Mechanical specifications for a closed leaflet valve prosthesis

MECHANICAL SPECIFICATIONS FOR A CLOSED LEAFLET VALVE PROSTHESIS

E.P.M. ROUSSEAU

MECHANICAL SPECIFICATIONS FOR A CLOSED LEAFLET VALVE PROSTHESIS

MECHANICAL SPECIFICATIONS FOR A CLOSED LEAFLET VALVE PROSTHESIS

PROEFSCHRIFT

TER VERKRIJGING VAN DE GRAAD VAN DOCTOR IN DE TECHNISCHE WETENSCHAPPEN AAN DE TECHNISCHE HOGESCHOOL EINDHOVEN, OP GEZAG VAN DE RECTOR MAGNIFICUS PROF. DR. S.T.M. ACKERMANS VOOR EEN COMMISSIE AANGEWEZEN DOOR HET COLLEGE VAN DEKANEN IN HET OPENBAAR TE VERDEDIGEN OP DINSDAG 2 APRIL 1985 TE 16.00 UUR

DOOR

EDUARD PIERRE MARIE ROUSSEAU

GEBOREN TE MAASTRICHT

Druk: Dissertatiedrukkerij Wibro, Helmond.

Dit proefschrift is goedgekeurd door de
promotoren: prof.dr.ir. J.D. Janssen
prof.dr. H.A. Huysmans
co-promotor: dr.ir. A.A. van Steenhoven

Het onderzoek, beschreven in dit proefschrift werd gefinancierd door de Stichting Technische Wetenschappen.
Het verschijnen van dit proefschrift werd mede mogelijk gemaakt door steun van de Nederlandse Hartstichting.

Mechanical specifications for a closed leaflet valve prosthesis

Chapter 1 General introduction

1.1. Concise survey of heart valve prostheses

Presently, basically three different types of heart valve prostheses can be distinguished:

i) the mechanical prostheses, in which a ball, a disc or rigid leaflets regulate the blood flow. Examples are the Starr-Edwards ball valve (Starr, 1960), the Björk-Shiley tilting disc valve (Björk, 1969) and the St Jude Medical bi-leaflet prosthesis (Emery et al., 1978);

ii) the biological leaflet valve prostheses which have three flexible leaflets suspended in a flexible or non-flexible frame. The leaflets are of different biological origin: glutaraldehyde treated porcine aortic valve leaflets (Hancock, Carpentier-Edwards, Angell-Shiley: Cohn and Collins, 1979) (see figure 1.1), glutaraldehyde treated porcine pericardial tissue (Tandon et al., 1978), human fascia lata tissue (Senning, 1967; Ionescu and Ross, 1969) or human Dura mater tissue (Zerbini, 1975);

iii) the artificial leaflet valves in which the leaflets are made from synthetic materials. There are valves made from silicone rubber reinforced with polyester fabric (Gerring et al., 1974), Avcothane (Ghista and Reul, 1977), polyolefin rubber Hexsyn (Kiraly et al., 1981) and segmented polyurethane (Wisman et al., 1982). All these synthetic valves, however, are not yet clinically available.

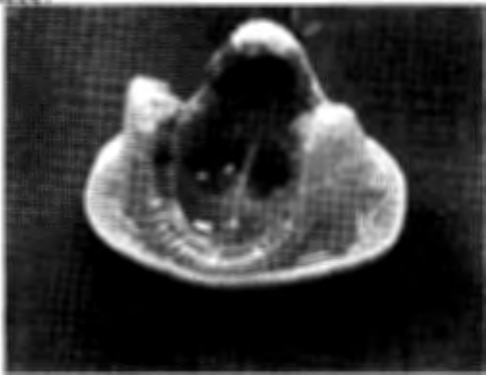

Fig. 1.1. The Hancock leaflet valve prosthesis.

All types of valves have important advantages and disadvantages. The main advantage of the mechanical prostheses is that they are mechanically strong and durable. However a serious disadvantage is that they carry a high risk of thrombus formation due to the flow behaviour, the valvular geometry and the material used (Mueller et al., 1981; Stevenson et al., 1982). Therefore, all mechanical prostheses require lifelong use of anticoagulants (Brawley et al., 1975; Cooley, 1977). Furthermore, from literature it is known that when using these valves, some damage of red blood cells (hemolysis) is inevitable (Eyster et al., 1971; Williams et al., 1971) due to the high shear stresses in the vicinity of the occluder (Figliola and Mueller, 1977; Yoganathan et al., 1978; Figliola and Mueller, 1981) and the mechanical interaction between occluder and frame (Lefemine et al., 1974). Finally, in the mechanical prostheses there may be a considerable pressure difference across the fully opened valve (Liotta et al., 1970; Brawley et al., 1975; Yoganathan et al., 1982).

Biological leaflet valve prostheses, which resemble the natural human aortic valve, have the main advantage of almost complete absence of thrombus formation, when the valve is implanted in the aortic position. Furthermore, the rather physiological hemodynamic characteristics like central flow and a lower pressure drop are mentioned, and only a low incidence of hemolysis is reported (Austen and Hutter, 1977). The main disadvantage of these biological valves is the relatively short lifetime due to tissue failure (Schoen et al., 1983). The failure phenomena described are cusp rupture and calcium deposition followed by insufficiency and stenosis respectively (Wright, 1972; Lennox, 1973; Wallace, 1975; Austen and Hutter, 1977; Muller and Nolan, 1977; Clark and Swanson, 1979; Lefrak and Starr, 1979; Davies, 1980; Ishihara et al., 1982; Thubrikar et al., 1983).

Finally the same list of advantages and disadvantages of the biological valves holds for the artificial leaflet valves. It is clear that such a type of valve also could have some important additional advantages over a biological tissue valve: it can be made at any desired geometry and material properties at probably a much lower cost price. The main disadvantage of these valves has been so far, just like for the biological valves, their limited lifespan in comparison with the mechanical valves. In the initial phase of valve

development this was partly due to the lack of proper durable synthetic materials and due to the defective surgical techniques and equipment (Akutsu et al., 1959; Braunwald and Morrow, 1964). Later types of valves were made of materials which were used and tested in bloodpumps and found to be suitable for biological purposes (Szycher et al., 1977; McMillin, 1983). The design of these valves was partly based on the requirements of gradual valve closure, fibre reinforcement and a large cross-sectional orifice area, and the design parameters were sometimes formulated by using a simple mathematical model (Ghista and Reul, 1977). However, most frequently the design was brought about empirically (Mohri et al., 1973; Gerring et al., 1974; Kiraly et al., 1981; Wisman et al., 1982). This led to valves which functioned quite well in-vitro, showing full opening and closing, physiological pressure- and flow patterns, small backflow and small energy loss (Mohri et al., 1973; Haworth et al., 1978; Haüssinger and Reul, 1981; Wisman et al., 1982), but failed in-vivo. This is partly due to an unfavourable mechanical stress situation in the closed and opened situation in comparison with the natural valves. Hence the design study of an artificial leaflet valve should be focussed on the creation of an optimal stress situation within the leaflets of such a valve. To specify that situation into more detail the failure behaviour of presently available leaflet valves has to be analysed and some hypotheses as to failure mechanisms need to be formulated. This will be the subject of the next section.

1.2. The failure behaviour of leaflet valve prostheses

1.2.1. Introduction

In literature some morphological observations are described on explanted bioprostheses which had functioned in patients for a certain time. The failure behaviour of artificial leaflet valve prostheses is only studied in in-vitro experiments or during animal experiments. Firstly, the observed failure phenomena of both groups of valves will be summarized and discussed. Subsequently, some hypotheses about the mechanisms of those failure phenomena are postulated.

1.2.2. Failure phenomena: a review of literature

The failure behaviour of bioprosthetic valves explanted from patients was thoroughly studied by Carpentier et al. (1974). All specimens removed for tissue failure exhibited similar lesions: tears and perforations in the central portions of the valve cusps. Furthermore degeneration of fibres and matrix was observed predominantly in the central portions of the leaflets, and calcium depositions were found at the base of the cusps. Clark and Swanson (1979) investigated the failure behaviour of two Hancock valves in a testing device in which the valves are loaded at a high frequency (Steinmetz et al., 1964). They found that first multiple fenestrations near the commissure in the coaptation area developed and that later holes and tears in the thinner portions of the leaflet base appeared between the collagen bundles. One leaflet of one prosthesis completely prolapsed during closure which resulted in gross valvular insufficiency. Davies (1980) concludes that for tissue valves, valve failure is associated with either tears or splits in the cusps, initiated near the commissures by cusp perforation, or by dystrophic calcification within the cusps with retraction and shriveling. Bodnar and Ross (1982) observed two important failure modes in 226 bioprostheses, namely the appearance of perforations, small tears or gross ruptures in one or more of the cusps while no clinical or pathological evidence of infection being present, and secondly calcifications were noted macroscopically by histological or in-vitro x-ray examination. Next, Ishihara et al. (1982) presented detailed morphological observations on 16 explanted porcine valve prostheses. They observed tears in the coaptation areas in the vicinity of the frame tops perpendicular to the free edge, perforations extended along the basal regions of the cusps forming an arc parallel to the sewing ring, and small perforations usually multiple and localized in central regions of the cusps often in association with multiple calcific depositions. Thubrikar et al. (1983) studied calcification phenomena of the Hancock valve implanted in calves. Initially calcification (within 49 days) was found mainly along the leaflet attachment. But also calcification appeared as streaks along the collagen bundles. At longer terms, calcification was also found in the middle part of the leaflet. Also the following case reports of explanted bioprostheses from patients are worth mentioning. McIntosh et al. (1975) found

small tears in the leaflets in the vicinity of the leaflet suspension near the commissures. Thereby also calcification was noted. Stinson et al. (1977) found leaflet perforations in the vicinity of the commissures of a one year old porcine valve, while Brown et al. (1978) ascertained at a Hancock valve, which had functioned for three years in a patient, heavy calcification of all three leaflets and noted a small perforation at the base of one cusp. Finally, Housman et al. (1978) described a case of sudden mechanical failure (leaflet disruption) where a major tear was found in one cusp just beneath the coaptation area in the vicinity of the leaflet suspension.

Until now, the failure behaviour of artificial leaflet valve prostheses has been studied only in-vitro or animal experiments. For example, Haworth et al. (1978) performed an in-vitro study of the failure behaviour of two types of artificial valves by loading them at a high frequency, and describing the observed failure phenomena. The first type, the so-called Oxford valve, was a valve with leaflets made from silicone rubber reinforced with a polyester fabric. This valve showed in course of time initial wear of the silicone rubber, and delamination of the composite near the free edge at the centre of each cusp and in areas close to each commissure. This initial wear was followed by rupture of some fibres in both mentioned cusp regions which led to propagation of a tear from one or more of the commissures to the cusp base. The failure behaviour of the second type, a valve with polyurethane leaflets, was similar to the first type, although failure tended to come about more abruptly as no strong fibres were present to arrest the tear. Besides, the Oxford valve (Gerring et al., 1974) was implanted in 4 goats and 7 calves. The valves in the goats had a limited lifetime of 0.5 - 20.5 months. Important causes of valve failure were thrombus formation and colonisation of thrombus by bacteria followed by stenosis or cusp rupture. The silicone/polyester cusps deteriorated in a characteristic way by delamination. This was aggravated by deposition of material from the blood on any exposed polyester which stiffens the cusps and accelerates the process of deterioration. However, the same type of valve was implanted also in 7 calves which were still alive after 18 - 30 months implantation time. Another report on failure of artificial leaflet valves was given by Hennig et al. (1981). They implanted the Aachen-valve, made of Avcothane and

developed by Ghista and Reul (1977), in 3 calves. After 4 months of implantation the leaflets were completely calcified. Finally, Wisman et al. (1982) implanted valves made of segmented polyurethane in sheep and goats. All the valves implanted in calves showed calcification especially along the free edges of the leaflets. Furthermore, thrombus formation always occurred. On the contrary, most goats and sheep were still alive. The valves of 3 sheep and 2 goats, who died owing to an other reason, showed no or just little calcification.

From this review of literature it may be stated that, although the experimental evaluations show great discrepancies, the failure phenomena of leaflet valve prostheses basically may be divided into the next three types (see also figure 1.2):

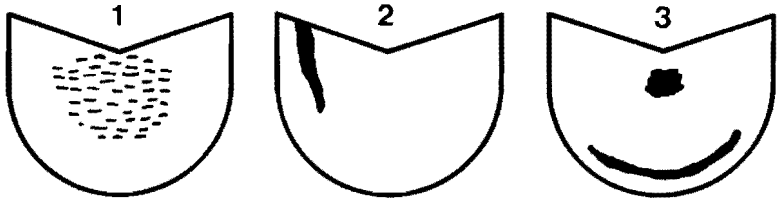

Fig. 1.2. The failure phenomena in leaflet valve prostheses.
1: tears and perforations in the central portions of the leaflets.
2: tears in the leaflets near the commissures.
3: calcification in central leaflet parts and at the base.

1) tears and perforations in the central portions of the leaflets (Carpentier et al., 1974; Brown et al., 1978; Haworth et al., 1978; Clark and Swanson, 1979; Ishihara et al., 1982);
2) tears in the leaflets in the vicinity of the commissures (McIntosh et al., 1975; Stinson et al., 1977; Housman et al., 1978; Haworth et al., 1978; Clark and Swanson, 1979; Davies, 1980; Ishihara et al., 1982);
3) calcification in central leaflet regions and at the base along leaflet attachment (Carpentier et al., 1974; McIntosh et al., 1975; Brown et al., 1978; Davies, 1980; Bodnar and Ross, 1982; Ishihara et al., 1982; Thubrikar et al., 1983).

In the next section some causal factors will be discussed which may lead to the failure phenomena described here.

1.2.3. Failure mechanisms

It is plausible that the tears and perforations in the leaflets near the commissures are caused by high tensile stresses during the closed phase of the cardiac cycle (Haworth et al., 1978). The fact that tears may grow perpendicular to the free edge (Ishihara et al., 1982) may indicate that in that region, beside rupture of the membrane parts, also fibre break occurs due to high tensile stresses. Moreover, as a consequence of the fibre network, it may not be excluded that in parts of the coaptation area which are not loaded the membraneous parts between the fibres wrinkle (see chapter 2). This is expected to be very unfavourable due to the accompanying high bending strains. Till so far the membranes and fibres were discussed separately. However, from fibre composite analysis (Munro and Beaumont, 1979) also the fibre-matrix connection is known to be very critical. Due to loading, tearing of a fibre from the matrix may occur. In conclusion, it is hypothesized that leaflet rupture in a loaded closed valve prosthesis is caused by: rupture of a membrane part between fibres, fibre break, wrinkling of membrane parts in the coaptation area and fibres tearing from the membrane.

The other failure mechanism is associated with the opening and closing behaviour of the valve leaflets. More specifically, it is hypothesized that the tears and perforations in the central part of the leaflet in the vicinity of the leaflet attachment (see figure 1.2) are caused by high bending strains. To justify this, Thubrikar et al. (1982) investigated leaflet flexions of Hancock valves implanted in calves, using small radiopaque markers placed on the leaflets. The movement of the markers was observed roentgenographically. From these measurements the greatest flexions were found along the leaflet attachment in radial direction and in the central portion of the leaflet in circumferential direction, during opening and closing. Also Broom and Thomson (1979) observed leaflet movements in a Hancock valve during a cardiac cycle but now in-vitro. From these observations, kinks were found at the free edges of the leaflets. These were the regions where large flexure was expected. Broom (1978) has also shown that glutaraldehyde treated porcine mitral tissue does suffer serious disruption confined to the regions of flexure.

The last hypothesis is concerned with the observed leaflet calcification. The regions of calcification in the leaflets agree with the

regions with high bending strains (Thubrikar et al., 1982, 1983). A possible relation between magnitude of varying bending strain and the amount of calcification is reported frequently in literature concerning membranes of artificial heart pumps (Coleman, 1981; Coleman et al., 1981; Hennig et al., 1981; Nosè et al., 1981). It is supposed that the varying bending strains introduce microtears in the leaflet surface where calcification is then expected (Coleman, 1981). Also, it is hypothesized by Bruck (1981) that a varying bending strain could accelerate the diffusion of calcium deposits into the leaflet material. A further understanding of the calcification process is very complex as this process seems to depend on many biological and mechanical factors like surface structure (Merrill, 1977), surface charge (Coleman, 1981), chemical structure of the material (Long and Urry, 1981) and local hemodynamic conditions (Coleman, 1981).

In conclusion it is postulated that the stress- and strain distribution during two phases of the cardiac cycle may lead to the failure of artificial leaflet valve prostheses:

i) the closed loaded situation where high tensile stresses cause membrane rupture and/or fibre break, and where wrinkling of the membranes in the coaptation area may occur. In this situation also tearing of the fibres from the membranes is expected.
ii) the opening- and closing phase of the cardiac cycle with high bending strains due to kink formation and large leaflet curvatures. These high bending strains cause tears in the leaflets often associated with calcification and hence stiffening of the leaflets.

1.3. Purpose and scope of the present study

The investigations described in this thesis were intended to formulate mechanical specifications for the design of an improved artificial leaflet valve prosthesis. This research is part of a larger project founded upon the opinion that a detailed analysis of the behaviour of the natural aortic valve may lead to better insights into the relevant design parameters for such a valve (figure 1.3). To that end in earlier studies, the hydrodynamical (van Steenhoven, 1979),

the mechanical (Sauren, 1981) and the kinematical (van Renterghem, 1983) aspects of the natural aortic valve behaviour were studied.

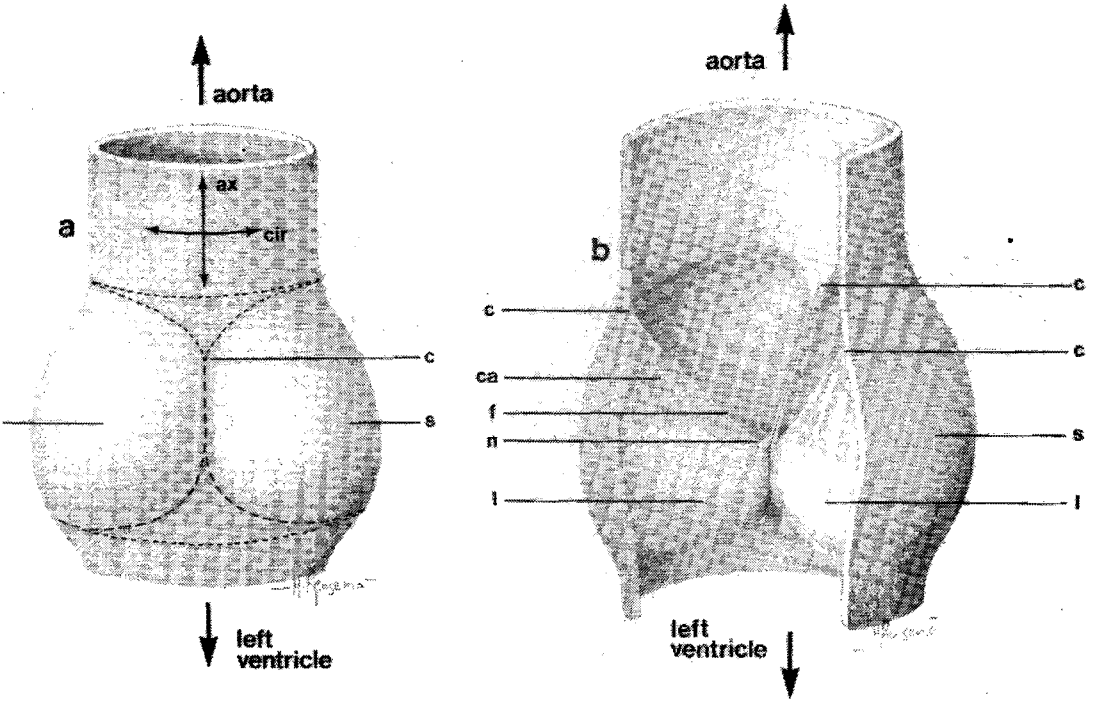

Fig. 1.3. Diagrammatic representation of the aortic valve (see van Renterghem, 1983).

a: side view of the valve.
b: the aortic valve in the closed configuration after dissection of one leaflet and the corresponding sinus wall.
c = commissure; f = free edge of the leaflet; ca = coaptation area; l = leaflet; n = node of Arantius; ax = axial direction; cir = circumferential direction; s = sinus of Valsalva;

These three basic studies revealed that:

- the aortic valve closes gradually. In in-vivo experiments it was observed that during the deceleration phase of systolic aortic flow the valve already closes for 75% of the cross-sectional orifice area and that only a slight backflow is necessary to close the valve completely (van Steenhoven et al., 1980, 1981 and 1982b).

From model experiments it was found that this early closing behaviour is essentially caused by the positive pressure gradient in the axial direction when the liquid flow is decelerating. The most important factor which enables this gradual closure was found to be the presence of a cavity behind the leaflets (van Steenhoven and van Dongen, 1979 and 1980). In-vivo, such a cavity is present behind each leaflet and is denoted as the sinus of Valsalva;

- the aortic valve leaflet has a fibre reinforced structure. From histological observations it followed that the leaflet consists of an elastin meshwork reinforced with circumferentially oriented bundles of collagen and that in the middle portion of the leaflets, close to the attachment to the aortic wall, constrictions were present which may act as a hinge (Sauren et al., 1980). Uniaxial tensile experiments showed that the collagen bundles in the leaflet have a stiffening effect and cause a marked anisotropy. Furthermore, it was found that the leaflets show a considerable stress relaxation (Sauren et al., 1983). Finally, from a numerical model study of a closed valve, it was concluded that the bundles in the leaflet transmit the pressure load on the membraneous parts to the aortic wall thereby creating an approximately homogeneous stress distribution with two equal positive principal stresses (Sauren, 1981). Hence the leaflets combine a high degree of mobility during opening and closing with great strength and stiffness in the closed situation.
- the geometry of the aortic ring, to which the leaflets are suspended, changes considerably during a cardiac cycle. From animal experiments it was found that the movements of the commissures are in phase with the aortic pressure variations during a cycle and amounts to about 20% of the diastolic radius. Also the strains in the base plane appeared to vary with maximum amplitudes of about 5% for the valve segments close to the myocardial wall (right valve part) and 15% for the segment adjoining the anterior mitral valve leaflet (left and posterior part). So, the deformation of the base plane is essentially non-symmetric. Finally, the relative displacement between a base and a commissure point of the aortic ring was negligible (van Renterghem, 1983). It is not yet quantified how these geometrical changes influence the instantaneous value of the stresses in the leaflets of the natural aortic valve, although it

is expected that a flexible leaflet suspension will reduce the instantaneous stress peak values, for example, just after valve closure.

Because of the stress reducing mechanisms found to be present in the natural aortic valve, e.g. gradual valve closure, leaflet reinforcement and flexible leaflet suspension, a leaflet valve prosthesis is pursued which exhibits the main characteristics of the natural aortic valve. However, for clinical practice some design restrictions have to be made such as:

- the valve prosthesis has to be implantable in an easy and quick manner;
- the prosthesis has to be applicable to different pathological situations;

Therefore, this study will focus on the design of a leaflet valve prosthesis which in essence should fulfil the following requirements:

- the valve is constituted around a frame to suspend the leaflets. This enables quick and easy implantation;
- the frame is allowed to be flexible to ensure commissure displacements throughout the cardiac cycle;
- because mostly the natural aortic valve has three sinusses, the number of leaflets is three to make use of these natural sinusses;
- the geometry of the frame and the leaflets is such that it fits optimally the sinusses to provide gradual valve closure. This means that the frame posts need to be low and narrow. Furthermore, prestresses in the leaflets are undesirable (van Steenhoven et al., 1982)
- the leaflets are reinforced in circumferential direction to ensure approximately a homogeneous stress distribution during diastole;
- the leaflets are made of a synthetic material instead of biological tissues to overcome fabrication problems such as treatment and storage of the tissues, biological deviations between tissues and the necessity to sacrifice many animals. Besides, the material properties can also be varied which gives an extra design parameter in the design study,
- a sewing ring at the base of the frame has to be added to enable implantation in different pathological situations without damage of the sinus cavities.

1.4. Contents of this thesis

In this thesis the main attention is focussed on the first of the two unfavourable valve loading situations during the cardiac cycle postulated in the foregoing, namely,the closed loaded situation. For this situation, a numerical model was developed to predict stresses and strains in the valve leaflets. In order to check this numerical model some displacements in the valve were measured in-vitro. For this purpose, a Hancock porcine leaflet valve is taken because of the following reasons:

- it is a valve that has been implanted frequently and it functions reasonably well;
- it resembles the valve which we wish to develop (3 reinforced leaflets, flexible frame, sewing ring);
- the valves are available for experimental studies;
- all relevant geometrical parameters and material properties can be determined.

First, the geometry and viscoelastic material properties of the frame and the leaflets of the Hancock valve were determined as basic input data for the mechanical model (chapter 2).

Next, a numerical model is developed for the Hancock valve to predict the stresses, strains and displacements in the loaded closed valve. Also the frame itself is analysed. These models are based on the finite element method, and incorporate both non-linear relationships between deformations and displacements and viscous material properties. The numerical model is verified experimentally by analysing the displacements of the commissures and the central part of the leaflets during a time varying loading. In the case of the artificial leaflet valve aimed at, viscous properties of frame and leaflet material may be chosen such that they affect the stress situation during the closed valve phase of the cardiac cycle. Hence, it is important that the viscous properties of the frame and leaflets are incorporated in the model. However, in the case of the Hancock valve the difference between the relevant time constants of the frame material and leaflet material is so large, that two separate experiments with the total valve prosthesis were performed at a high and a low value of loading rate, respectively. The numerical model of

the Hancock valve together with the experimental verification is described in chapter 3.

With the developed numerical model the construction of a rather arbitrary leaflet valve prosthesis is evaluated in chapter 4. As a basic design a much simpler construction than the Hancock valve was chosen. It is constituted around a frame with very narrow posts to which directly the leaflets are suspended. Furthermore, the fibre reinforcement is chosen to be oriented almost in a parallel way and all fibres have the same thickness. Next, the (visco)elastic material properties of frame and leaflets, the geometry of frame and leaflets and the amount and thickness of the fibres were varied and the influences on the stress distribution within the leaflets were determined. To characterize this stress distribution, four stress quantities in the valve leaflets were analysed. These are: i) the von Mises intensity for the membranes, giving an overall idea of the membraneous stress situation, ii) the tensile stress in the fibres, iii) the minimum principal stress in the membranes between the fibres and iv) the shear force between fibre and membrane. Although it is unknown how these stress parameters are related to the failure mechanisms for the closed loaded valve (section 1.2) it is still believed that they describe the stress situation in the leaflet adequately. On the basis of this analysis mechanical specifications will be formulated for geometry and material properties of a leaflet valve prosthesis.

Finally, chapter 5 is concerned with the progress of this study. As a preparatory study an attempt is undertaken to investigate the possible relation between time varying bending strain and the phenomenon of calcification. Also a proposal for further research will be given.

Chapter 2 Input data for the mechanical model of the Hancock valve

2.1. Introduction

To check the numerical model for a leaflet valve prosthesis, a Hancock valve is analysed and tested. The Hancock leaflet valve prosthesis (model 242) is schematically shown in figure 2.1. It consists of a polypropene frame (figure 2.2.a), covered with Dacron cloth, in which a glutaraldehyde-treated

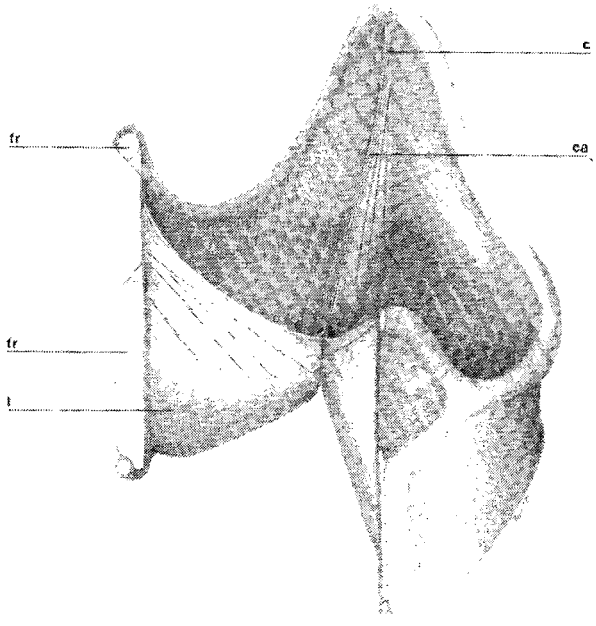

Fig. 2.1. The Hancock leaflet valve prosthesis.

fr = frame, c = commissure, l = free leaflet area, ca = coaptation area; The sewing ring is not drawn.

porcine aortic valve is mounted. The base of the frame is reinforced with a hard metal (Stellite) ring. To implant the valve prosthesis in the patient, a sewing ring is positioned just above that ring. The valve is essentially a-symmetrical due to the a-symmetrical geometry of the porcine aortic valve (Sauren, 1981). Before mounting the aortic valve in the frame, the entire valve is treated with glutaraldehyde under a hydrostatic pressure of about 13 kPa (Rousseau et al.,

1983). After the treatment, the leaflets and a small part of the surrounding sinus- and left ventricle tissue are cut out from the total valve. This piece of tissue, shown schematically in figure 2.2.b, is then mounted in the frame using Dacron cloth. After mounting, this cloth covers the frame, the sewing ring, the hard metal ring and a

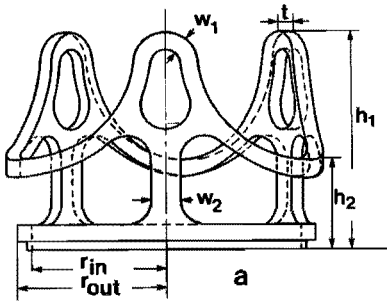

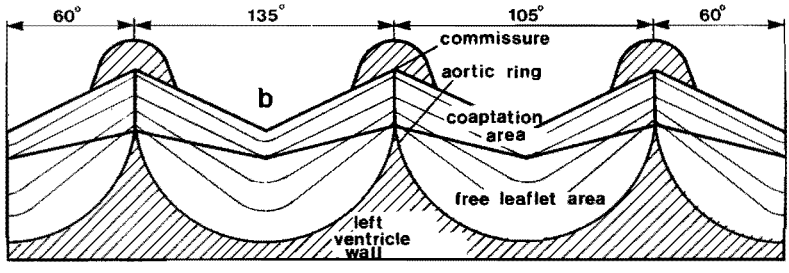

Fig.2.2. a. The frame

b. A schematic outline of the crownlike piece of tissue cut from a treated porcine aortic valve.

small part of the sinus- and left ventricle tissue. The use of a part of the sinus and left ventricle, including the aortic ring, allows the preservation of the natural anchorage of the leaflets to their surroundings.

In order to be able to analyse the mechanical behaviour of the closed Hancock valve prosthesis, the geometry and material parameters of this valve have to be accurately known. In this chapter, the determination of these parameters is described.

2.2. The valve geometry

The frame construction is shown in figure 2.2.a and consists of three similar parts with unequal cross sectional angles (120^{o} - 135^{o} - 105^{o}). The geometrical data of several frames are summarized in table 2.1.

The a-symmetric geometry of the porcine aortic valve mounted in the Hancock valve is sufficiently described by the next three parameters (see figure 2.3):

i) leaflet surface A_i/A_t, being the quotient of the projected leaflet area belonging to frame top i (i = 1,2,3) (A_i) and the total projected leaflet surface: $A_t = \sum_{i=1}^{3} A_i$.

ii) commissure height: H_i (i = 1,2,3) which is defined as the distance between commissure point i and the valve base.

iii) angle φ_i (i = 1,2,3) made by the upper boundary of the coaptation area i, and the "horizontal axis".

Frame size [mm]	19	21	23	25	27
geometry data [mm]					
h_1	14.6	16.0	17.2	18.8	19.6
h_2	6.1	6.7	7.1	7.8	8.2
r_{out}	9.4	10.4	11.4	12.4	13.2
r_{in}	8.3	9.3	10.3	11.2	11.9
w_1	1.3	1.4	1.5	1.6	1.6
w_2	2.0	2.2	2.4	2.5	2.7
t	1.1	1.1	1.1	1.2	1.3

Table 2.1. Geometrical data for the different frame sizes

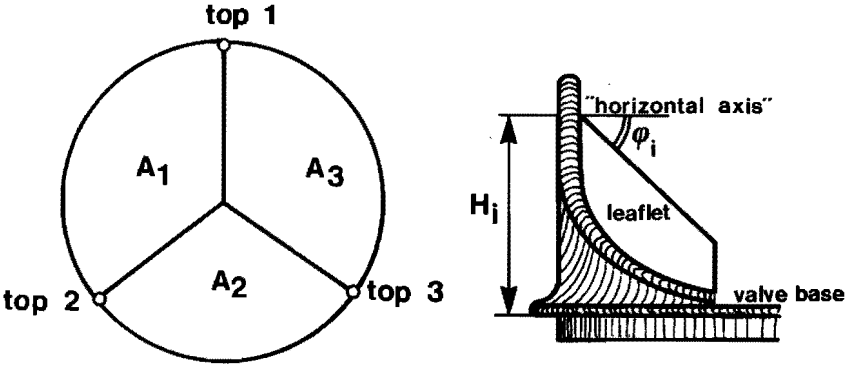

Fig. 2.3. Definition of the geometry parameters A_i/A_t, H_i and φ_i.

The values of A_i/A_t (i = 1,2,3) were determined from photographs of the bottom of the valve. The commissure height H_i and the angle φ_i were measured using a moving crosstable (Carl Zeiss) having an absolute measurement accuracy of 0.001 mm in each point. The measurement data for the 4 valves considered are listed in table 2.2. Besides, for the numerical modelling (see section 3.2.2 and figure 3.3) another geometrical characterization is given by the coordinates of the points A, B, C, D and E. Here, the surface BCDE represents the coaptation area and ABE represents the free leaflet area. BC, CD, DE and AE are straight lines. The z coordinates of the points A, B, C, D and E were measured in the same way as H_i and φ_i were measured. For one 23 mm valve these data are also given in table 2.2. The thickness of the leaflet in all cases is about 0.4 mm (Rousseau et al., 1981).

	A_i/A_t [-]			H_i [mm]			φ_i [°]		
frametop	1	2	3	1	2	3	1	2	3
valve									
19	0.37	0.32	0.31	8.8	6.8	9.1	50	75	60
21	0.35	0.37	0.28	9.6	9.0	11.9	64	61	68
23-1	0.29	0.32	0.39	12.1	14.3	14.5	50	48	45
23-2	0.37	0.32	0.31	12.2	10.9	12.0	41	58	44

	Z(A)	Z(B)	Z(C)			Z(D)	Z(E)
	1 - 2 - 3	1 - 2 - 3	1	2	3	1 - 2 - 3	1 - 2 - 3
23-1	0.5	7.0	10.6	12.9	13.1	6.5	4.6

Table 2.2. The geometry of the Hancock valve as characterized by the leaflet surface areas A_i/A_t, the commissure heights H_i and the angles φ_i (see fig. 2.3). The standard deviation of each parameter amounts to $\pm$ 0.05, $\pm$ 0.1 mm and 1° respectively. For the 23-1 mm valve also the z coordinates of the points A, B, C, D and E as used in the numerical model are given (see section 3.2.2 and fig. 3.3.a). For A, B, D and E these z-coordinates are taken to be equal for the 3 valve parts (standard deviations are 0.2 mm).

Finally, leaflets of the Hancock prosthesis are reinforced with collagen bundles. A typical fibre pattern is illustrated in figure 2.1.

2.3. The mechanical properties of the glutaraldehyde treated tissue

2.3.1. Experimental procedure

The viscoelastic material properties of the Hancock leaflet tissue and of fresh and glutaraldehyde treated porcine aortic valve leaflets were determined using the experimental procedure developed by Sauren et al. (1983). The experiments were performed on strips of about 3 mm wide which were cut in the circumferential direction from the leaflets (see fig. 1.3) (Rousseau et al., 1983). This direction globally corresponds to that of the collagen network. After mounting, the tissue strips were preconditioned in the same way as described by Sauren et al. (1983). After this, the actual experiments were started which involved straining of the specimen with a constant elongation rate, followed by maintaining the specimen length at a predetermined level during 120 s. As a check on the reproducibility, the experiment was repeated three times inserting a rest period of 120 s whilst keeping the specimen at reference length. This reference length was the length of the specimen when the load was just zero. Thereafter, the thickness and width of the unloaded specimen were determined, using a microscope and a crosstable with a micrometer.

After conclusion of the experiments with the fresh leaflet strips, the same tissue strips were treated with glutaraldehyde according to the method of Carpentier and Dubost (1972). The treatment was performed at $4^{o}C$. 100 ml solution of glutaraldehyde was composed of 2.6 ml 25% glutaraldehyde solution and 97.4 ml 1/15 M phosphate buffer, pH = 7.4. The glutaraldehyde treatment for manufacturing a bioprosthesis was applied to an entire valve root under a hydrostatic pressure of about 13 kPa (Broom and Thomson (1979)). In the present study, this condition was simulated by treating the strips under a preload of approximately 0.3 N, which corresponds with the physiological strain value of about 0.08. This value is the average local strain in the circumferential direction in the leaflets of an intact porcine valve under an internal hydrostatic pressure of approximately 13 kPa, as measured stereophotogrammetrically by

Missirlis and Chong (1978). Next, these treated specimens were subjected to the same experimental procedure as described above. The advantage of the evaluation of the material properties before and after the glutaraldehyde treatment is that the biological deviations between various tissue strips is eliminated for the most part. Finally, the properties of strips of a Hancock bioprosthesis (342 M, 31 mm) were determined.

The elastic behaviour was described by the stress-strain relation measured when straining from the reference length to the maximum length. Here, stress was defined as the quotient of the loading force and the initial (unloaded) cross-sectional area, and strain was defined as the quotient of the elongation and the initial length. Two parameters were defined in order to quantify the elastic behaviour: E_0 being the slope of the stress-strain curve for the unloaded situation and E_{13} being the slope of the curve for the situation corresponding with a pressure load of 13 kPa. The procedure for the determination of the latter parameter was as follows: From the curve for the fresh tissue, the stress corresponding with a strain of 0.08 was determined. The slope in that point of the stress-strain curve was used as the E_{13} value for the fresh tissue. For the treated tissue, we hypothesized that the loading force (= stress multiplied by cross-sectional area) is the same as for the fresh one under a pressure load of 13 kPa. From the change in cross-sectional area, due to the treatment, the stress in the treated tissue could be obtained and consequently E_{13}.

The viscoelastic behaviour was characterized by the reduced relaxation function G(t), used by Fung (1972). This function is defined as:

$$G(t) = \frac{F(t)}{F(t=0^+)} \qquad (2.1)$$

where F(t) is the measured force response at time t to a step change in the length at time t = 0. Fung (1972) has proposed to describe the material behaviour using a so-called continuous relaxation spectrum between two boundaries θ_1 and θ_2 (see appendix I). The reduced relaxation function G(t) can then be expressed as:

$$G(t) = \frac{1+K\int_{\theta_1}^{\theta_2} \frac{1}{\tau} e^{-t/\tau} d\tau}{1+K \ln(\theta_2/\theta_1)} \qquad (2.2)$$

In this equation, K, θ_1 and θ_2 are the viscoelastic parameters which have to be determined. K is the parameter which has the greatest influence on the total amount of relaxation after a large time interval. The time constant θ_1 has an influence on the slope of the relaxation function just after the beginning of relaxation and the time constant θ_2 is a measure for the time which is necessary to reach the maximum relaxation. Further physical interpretation of the parameters K, θ_1 and θ_2 should be handled carefully (Sauren and Rousseau, 1983). The reduced relaxation function G(t) has to be determined from the load response of the specimen to a step change in the length of the specimen. As it is physically impossible to realize a true step change, a finite time interval t_s of about 0.1 s was considered. This quasi-step change was obtained with an elongation rate of approximately 10 mms^{-1}.

From the response, first the stress-strain curve was determined and the parameters E_0 and E_{13} were obtained. Next, the parameters K, θ_1 and θ_2 were determined by fitting the measured relaxation curve on relation (2.2) using the least squares method. These experiments were repeated for the two fresh and glutaraldehyde-treated strips and three Hancock leaflet strips (Rousseau et al., 1983).

2.3.2. Results

Figure 2.4 shows typical stress-strain curves for the different

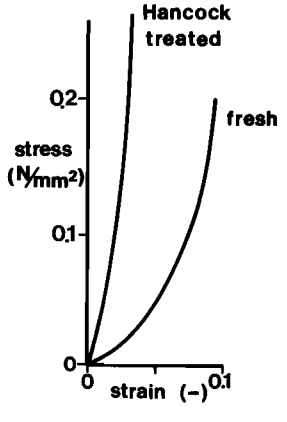

Fig. 2.4. Typical stress-strain curve for the fresh, the treated and the Hancock leaflet tissue. The curve for the treated tissue is very close to the curve for the Hancock leaflet tissue.

tissues. From these curves it is concluded that as a result of the glutaraldehyde treatment, the stress-strain curve for the leaflet tissue shifts towards the stress-axis with respect to the curve obtained in the fresh state. The results of the fitted parameters are summarized in table 2.3. It is seen that the values of both parameters E_0 and E_{13} strongly increase due to the glutaraldehyde treatment. Besides, the observed stress-strain curves for the glutaraldehyde treated tissue are in fair agreement with those given by Broom and Thomson (1979).

	E_0 [N/m^2]	E_{13} [N/m^2]	K[-]	θ_1[s]	θ_2[s]
fresh tissue	0.18 10^6 (0.04 10^6)	6.6 10^6 (1.1 10^6)	0.085 (0.013)	0.0054 (0.0009)	71 (18)
treated tissue (13 kPa)	1.7 10^6 (0.5 10^6)	23.0 10^6 (7.1 10^6)	0.024 (0.010)	0.0034 (0.0009)	37 (14)
Hancock tissue	1.8 10^6 (0.7 10^6)	23.0 10^6 (7.1 10^6)	0.050 (0.005)	0.0019 (0.0015)	23 (13)

Table 2.3. Elastic and viscoelastic material parameters of fresh and glutaraldehyde-treated porcine aortic valve leaflet tissue and of Hancock leaflet tissue (Rousseau et al., 1983). Between parentheses the standard deviation of the mean is given.

In figure 2.5.a a characteristic result of the measured and the fitted relaxation function for the Hancock-leaflet tissue is given. The accordance between both is good. Figure 2.5.b shows the relaxation functions for the fresh, the treated and the Hancock leaflet tissue, which are computed with the averaged values of the viscoelastic parameters K, θ_1 and θ_2 as given in table 2.3. From this it is observed that the fresh leaflet tissue shows much more relaxation than the treated one and remarkable more than the Hancock leaflet tissue (G(t=120 s) = 0.81, 0.69 and 0.59 for the treated, the Hancock and the fresh tissue respectively).

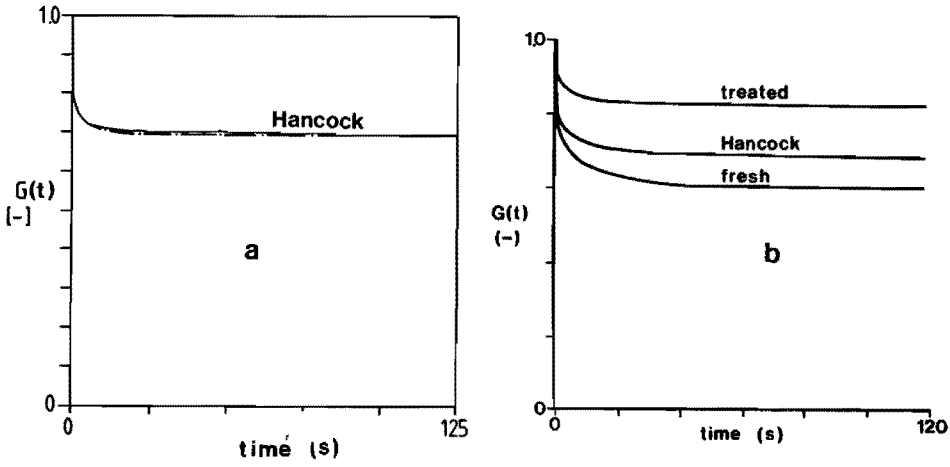

Fig. 2.5.a. A characteristic result of the measured and fitted reduced relaxation function for the Hancock leaflet
b. Computed reduced relaxation functions for the fresh, the treated and the Hancock leaflet tissue, using the mean values of the viscoelastic parameters K, θ_1 and θ_2

The experimentally observed changes of material properties due to the treatment with glutaraldehyde were expected to be related to changes in the leaflet histology (Sauren et al., 1980). The increase of E_0 and E_{13} could then be explained by the preservation through the treatment of the stretched state of the collagen bundles as caused by the preload. The decrease of K, corresponding with the decreasing relaxation after treatment might be the result of the reduction of the layer of the loose connective tissue (Rousseau et al., 1983). The difference of the amount of relaxation of the Hancock strips and the treated strips is possibly explained by the difference between the treatment conditions of the entire valve root under hydrostatic pressure and the treatment conditions of the tissue strip under uniaxial preload (Rousseau et al., 1983). Therefore, in the numerical model we will work with the obtained data of the Hancock valve.

2.4. The mechanical properties of the frame material

2.4.1. Experimental procedure

From some preliminary experiments on test specimens and from data obtained in the literature (Crissman and Zapas, 1983) it is expected that the polypropene, the frame is made of, behaves as a viscoelastic material. Hence, some relaxation experiments were performed on

polypropene test specimens (60 mm long, 3 mm wide, 0.5 mm thick) which were clamped in a Zwick (1434) testing equipment. The test specimens were strained in a steplike way within 0.5 s and the viscoelastic properties were determined. Due to the observed non-linear relation between the normalized relaxation function, defined by

$$H(t) = \frac{G(t)-G(\infty)}{1-G(\infty)} \qquad (2.3)$$

and the logarithm of time, see for example figure 2.8, the description of the viscous properties as explained for the leaflet tissue in section 2.3 has to be adapted. In appendix I it is outlined that in this case the relaxation spectrum as proposed by Fung (1972) does not give a appropriate description of the material behaviour and that an extra parameter (S_0) has to be added to the continuous relaxation spectrum to get a better fit. This gives:

$$G(t) = \frac{1+S_0 \int_{\theta_1}^{\theta_2} e^{-t/\tau}\, d\tau + K \int_{\theta_1}^{\theta_2} \frac{1}{\tau} e^{-t/\tau}\, d\tau}{1+S_0(\theta_2-\theta_1)+K \ln(\theta_2/\theta_1)} \qquad (2.4)$$

The viscoelastic material parameters of the polypropene θ_1, θ_2, S_0 and K were determined by fitting relation (2.4) to the measured reduced relaxation function by means of a least squares method.

2.4.2. Results

The Young's modulus of the polypropene was determined by DSM using a torsional damping test (DSM-information, Stamylan P, 1977) and was found to be 1582 N/mm^2 at a temperature of 23°C. The Poisson ratio has a constant value of $\nu = 0.4$.

The results of the relaxation experiments are shown in Figure 2.6. In this figure the reduced relaxation function is given as found by Crissman and Zapas (1983) and as found in our laboratory. The standard deviation of our relaxation function was obtained from five repetitions and found to be equal to 0.035. With regard to this standard deviation the agreement between the curves is fair.

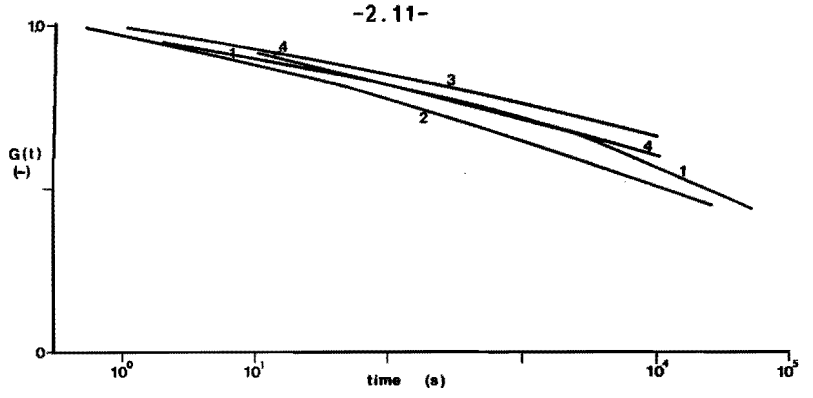

Fig. 2.6. Reduced relaxation function of polypropene measured in our laboratory and measured by Crissman and Zapas (1983).
1: own experiment; strain = 0.007
2: own experiment; strain = 0.010
3: Crissman and Zapas; strain = 0.004
4: Crissman and Zapas; strain = 0.008

In figure 2.7 the normalized relaxation function is plotted on a logarithmic time scale, from which it is concluded that this function is essentially non-linear. The parameters obtained from the fit with equation (2.4) are θ_1 = 3.4 s, θ_2 = 63270 s, S_0 = 0.9265 10^{-5} s^{-1} and K = 0.1051.

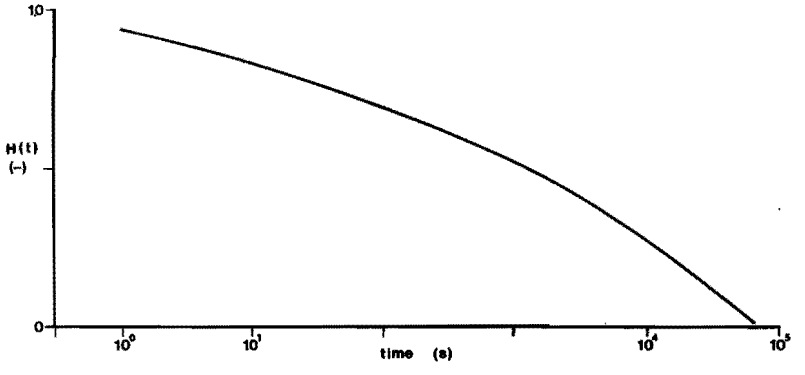

Fig. 2.7. The normalized relaxation function H(t) for the relaxation curve 1 in fig. 2.6. It is observed that this function is non-linear with ln(t).

2.5. Concluding discussion

In this chapter the geometry and material properties of frame and leaflets were determined. The frame geometry was exactly known by the

Hancock designs. The leaflet geometry was characterized by the projected leaflet surface areas, the commissure heights and the suspension angle. The tensile and relaxation experiments revealed the elastic properties of the leaflets to be non-linear while both frame and leaflet material exhibit significant viscous properties.

From the relaxation experiments a clear difference is observed between the viscoelastic material behaviour of the polypropene and the glutaraldehyde treated tissue. This is also elucidated by the frequency dependency of the loss modulus. This parameter, which describes the amount of energy dissipation and hence correlates with the amount of hysteresis, can be calculated from the continuous relaxation spectra (see: appendix I). Figure 2.8 shows the loss modulus versus frequency for both materials. From this figure it is concluded that the loss modulus of polypropene has a maximum at f $\approx$ 1 10^{-5} Hz (periodic time T $\approx$ 10^{5} s). On the contrary the maximum of the loss modulus of the leaflet has a maximum at about f $\approx$ 1 Hz (periodic time T $\approx$ 1s). This means that the viscoelastic phenomena of the frame are just notable in case of a very low loading rate and those of the leaflets at a much higher one. More specifically, the results indicate that the viscous properties of the valve leaflet are quite well notable during a cardiac cycle (f $\approx$ 1 Hz), while the influence of the viscous properties of the frame may then be neglected.

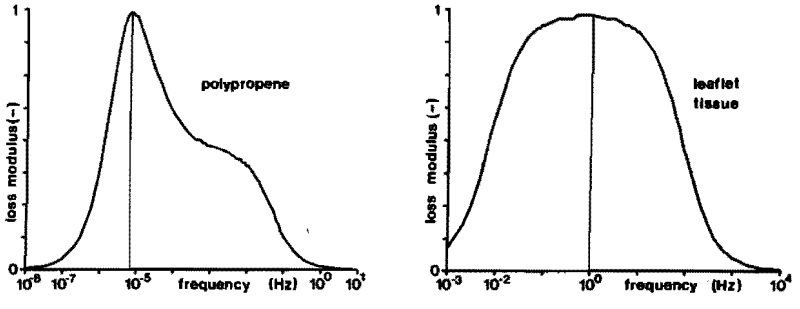

Fig. 2.8. The loss modulus of the polypropene (a) and of the glutaraldehyde treated tissue (b). The loss modulus is given as a dimensionless quantity: the values are divided by the maximum value.

Chapter 3 A mechanical model of the closed Hancock valve

3.1. Introduction

Earlier attempts to make a mechanical model of a leaflet valve have been undertaken by Ghista and Reul (1977) who used relatively simple linear expressions for the calculation of the membrane stresses in an isotropic model without fibre reinforcement and without flexible leaflet suspension. Christie and Medland (1982) performed a non-linear finite element analysis of bioprosthetic heart valves with fibre reinforcements. In their model, purely elastic material behaviour was assumed and the leaflet suspension was a rigid one. Experimental analyses of the mechanical behaviour of a closed leaflet valve prosthesis were also performed. For example, Thomson and Barratt-Boyes (1977) measured optically the radial commissure displacements of 2 Hancock valves in a mock circulation device, while Pohlner et al. (1979) studied the quasi-static behaviour of a flexible stent. Thubrikar et al. (1982) determined stresses in the leaflets of a porcine bioprosthesis in the closed and opened position. They put radiopaque markers on the valves and analysed their displacements under x-ray control. From these measured displacements, approximate bending strains in the leaflets were calculated.

The frame itself has also been the subject of investigation. For example a numerical analysis of the frame behaviour has been performed by Wright et al. (1982). They developed an a-symmetrical numerical model of a flexible frame without leaflets and determined frame stiffness, stress contours and maximum stress levels using the ANSYS finite element program package. Their analysis was restricted to geometrically linear and purely elastic behaviour of the frame and results were only given for 27 and 33 mm frame sizes. Experimentally the frame stiffness was determined earlier by Wright et al. (1982) and by Drury et al. (1981). The latter performed flexibility measurements on injection moulded valve frames. They investigated the influence of the geometric design, the kind of plastic used and the frame size on the flexibility of the frame. Both authors only analysed the elastic behaviour of the frame. No numerical model studies of leaflet valve prostheses were found which took into account the flexible frame as well as the leaflets. In all these

studies the influence of viscous properties of leaflet and frame were neglected.

In the present study a mechanical model of a leaflet valve prosthesis is aimed at, which incorporates a non-linear relationship between deformations and displacements and the viscoelastic properties of frame and leaflets. In case of the Hancock valve the viscoelastic properties of the frame are such (see chapter 2) that they probably hardly affect the stress distribution within the leaflets during a cardiac cycle. However, for the design study a mechanical model of a leaflet valve needs to be available in which the viscoelastic properties of the frame can be changed such that they may influence the stress situation in the closed valve during diastole. To verify such a mechanical model in case of the Hancock valve various experiments have to be performed which differ mainly in loading rate; a slow rate for the frame denoted by quasi-static loading and a faster one for the leaflets denoted by physiological loading. Besides, in a separate experiment the viscoelastic deformation of the frame itself has to be examined to separate the influence of frame and leaflet suspension shown in figure 2.2.b.

The mechanical behaviour of the closed Hancock valve has been examined using a non-linear finite element program package (MARC, 1983). For the sake of reduction of calculation time, the numerical model has been primarily restricted to 1/6 part of the valve, hence assuming 120^{o}-symmetry. As the Hancock valve is essentially a-symmetric (see section 2.2), also a simplified a-symmetric valve model is used to analyse the relation between numerical model and experiment. The numerical results will be verified by measuring the radial frame top displacements both in case of the frame itself and in case of an entire valve (i.e. commissure displacement) and by measuring the vertical displacement of the valve centre, all during the different load conditions mentioned above and for several sizes of frame and valve prosthesis. The different frames are denoted as 21, 23, 25 and 27 mm while the entire valves are denoted as 29, 21, 23-1 and 23-2 mm.

3.2. The numerical model

3.2.1. The frame

In the numerical model of the frame a 120^{o} symmetry is assumed, so that the calculations could be restricted to 1/6 part of the total frame. This part is schematically shown in figure 3.1a and the geometrical data are summarized in section 2.2. This 1/6 part was modelled with 16 nodes and 15 cylindrical beam elements; the mesh is shown in figure 3.1b. The material behaviour of

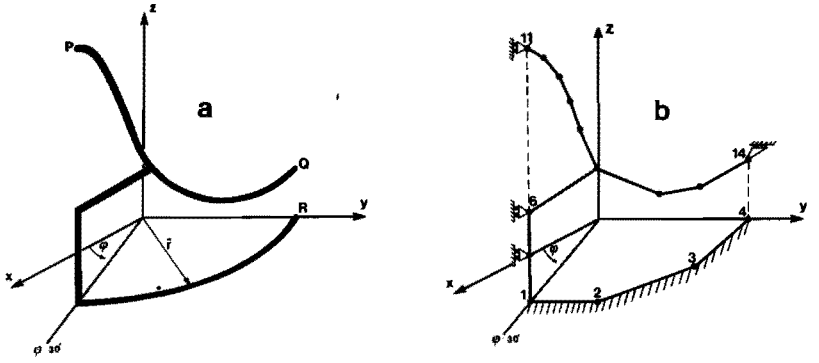

Fig. 3.1.a. The geometry of 1/6th part of the frame.

3.1.b. The mesh of the numerical model of the frame. The nodes 1, 2, 3 and 4 are fixed rigidly; for the nodes 5, 6, 11 and 14 the symmetry conditions hold.

the polypropene is described in section 2.4. In this description, use was made of the continuous relaxation spectrum (2.6) determined by the parameters K, θ_1, θ_2 and S_0. For the numerical model study, this continuous spectrum had to be transformed into a generalized Maxwell model with n branches (2n + 1 parameters) (see: figure 3.2) as required for the input deck of the MARC program package (MARC, 1983).

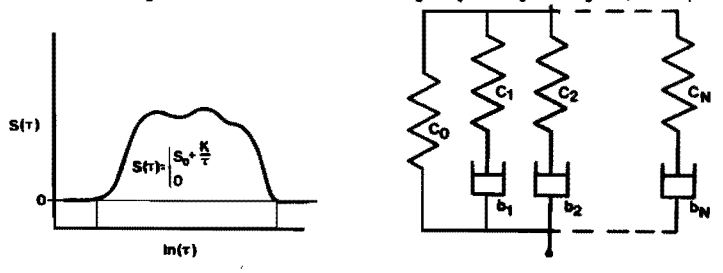

Fig. 3.2. Transformation of the continuous relaxationspectrum into a generalized Maxwell model.

This transformation is outlined in appendix II and the results of this transformation are given in table II.1 of the same appendix. The frame was fixed rigidly at the base (z=0) and symmetry conditions hold at the planes $\varphi = 30^{o}$ and $\varphi = 90^{o}$.

The numerical model of the frame was loaded with a radial frame top displacement (node 11), built up incrementally. First the frame top was loaded with a constant velocity until a frame top displacement of 1.5 mm was realized. Then the frame was unloaded with the same velocity until the starting point was reached. The loading velocity was varied in the range of 0.05 - 10.0 mm/s. The value of 1.5 mm is based upon the values used by Wright et al. (1982). They used displacements of 0.5 - 2.5 mm in their static creep experiments on cloth-covered polypropene frames.

3.2.2. The entire valve

In the geometry of the 1/6 part of the valve, which is shown in figure 3.3, the surface BCDE represents the coaptation area and ABE represents the free leaflet area. The geometric data as obtained from table 2.2 were averaged over the 3 valve parts. These averaged values are given in figure 3.3a. The free leaflet surface ABE is further

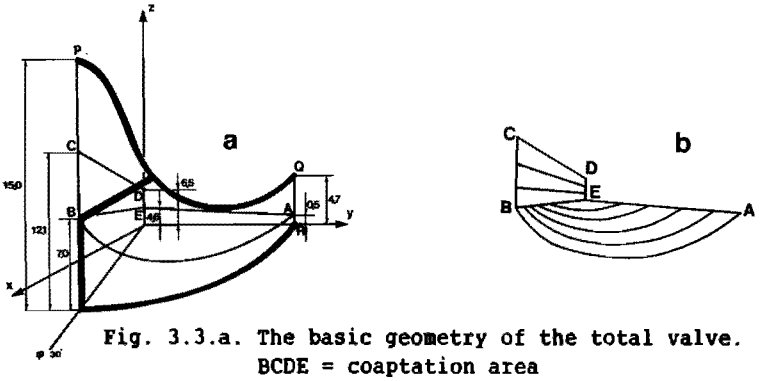

Fig. 3.3.a. The basic geometry of the total valve.
BCDE = coaptation area
ABE = free leaflet area
ABC = aortic ring
some z coordinates are given for the 23 mm valve

3.3.b. Geometry of the fibre reinforcements.

described by straight lines between AB and BE. For AB the intersection of a sphere, with its central point in the y-z plane, and the cylinder surrounding the frame, is taken. As outlined in section 2.2 the leaflets of the Hancock valve are reinforced with

collagen bundles (see figure 2.1). Figure 3.3b shows how this fibre reinforcement is modelled in the numerical model. Finally, a constant leaflet thickness amounting to 0.4 mm is assumed (Rousseau et al., 1981), the fibre diameter is 0.4 mm, the diameter of the aortic ring amounts to 0.8 mm and the sinus wall tissue has a thickness of 1.6 mm (see table 3.1).

To incorporate the viscoelastic material properties of the leaflet tissue the continuous relaxation spectrum of the glutaraldehyde treated tissue has been transformed into a generalized Maxwell model (see section 3.2.1). This transformation is outlined in appendix II and the resulting material parameters are also given there. In the numerical model, it was furthermore assumed that the time-dependent material behaviour of the membranes and the fibres was the same. This means that the transformed parameters C_i (i = 1,N) and τ_i (i = 1,N) (see figure 3.2) are the same for the membranes and the fibres. Finally, for the glutaraldehyde treated tissue a Poisson ratio of $\nu \approx 0.5$ was chosen as this is the value of the most biological tissues. The sinus wall tissue was assumed to be purely elastic. The Young's modulus of this tissue was estimated from some tensile experiments analogously to those described in section 2.3, its value being about 5 N/mm^2. Not much was known about the material properties of the aortic ring. Sauren et al. (1983) stated that the aortic ring is much stiffer than the other valve parts. Therefore we assumed the aortic ring to have a Young's modulus of 1000 N/mm^2. For Dacron some data are known. When the Dacron is in the form of patch material, it has a Young's modulus of about 30 N/mm^2 (Gilding et al., 1984); when it is in the form of fibres, the Young's modulus ranges between 4000 and 7500 N/mm^2 (Roff et al., 1971). For the Young's modulus of the Dacron used in the valve prosthesis the arbitrary value of 1000 N/mm^2 was chosen.

The 1/6 part of the valve was modelled with 75 nodes and 136 elements; the mesh is shown in figure 3.4. The used elements are described in table 3.1. In this table the element numbers, element types, geometric data and material parameters are given.

The valve was fixed rigidly at the base while symmetry conditions were applied at the planes $\varphi = 30^o$ and $\varphi = 90^o$ (see figure 3.3).

element number	element type	modelled valve part	geometry	material description	material parameters
1-14	cylindr. beam	polypropene frame	diameter 1-1.5 mm	viscoelastic with a continuous relaxation spectrum $S(\tau)$ $S(\tau)= S_0+K/\tau \quad \theta_1<\tau<\theta_2$; $0 \quad \tau<\theta_1 \quad \tau>\theta_2$	$S_0 = 0.926\ 10^{-5}$ (s^{-1}) $K=0.1051$ (-) $\theta_1 = 3.4$ (s) $\theta_2 = 63270$ (s) $M = 1582$ (N/mm^2) $\nu = 0.4$ (-)
15-26	membrane	leaflet suspension	thickness = 0.4 mm	linear elastic	$M = 5.0$ (N/mm^2) $\nu = 0.5$ (-)
27-46	membrane	free leaflet area	thickness = 0.4 mm	viscoelastic : $S(\tau)= K/\tau \quad \theta_1<\tau<\theta_2$; $0 \quad \tau<\theta_1 \quad \tau>\theta_2$	$K = 0.05$ (-) $\theta_1 = 0.0019$ (s) $\theta_2 = 23.0$ (s) $M = 1.8$ (N/mm^2) $\nu = 0.5$ (-)
47-73	membrane	coaptation area			
74-125	truss	fibre reinforcement	diameter = 0.4 mm		$K = 0.05$ (-) $\theta_1 = 0.0019$ (s) $\theta_2 = 23.0$ (s) $M = 23.0$ (N/mm^2) $\nu = 0.5$ (-)
126-132	truss	aortic ring	diameter = 0.8 mm	linear elastic	$M = 1000$ (N/mm^2) $\nu = 0.5$ (-)
133-136	truss	Dacron	diameter = 0.4 mm	linear elastic	$M = 1000$ (N/mm^2) $\nu = 0.4$ (-)

Table 3.1. Description of the elements,geometric and material properties.

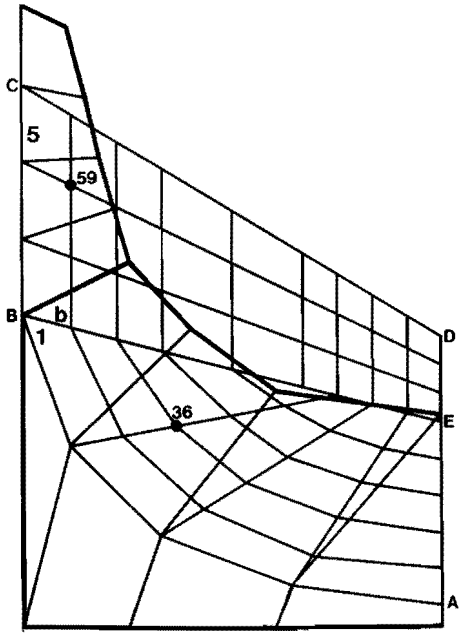

Fig. 3.4. The total mesh of the leaflet valve prosthesis.

During calculation the valve was loaded incrementally with a time varying uniform pressure load over the free leaflet area. The model was then first prestrained by loading the initial mesh with a very small pressure load. This was done for the first increments (Δp_0, Δp_0, 10 Δp_0 and 50 Δp_0, $\Delta p_0 = 7.5\ 10^{-4}$ kPa for increment 0, 1, 2 and 3 respectively). From increment 4, the valve was loaded according to the following patterns:

i) a load increasing linear with time until a pressure difference of 12 kPa was obtained, followed by a decreasing load with the same velocity, until the starting point was reached (figure 3.5a). The total loading- and unloading time was varied (0.02 ÷ 3600 s). This loading will be denoted by quasi-static loading.

ii) a physiological loading (figure 3.5b), which resembles the in-vitro measured pressure difference across the valve during a simulated cardiac cycle.

These load patterns were chosen to investigate the influence of the different viscoelastic properties, especially the different relaxation times of frame and leaflets.

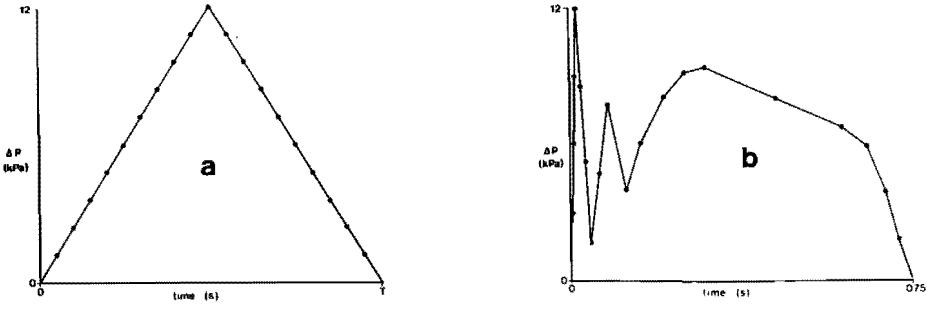

Fig. 3.5. Loading patterns for the numerical model:
a. linear with time, loading and unloading.
b. physiological loading

With regard to the design study described in the next chapter the following stress quantities were determined:

i) The stress distribution in the leaflet, illustrated by the von Mises intensity $\bar{S}$ for the membranes, defined as:

$$\bar{S} = \sqrt{\frac{3}{2} S_{ij} S_{ij}} \qquad (3.1)$$

where S_{ij} are the components of the deviatoric stress tensor

ii) The tensile stresses in the fibres.

iii) The minimum principal stress in the membranes between the fibres. The membrane element of the MARC program package has the same constitutive behaviour for positive as for negative strain. When the strain has a negative value, for example in the coaptation area, actually the membrane has to collapse. When observing the minimum principal stresses, an indication of the magnitude of wrinkling is obtained.

iv) Fibre tearing from the membranes may be introduced by "shear forces" between fibre and membrane. An approximation of this shear force may be obtained from the numerical model by splitting up the nodal force into the separate contributions of membranes (F_m) and fibres (F_f). The difference between the two fibre-directed components of those nodal forces (F_{mf} and F_{ff} respectively) is a measure for the shear force between fibre and membrane. The shear force is divided by the circumferential length of the fibre to find a physical measure. The shear force per unit length is defined as $|F_{ff} - F_{mf}|/\pi d$, with d is the fibre diameter.

Furthermore, for experimental verification the following displacements in the valve were calculated:

v) The radial commissure displacement as a function of time and of pressure load.

vi) The axial displacement of the valve center both as a function of time and of pressure load.

3.2.3. An a-symmetrical model

To analyse numerically the influence of the a-symmetry of the valve upon the displacements of leaflet center and commissures, a numerical model of the total valve was designed the geometry of which was described using the geometric parameters as outlined in section 2.2 (table 2.2). Due to the too large amount of computation time we simplified the total valve model by assuming linear elastic material behaviour of the different valve parts and by assuming a linear relationship between strain and elongation.

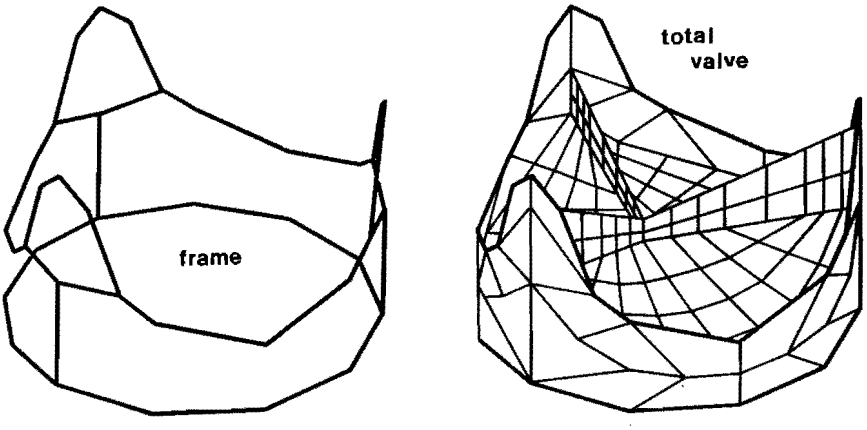

Fig. 3.6. The mesh of the total a-symmetrical model.

For comparison, also the commissure displacements of 1/6th part of the symmetric valve model was calculated under the same assumptions. The mesh of the total model is given in figure 3.6. The valve was loaded with a pressure load of 12 kPa across the free leaflet areas. Next, the commissure and leaflet center displacements of the a-symmetrical and symmetrical valve model were compared. To that end the initial slope of the curves representing the commissure displacement versus pressure load as well as the leaflet center displacement versus pressure load were determined.

3.3. Experimental verification

3.3.1. The frame

To verify the numerical prediction of the frame behaviour, the frame was loaded using a Zwick (1434) testing equipment.

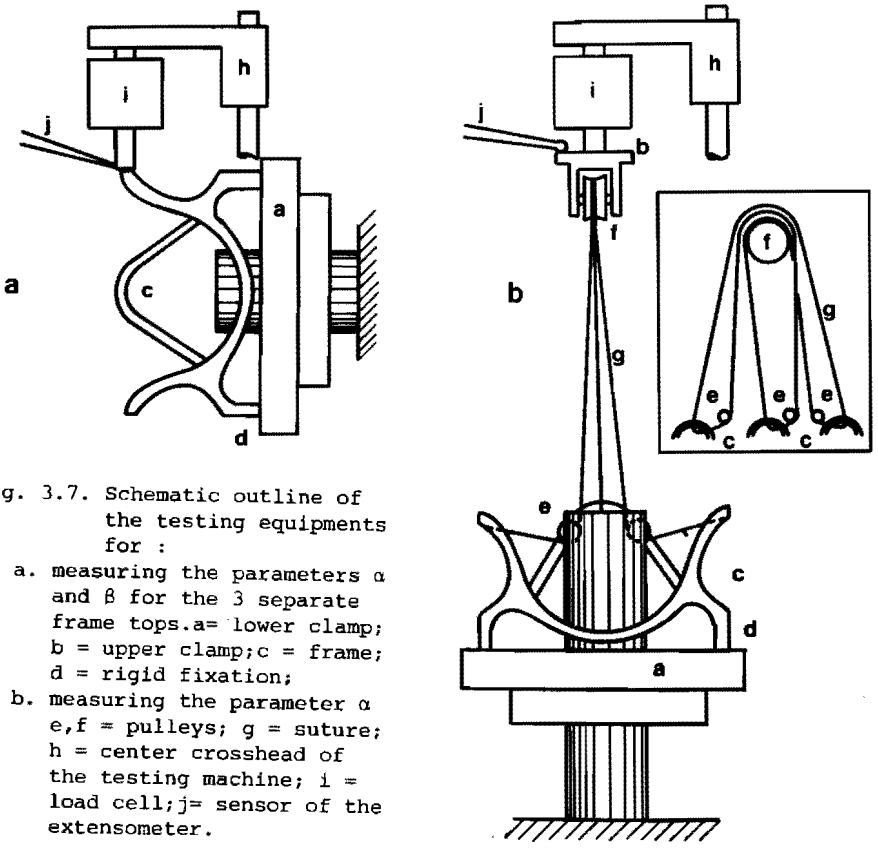

Fig. 3.7. Schematic outline of the testing equipments for :
a. measuring the parameters α and β for the 3 separate frame tops.a= lower clamp; b = upper clamp;c = frame; d = rigid fixation;
b. measuring the parameter α e,f = pulleys; g = suture; h = center crosshead of the testing machine; i = load cell;j= sensor of the extensometer.

A schematic outline of the experimental set-up is shown in figure 3.7. First the frame tops were loaded separately (see fig. 3.7.a) by moving the upper clamp of the testing equipment. Force was recorded by a load cell (Hottinger, U1), while the displacement was recorded by an extensometer (Zwick, 1400). The analog signals (force and displacement) were recorded on magnetic tape with an instrumentation recorder (HP3968A) whereafter the signals were plotted on a XY-recorder (Yokogawa, 3078). During each experiment five loading- and unloading cycles were performed with a constant loading velocity between two boundary values for the force on the frame top. As in all cases the fourth and fifth cycle were not significantly different from each other, the fifth cycle was considered as the measuring cycle.

From the resulting force-displacement curves of each top the mean slope of the ascending line (α) and the amount of hysteresis (β) were determined. The latter quantity was thereby defined as the quotient of the area enclosed by the ascending and descending line and the area enclosed by the ascending line, the horizontal axis and the vertical line Δl_{max} (see figure 3.12). The standard deviations of α and β were determined by performing five times the complete measuring procedure and data processing. Varied parameters were the frame size (21, 23, 25 and 27 mm diameter) and load velocity (range: 0.1 ÷ 1.0 mm/sec).

Finally, to check the assumptions for the numerical model with regard to the symmetry of the frame, all frame tops were also loaded simultaneously (see fig. 3.7b). To that end a long Mersilene suture was put between the 3 frame tops and the 4 pulleys in the experimental set-up. The extensometer then registered the sum of the suture elongation and the radial force-displacement relation for the frame tops. The same experiment was performed twice: one time the total strain was measured and one time only the suture elongation was measured by fixing the frame top displacements with a rigid metal ring put over the frame tops. Next, both force-displacement curves were subtracted. With this set-up the mean frame stiffnesses were determined for various valve sizes and load velocities, and the values were compared with those for each top separately. Furthermore, with this set-up the influence of the Dacron cloth around the frame was

investigated through a comparison of the mean slope α for the clothed and the non-clothed frame.

3.3.2. The entire valve

For experimental verification of the numerical model of the entire valve prosthesis, a Hancock prosthesis (242 Aortic) was mounted in a rigid valve housing such that the base of the valve was fixed. This was realized by fixing the valve using the sewing ring and using a well fitting valve housing. First, the valve was loaded in a quasi-static way. To that end a hydrostatic pressure was applied to the closed valve prosthesis by means of a fluid column, the height of which was controlled using a gear-wheel pump (Verder 114-1), see figure 3.8. The pressure load was first increased up to a level of 20 kPa immediately followed by a decrease to 1.4 kPa. To determine the influence of the loading velocity the valve was loaded within 150 s as well as within 1800 s with a constant velocity.

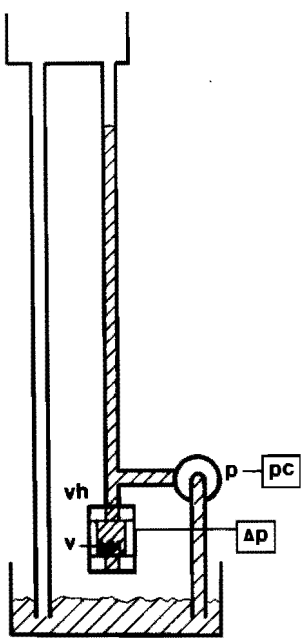

Fig. 3.8. Schematic outline of the quasi-static loading system. p = pump; p.c. = pump control: vh = valve housing; v = valve; Δp = recording of the pressure load.

Next, the valve was subjected to a physiological loading in a mock circulation device developed by Leliveld (1974). This mock circulation device which has been described earlier by van Steenhoven et al. (1982a) mainly consists of a left ventricle, aorta and load

impedance (see figure 3.9). The left ventricle is simulated by a moving piston system in which the movements of the piston are controlled by a regulated air pressure. At the inflow side a sturdy silastic leaflet valve is mounted simulating the mitral valve. The inflow side of the pump is connected to a reservoir with overflow, simulating the left atrium. This reservoir provides a constant supply pressure during the pump relaxation phase. Between the ventricle and aorta different valve prostheses can be mounted within a perspex housing. A bottle compliance is connected at the beginning of the latex tube, to compensate for the rigidity of the valve house and the flow meter. However, due to the large valve housing necessary for these measurements, high pressure peaks just after valve closure are inevitable. The load impedance at the end of the aorta is designed as indicated by Westerhof et al. (1971). It consists of two fluid resistances, coupled by a bottle compliance. The fluid resistances are composed of a large number of parallel capillaries with an internal diameter of 0.6 mm. The values of the components of the load impedance are chosen in accordance with Westerhof's data for men. The fluid used is a physiological saline solution.

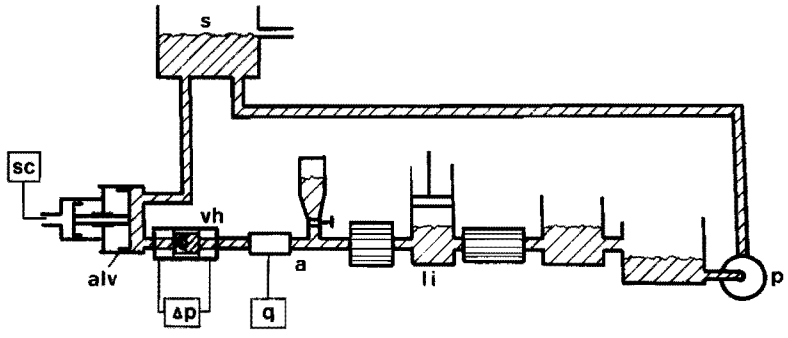

Fig. 3.9. Schematic drawing of the mock circulation system. sc: servo control; s: supply; alv: artificial left ventricle: vh: valve housing; a: aorta; li: load impedance; p: pump; Δp,q: recordings of pressure difference and flow.

Pressures at the left ventricular (P_{lv}) and aortic sides (P_{ao}) of the valve were measured in both types of loading with Statham P23dB pressure transducers (100 Hz, -3dB). The pressure difference across the valve (ΔP) was obtained by subtracting the two pressures electronically (Tektronic AM 502). In the mock circulation system the aortic

flow was also measured at the outflow of the valve housing by an extracorporeal electromagnetic flow probe (Transflow 601, 100 Hz, -3 db). The commissure displacement for each frame top was measured using an inductive measuring device as developed by Arts and Reneman (1980) and modified by van Renterghem (1983). It (100 Hz, -3 dB) consists essentially of 2 small electrical coils (fig. 3.10). One coil was sutured at the commissure whereas the other coil was glued to the nearest opposite wall of the valve housing. The time varying current (100 kHz) through the coil on the valve housing induced a voltage in the coil on the commissure. From the induced voltage, the distance between the 2 coils was derived:

$$\Delta r = (r - r_0) = r_0\{\exp(\frac{V}{C}) - 1\}$$

with: r_0 = distance between the 2 coils in unloaded condition (mm)
r = actual distance between the 2 coils (mm)
V = the induced voltage (V)
C = a constant factor with a value of 2.05 (1/V).

Finally, the leaflet center displacement was measured cinematographically in the quasi-static situation and assested by integrating the leaflet center velocity in the physiological loading case. In the case of the quasi-static loading use was made of a video camera and recorder which registered the vertical movement of the leaflet center. In the case of the physiological loading use was made of an adjusted ultrasonic Doppler device (Alvar 50 Hz -3dB). The position of the probe was such, that only the axial component of the leaflet velocity was measured in the plane of the pipe (see figure 3.11). Using the range gate the measuring volume ($\approx$ 0.8 mm^3) was focussed upon the underside of the coaptation area in unloaded situation. Care was taken that the measuring volume was in the leaflet during the whole period that the valve was closed. As no reflecting particles were added to the fluid only the leaflet velocity was measured.

The analog signals (pressures, pressure difference, flow, frame top displacement, leaflet center velocity and a triggering signal) were recorded on magnetic tape using an instrumentation recorder (HP 3968A). The signals of pressure difference, frame top displacement, aortic flow and leaflet center velocity were digitized

with a sampling frequency of 500 Hz. Before digitizing, the signals passed through a low pass filter (Krohn-hite 3750; 100 Hz, -3dB) to prevent aliasing. The digital data were then fed into a Prime (750) minicomputer. The digitized signals were all averaged over 10 periodic cycles. Next, the velocity of the leaflet center was integrated numerically from the moment of valve closure and shifted over about 8 msec to compensate for the electronical delay in the velocity meter system. Finally, the commissure displacement and leaflet center displacement were given as a function of the pressure difference across the valve.

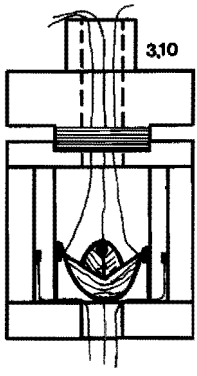

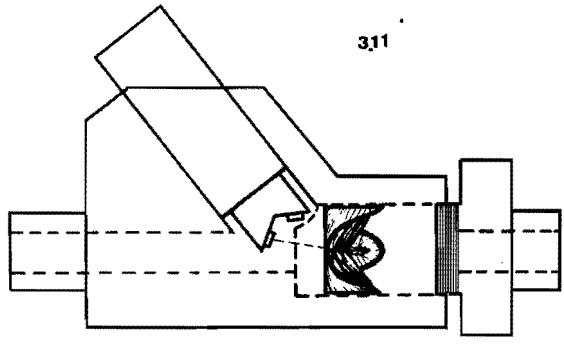

Fig. 3.10. Measurement of the commissure displacements by using 6 electrical coils.

Fig. 3.11. Measurement of the displacement of the leaflet center by using an Alvar ultrasonic measuring device. The double channel probe is positioned so that only the axial velocity is measured in the plane of the pipe.

3.4. Results

3.4.1. The frame top displacements

Figure 3.12 shows a typical result of the force-displacement relation for one top of the frame as obtained numerically and experimentally. The accordance of the ascending line and the amount of hysteresis is fair. The results of all experiments and numerical calculations are summarized in tables 3.2 and 3.3.

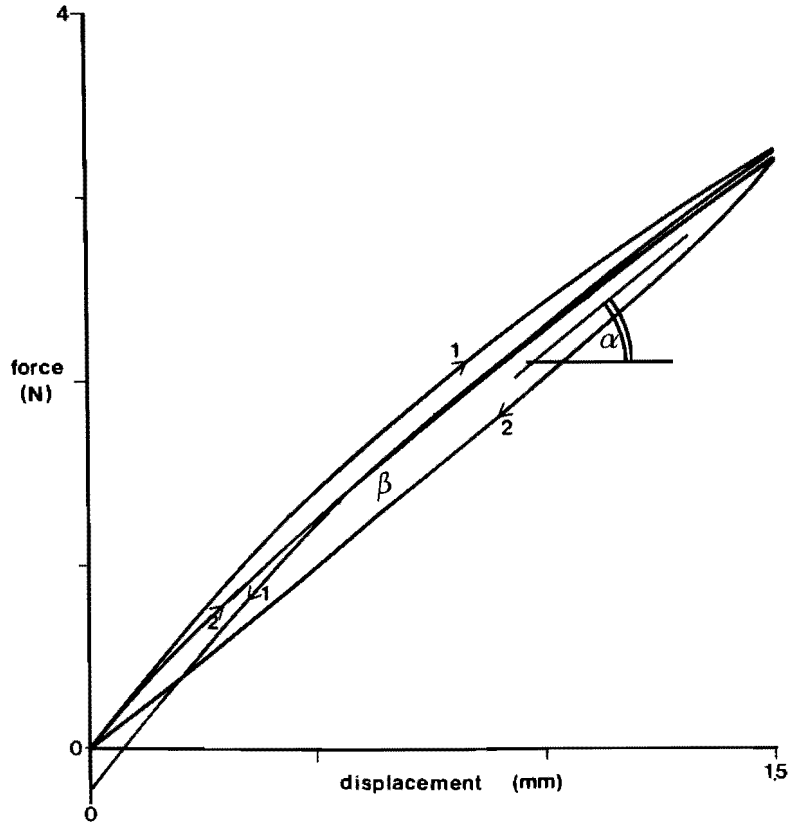

Fig. 3.12.

Typical numerical (1) and experimental (2) force-displacement relation for a 23 mm valve frame with a loading velocity of 0.1 mm/s.

Comparing the numerical and experimental results it is concluded that:

i) for both cases, α and β are in fair agreement;

ii) the slight increase of α at increasing loading velocity and increasing frame size is found numerically as well as experimentally;

Frame size (mm)	21					23					25					27				
Loading-velocity (mm/s)	exp*			exp**	num	exp*			exp**	num	exp*			exp**	num	exp*			exp**	num
	A	B	C			A	B	C			A	B	C			A	B	C		
0.1	1.8	1.6	1.7	2.7	-	1.9	2.1	1.8	2.7	2.7	2.4	2.4	2.5	2.6	2.8	2.4	2.3	2.4	2.8	2.9
0.5	2.0	1.7	1.8	-	-	1.9	2.3	1.9	-	2.8	2.5	2.5	2.6	-	-	2.5	2.4	2.5	-	-
1.0	2.0	1.9	1.9	-	-	2.0	2.3	2.0	-	2.8	2.5	2.5	2.6	-	-	2.5	2.4	2.5	-	-

Table 3.3. The mean slope of the ascending line of the force-displacement relation (α,N/mm).The data under exp* are the slopes of the separate frame tops, while those under exp** are the mean slopes obtained with the second set-up.The frame tops are denoted with A,B and C,corresponding with the cross-sectional angle of 105,120 and 135 deg.respectively. (standard deviation amounts to 0.2 N/mm)

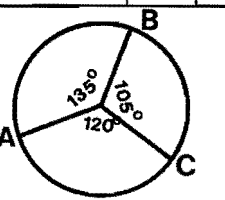

Frame size (mm)	21				23				25				27			
Loading - velocity (mm/s)	exp			num	exp			num	exp			num	exp			num
	A	B	C		A	B	C		A	B	C		A	B	C	
0.1	12.0	12.5	11.5	-	12.1	11.7	12.2	9.5	10.8	10.3	10.8	9.5	10.7	10.7	10.3	9.5
0.5	10.1	11.1	10.3	-	11.3	10.3	11.1	6.9	9.9	9.4	9.9	-	9.9	9.3	9.7	-
1.0	10.4	11.1	10.4	-	10.8	10.3	10.9	4.8	10.0	9.9	9.7	-	10.3	9.7	9.8	-

Table 3.3. The amount of hysteresis (%) as obtained experimentally (exp) and numerically (num). The frametops (A,B,C) are denoted as outlined in table 3.2.(stand.dev.= 1%)

iii) the amount of hysteresis found experimentally is slightly dependent of the frame size and loading velocity. However, numerically β is independent on frame size but decreases strongly for increasing loading velocity;

iv) for the greater valves (25 and 27 mm) the slope α of the separate tops hardly deviate from the data from all tops averaged. However for the 21 and 23 mm valve there is a remarkable difference.

From multiple regression analysis of the data of tables 3.2 and 3.3 it was concluded that the parameters α and β are not statistically significant dependent on frame top number, frame size or loading velocity. Finally, the influence of Dacron cloth around the frame is summarized in table 3.4. From this it is concluded that for all frame sizes the clothed frame is stiffer than the non-clothed frame, although the stiffness of the clothed frames show a large spreading. This is possibly caused by the method of fixation of the cloth to the frame.

frame size [mm]	clothed	non-clothed
21	3.1	2.7
23	6.6	2.7
25	3.1	2.6
27	4.5	2.8

Table 3.4. Frame stiffness α [N/mm] for the clothed and the non-clothed frames. (loadvelocity: 0.1 mm/s). The standard deviation for α is 0.2 N/mm.

3.4.2. The commissure displacements

For the case of quasi-static loading, the predicted commissure displacement of the entire valve model is given as a function of pressure load in figure 3.13b. For the case of physiological loading the displacements are given both as a function of time and of pressure load in figure 3.14b, c. Comparing these figures, it is

observed that the commissure displacement as a function of pressure load is nearly linear. The slope is equal to 0.0233 and 0.0225 mm/kPa respectively.

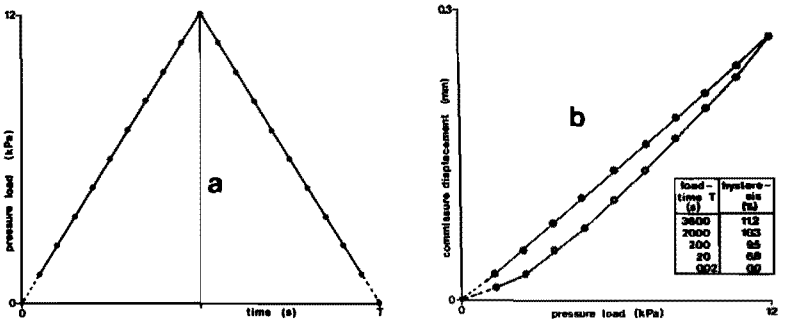

Fig. 3.13. Numerical results corresponding to a loading pattern as a linear function of time:
a. pressure load as a function of time.
b. commissure displacement as a function of pressure load. (T=3600 s)

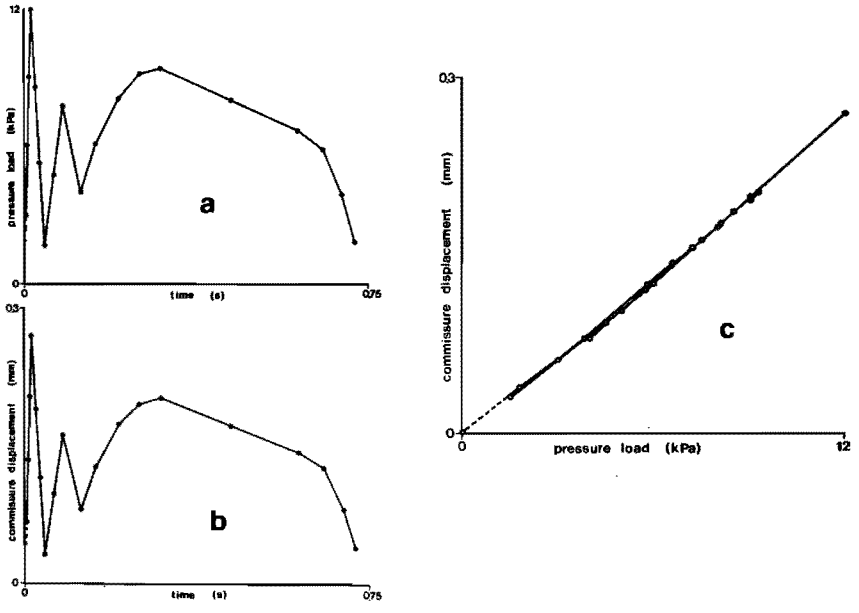

Fig. 3.14. Numerical results corresponding to a physiological loading pattern:
a. physiological loading pattern.
b. calculated commissure displacement as a function of time.
c. commissure displacement - pressure load relation.

So, for the range of load velocities studied here, with the numerical model no viscoelastic phenomena were found for the commissure displacement as expected from the viscous properties of the frame (see section 2.4). However, when the load velocity decreases, the amount of hysteresis increases (see table in figure 3.13).

A characteristic experimental result for a quasi-static loading pattern (loading- and unloading time is about 3600 s) is shown in figure 3.15. Here, the measured relation between commissure displacement and pressure load is given. From this a remarkable amount of hysteresis is noticed. The amount of hysteresis, averaged over the three frame tops, is 13% and 25% respectively for a high loading velocity (rise time is about 150 s) and a low loading velocity (rise time is about 1800 s), which is considerably higher than numerically predicted (9.5 and 11.2%, respectively).

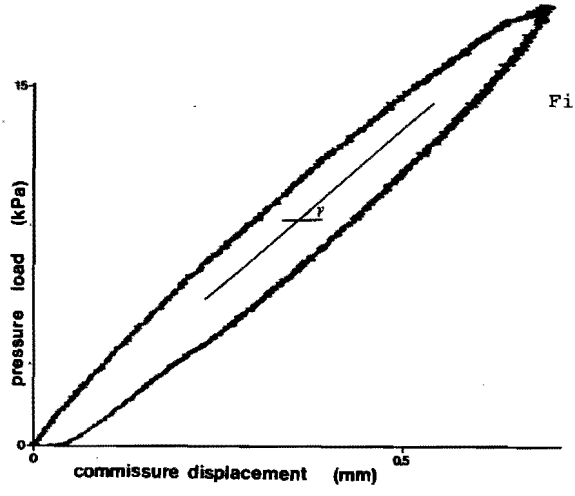

Fig. 3.15. A characteristic result of the quasi-static experiment. (top 3,23-1 mm valve, rise time : 1800 s.). A mean slope γ is defined in the pressure - displacement relation.

A characteristic result of the experimentally determined commissure displacement during a physiological loading pattern is given in figure 3.16.

It shows

- the pressure difference, averaged over 10 cycles, as a function of time during one cycle (fig. 3.16.a)
- the displacements for the 3 commissures, also averaged over 10 cycles, as a function of time (fig. 3.16b).

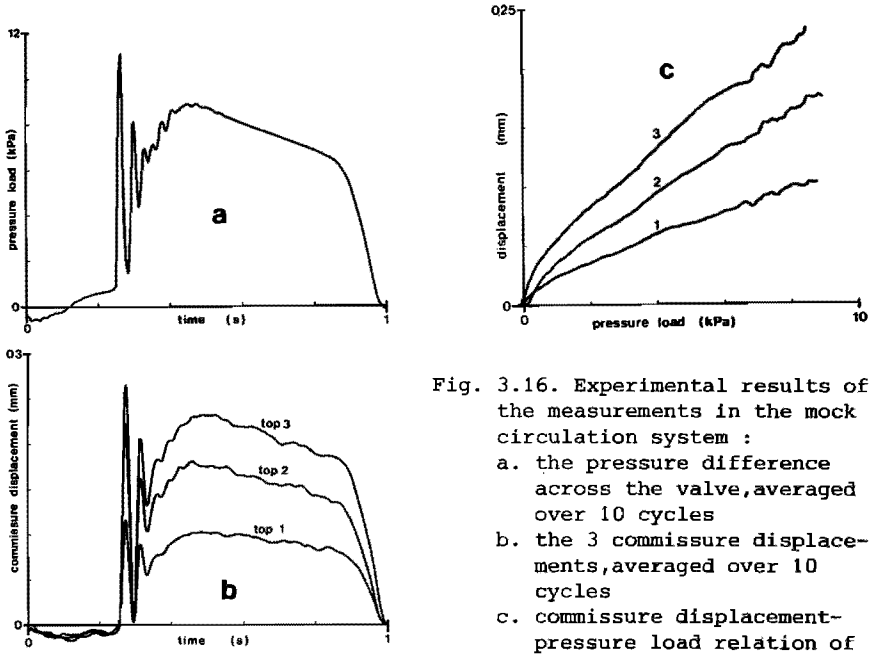

Fig. 3.16. Experimental results of the measurements in the mock circulation system :
a. the pressure difference across the valve, averaged over 10 cycles
b. the 3 commissure displacements, averaged over 10 cycles
c. commissure displacement-pressure load relation of the quasi-static part of the load cycle.

Next, from the signal two parts were analysed separately: the first part (fast fluctuations just after valve closure; time ≈ 0.2 ÷ 0.4 s) and the second part (valve behaviour during the remaining part of diastole; time ≈ 0.4 ÷ 0.9 s). For the second part, the relation between commissure displacement and pressure difference is given in figure 3.16c. From this figure, it is observed that during a cardiac cycle the relation between commissure displacement and pressure load is nearly linear for the second part of the loading cycle. For the first part also a nearly linear relationship was found. For both parts, the slope was determined by a linear regression analysis, the results of which are shown in table 3.5; they do not differ significantly. From the experiments it is furthermore concluded that there is a considerable difference between the 3 commissures and that no hysteresis can be observed.

C values in [mm/kPa] 23-1 mm valve	frame top number 1	2	3
C_1	0.0140	0.0200	0.0310
	(0.0005)	(0.0008)	(0.0014)
C_2	0.0131	0.0205	0.0304
	(0.0005)	(0.0006)	(0.0010)
C	0.0148	0.0231	0.0372
	(0.0010)	(0.0030)	(0.0035)
sym. model non-linear	0.0225		
sym. model linear	0.0183		
a-sym. model linear	0.0133	0.0192	0.0208

Table 3.5. Values for the slope of the relation between commissure displacement and pressure load, determined with the mock circulation system and with the quasi-static set-up, compared with the values found with the a-symmetrical numerical model and the symmetrical model (linear and non-linear). The standard deviations are given between parentheses.

Table 3.6 shows the slope of the displacement-pressure curves during the second part of the loading cycle for all measured valves. It is seen that the a-symmetry of the frame top displacement is present in all valves. For smaller valves, the slope C decreases. Finally, the mean slope of the displacement-pressure curve of the 23-1 mm valve under quasi-static loading conditions is also inserted in table 3.5. They are slightly higher than those determined under a physiological loading pattern.

To compare the experimental and numerical results into more detail, the a-symmetrical model as explained in section 3.2.3 is used.

C quasi-statical [mm/kPa]	frametopnumber		
valve	1	2	3
23-1	0.0131 (0.0005)	0.0205 (0.0006)	0.0304 (0.0010)
23-2	0.0224 (0.0005)	0.0107 (0.0003)	0.0164 (0.0010)
21	0.0058 (0.0003)	0.0062 (0.0002)	0.0047 (0.0003)
19	0.0062 (0.0002)	0.0012 (0.0001)	0.0043 (0.0002)

Table 3.6. The quasi-static pressure-commissure displacement slopes for all measured valves. The standard deviations are given between parentheses.

This model prediction is also inserted in table 3.5. From this it is concluded that the a-symmetrical commissure displacements are in good agreement with the experimental results for frame tops 1 and 2 while for frame top 3 an underestimation of its displacement is found. There is also a fair agreement between the slope obtained for the symmetrical linear model and the averaged slope of the a-symmetrical linear model. Also the slope of the 3 experimental commissure displacement-pressure load curves of one valve were averaged. The values of the slope measured with the mock-circulation system have an average value of 0.0227 ($\pm$ 0.0040) mm/kPa. When comparing this value with the slope found numerically with the symmetrical non-linear model (0.0225 mm/kPa), the conclusion is justified that the agreement between theory and experiment is fair.

3.4.3. The leaflet center displacement

For the case of quasi-static loading the predicted and measured displacement of the leaflet center (23-1 mm valve) are given as a function of the pressure load in figure 3.17.

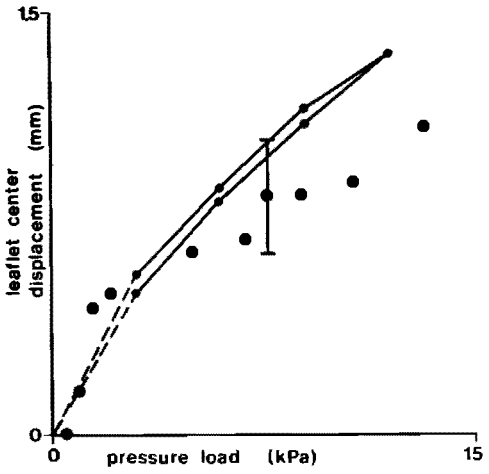

Fig. 3.17. Quasi-statical leaflet center displacement for the 23-1 mm valve.The solid line represents the numerical prediction. The measured displacements are indicated as dots.

In figure 3.18 the numerical predicted leaflet center displacement is given as a function of time and of pressure load for the physiological case (for the 23-2 mm valve). From these figures it is observed that the relation between the axial displacement of the leaflet center and the pressure load is non-linear, and shows a small amount of hysteresis.

In figure 3.19 a characteristic experimental result is given of the center displacement during a simulated cardiac cycle. In this figure the pressure load across the valve, the velocity of the leaflet center and the integrated velocity signal are shown as function of time during the fast fluctuations in the cardiac cycle. In figure 3.20 the leaflet center displacement of valve 23-2 is given as a function of the pressure load during the fast fluctuations just after valve closure. From this it is seen that also in the experiments the displacement-pressure relation is very non-linear. The hysteresis area has to be interpreted with caution as it is very sensitive to the adjusted time delay between pressure and velocity, see section (3.3.2). Finally, in table 3.7 the values of pressure and displacement after the fast fluctuations for the two measured valves are summarized together with the numerical predictions. From this table it can be seen that the numerical predictions are constantly about 40% higher than the measured leaflet displacements.

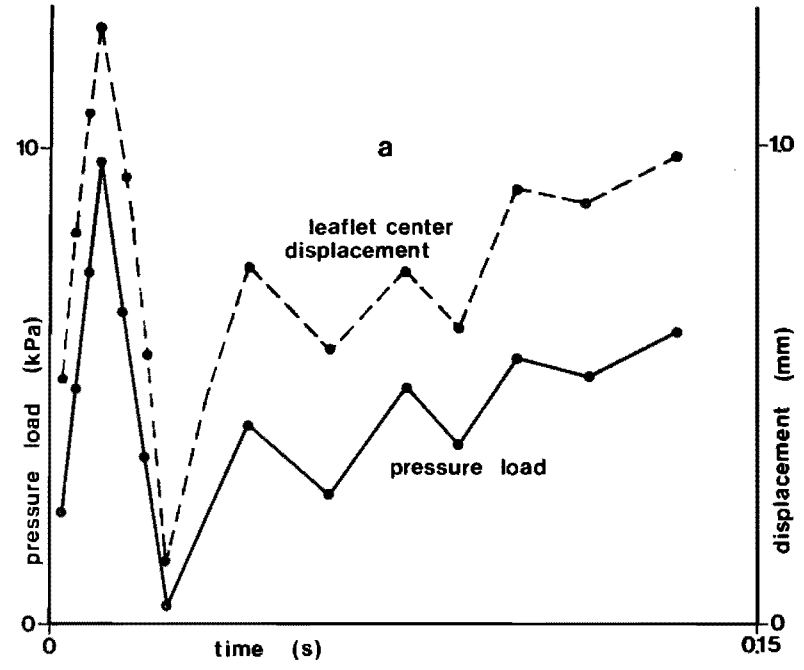

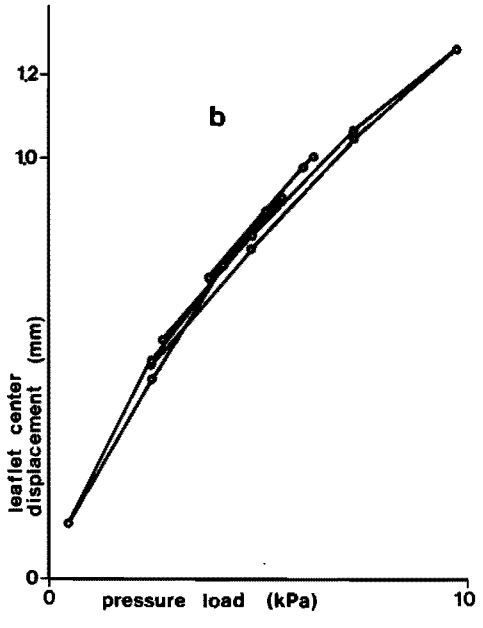

Fig. 3.18.
Numerical prediction of the leaflet center displacement during the fast fluctuations just after valve closure for the 23-2 mm valve.
a. pressure load and leaflet center displacement as a function of time.
b. displacement versus pressure load.

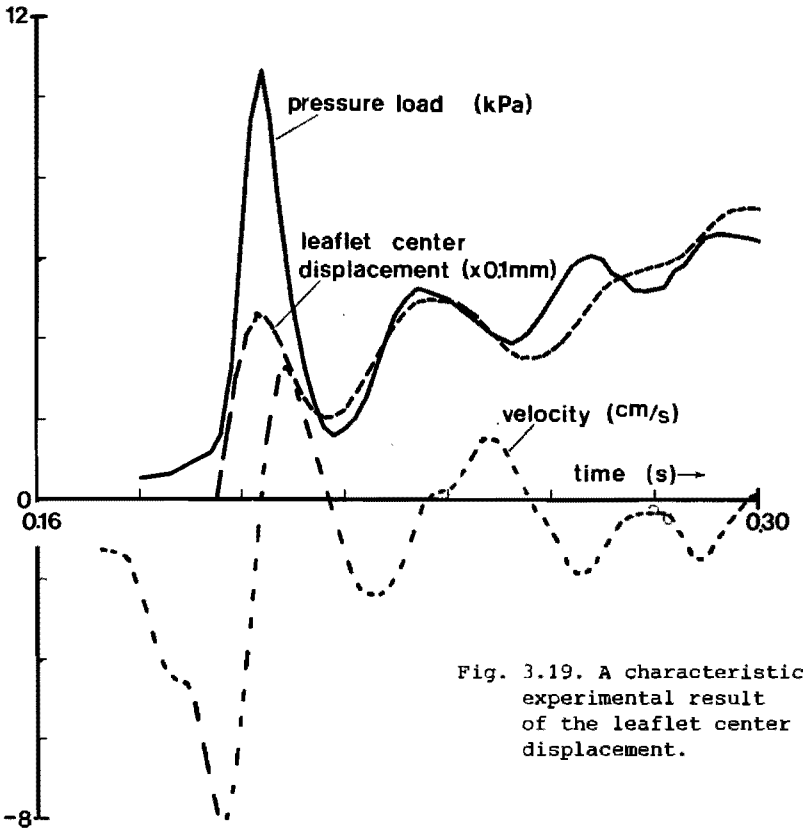

Fig. 3.19. A characteristic experimental result of the leaflet center displacement.

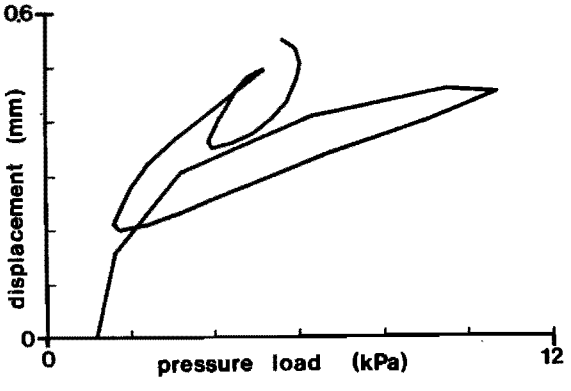

Fig. 3.20. The measured leaflet center displacement as a function of pressure.

valve	exp Δp (kPa)	exp Δu (mm)	num Δu (mm)
23-1	6.0	0.7	0.8
23-2	5.5	0.55	0.85
	3.7	0.3	0.55

Table 3.7.

Experimental and numerical results of the leaflet center displacement

3.4.4. The stress distribution within the leaflets

A contourplot of the von Mises intensity in the membranes of the valve loaded with 12 kPa is given in figure 3.21. From this figure it is seen that the von Mises intensity has a maximum in the vicinity of the commissure (point B) and amounts to about 0.20 N/mm^2.

In figure 3.22 a contourplot of the minimum principal stress is shown for the same loading situation as the one in figure 3.21. From figure 3.22 it is observed that at 12 kPa the minimum is mainly found in the coaptation area in the vicinity of the leaflet suspension (region between B and C).

The fibre stresses at a pressure load of 12 kPa are given in figure 3.23. From this figure it is seen that the maximum value of stress is found in fibre 5 and amounts to 0.64 N/mm^2 in the vicinity of the aortic ring. The fibre stress is nearly constant over the free leaflet area (minimum 0.3, maximum 0.5 N/mm^2) while in the coaptation area the stress varies from 0.64 to 0 N/mm^2. The shear force is approximated for the nodes 36 and 59 and amounts to 0.005 and 0.012 N/mm, respectively.

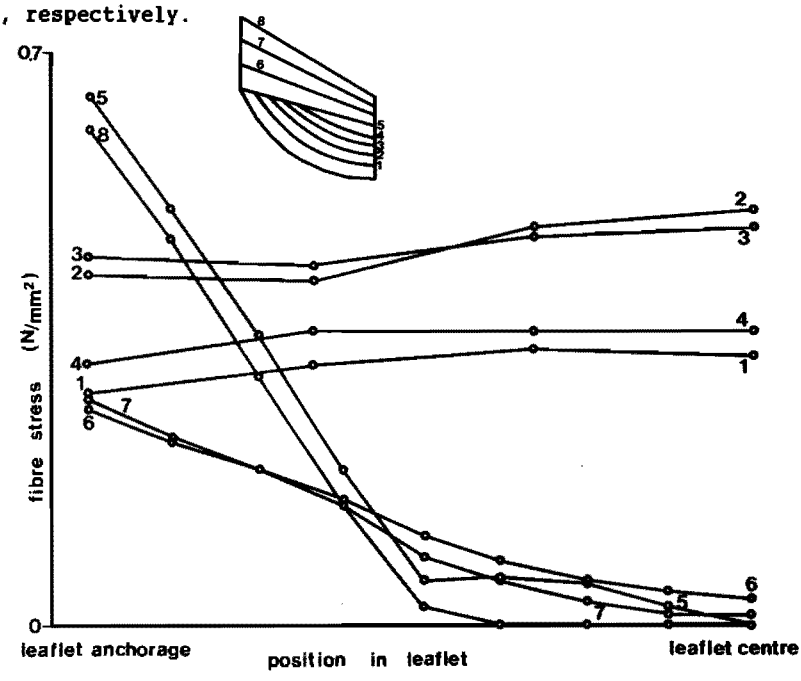

Fig. 3.23. Tensile stress in the fibres.

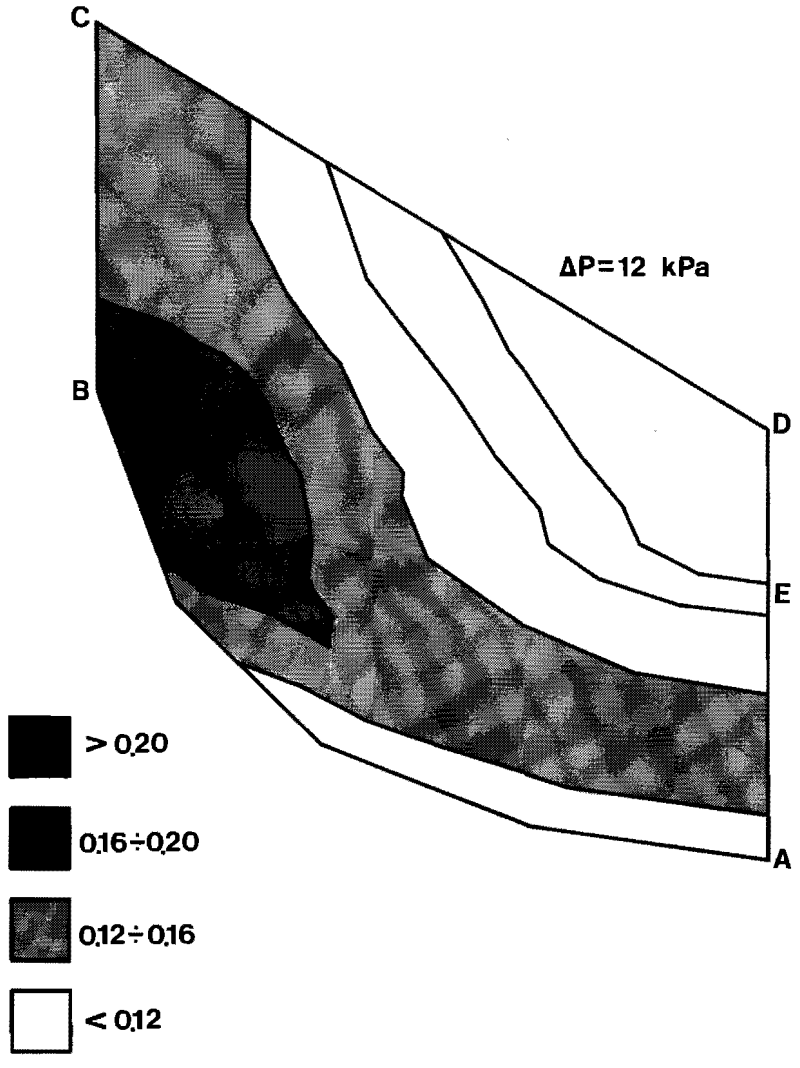

Fig. 3.21. Contourplot of the von Mises intensity in the membranes for a pressure load of 12 kPa.

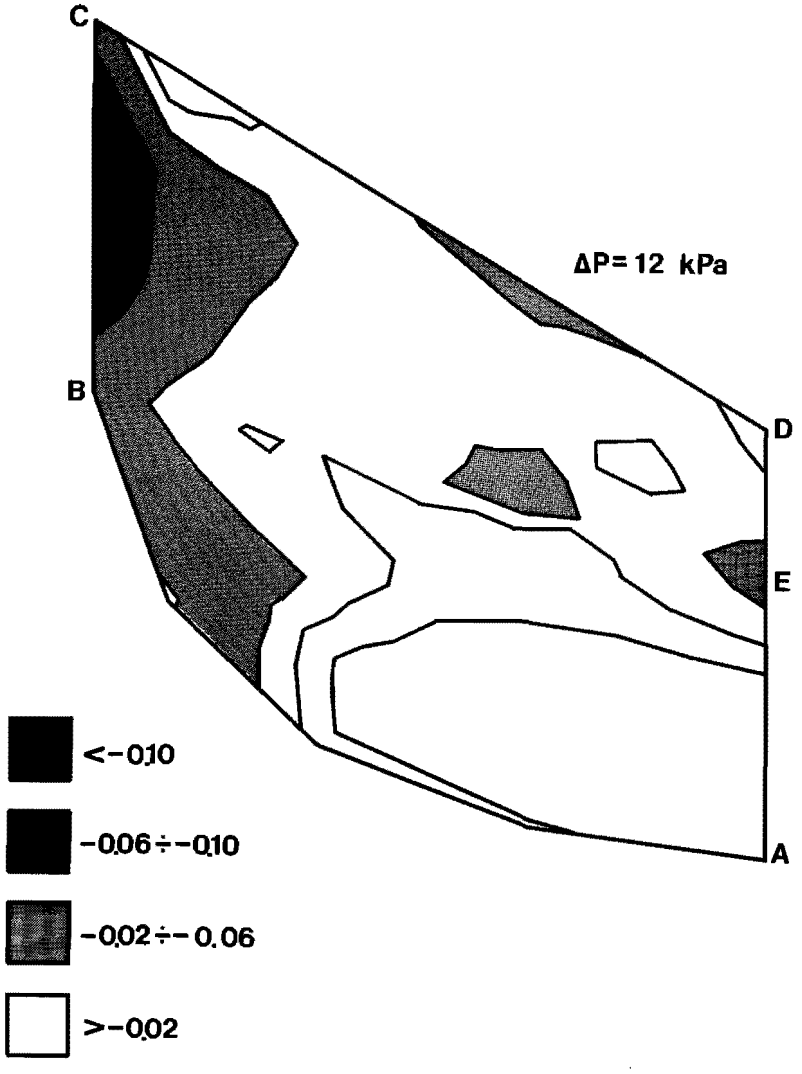

Fig. 3.22. Contourplot of the minimum principal stress in the membranes for the same load value of 12 kPa.

3.4.5. Model sensitivity

To get some insight into the sensitivity of the numerical results on the different geometry and material parameters some of these parameters were varied between some arbitrary boundary values. Table 3.8 shows the different situations analysed and summarizes the results for the calculated commissure displacement, leaflet center displacement, the von Mises intensity for point 1 in the membrane, the tensile stress in fibre b and the minimum principal stress in point 5 (see fig. 3.4). From this table it can be observed that the commissure displacement increases remarkably with decreasing frame stiffness and increasing z(C) and z(B), while the other parameters have only a slight influence. The leaflet center displacement is sensitive for allmost all parameters. The von Mises intensity in point 5 increases only when the fibres and membranes are very thin or when the membranes are stiffer, but is independent of the geometry parameters. Furthermore, the fibre stress in fibre B is dependent on d_f, d_m, E_m and z(c). Finally, the minimum principal stress is not very sensitive to the geometry and material parameters; only for the case d_m = 0.2 mm a large negative value is found.

3.5. Concluding discussion

3.5.1. The frame

From figure 3.12 and tables 3.2 and 3.3 it is observed that the numerical predictions of the frame top displacements are in agreement with the experimental results. Experimentally, the slope of the ascending line (α) and the amount of hysteresis (β) are not statistically significant dependent on frame top number, frame size or loading velocity. On the contrary, the numerically predicted value of α shows a slight increase with increasing frame size while β decreases with increasing loading velocity, which is probably due to a small mismatch of the viscoelastic material properties. Furthermore, the experimental results verify the model assumption that the influence of the a-symmetry of the frame on its force-displacement characteristic is negligible. Finally, it is found from the experiments that the clothed frames are stiffer than the non-clothed ones (table 3.4).

adjusted situation	boundary values	cd	lcd	vM1	fsb	mps5
basic model	E_{frame} = 1582 N/mm^2 d_f=d_m = 0.4 mm E_m = 1.8 N/mm^2 z_C = 12.1 mm z_D = 6.5 mm z_B = 7.0 mm z_E = 4.6 mm E_f = 23.0 N/mm^2	0.27	1.36	0.278	0.47	0.110
E_{frame}	1000 N/mm^2	0.39	1.48	0.287	0.48	0.110
	3600 N/mm^2	0.15	1.27	0.276	0.47	0.110
	100000 N/mm^2	0.06	1.16	0.272	0.45	0.106
d_f	0.1 mm	0.24	1.85	0.307	0.56	0.093
	0.7 mm	0.28	1.07	0.253	0.37	0.114
d_m	0.2 mm	0.30	1.61	0.502	0.76	0.173
	0.7 mm	0.27	1.16	0.195	0.33	0.078
E_m	1.15 N/mm^2	0.30	1.54	0.292	0.67	0.095
	3.5 N/mm^2	0.27	1.11	0.353	0.31	0.143
z_c	9.2 mm	0.16	1.67	0.318	0.60	0.105
	14.5 mm	0.38	1.17	0.285	0.40	0.111
z_D	5.0 mm	0.27	1.33	0.276	0.46	0.115
	7.9 mm	0.26	1.39	0.282	0.48	0.107
z_B	5.8 mm	0.22	1.49	0.277	0.46	0.116
	8.2 mm	0.32	1.25	0.246	0.52	0.098
z_E	6.0 mm	0.29	1.48	0.260	0.40	0.113
	3.1 mm	0.24	1.24	0.237	0.55	0.108

Table 3.8. Model sensitivities

cd = commissure displacement (mm)
lcd = leaflet center displacement (mm)
vM1 = von Mises intensity in point 1 (N/mm^2)
fsb = fibre stress in b (N/mm^2)
mps5 = negative values of min.princ.stress in 5 (N/mm^2)

(The different positions in the leaflet are illustrated in figure 3.4)

The flexibility of the frame as found in this study is in agreement with those in literature. Drury et al. (1981) performed flexibility measurements on injection moulded valve frames and found that for a polypropene frame the needed load for a 2 mm deflection amounted to 4.2 and 3.8 N for a low and high frame respectively. This is in agreement with our values of the frame stiffnesses. They also found that increasing frame size corresponds with increasing frame stiffness. Wright et al. (1982) investigated the stiffness of the polypropene frames of the Hancock valves numerically as well as experimentally. Numerically the frame was modelled with 778 4-node shell elements (896 nodes). The pressure load which normally acts on the valve was transferred to each frame top. Experimentally, they used a 3 lever system by which simultaneously a force was applied to each of the three frame tops. The radial force-displacement relations were measured, which resulted in a mean stiffness of about 2.45 N/mm. The force-displacement predictions of the numerical model agreed with the experimentally observed results with a variance of 12%. The value of 2.45 N/mm is close to our value. They further observed the frame stiffness to remain constant or to show a slight increase with increasing frame size which is in accordance with our results.

3.5.2. The commissure displacements

The commissure displacements in the entire valve are found to be linear dependent of the pressure load, both from the numerical predictions and from the experiments. The slope of the curves is hardly dependent on loading type and loading velocity (table 3.5). From the experiments a difference is found between the 3 commissure displacements, which is predicted numerically using a simplified a-symmetric total valve model. The agreement was fair for two frame tops. The observed discrepancy between the numerical prediction and the experimentally determined displacement of the third commissure is partly a consequence of the underestimation due to the linear theory, while also a change in the position of point B during valve loading may contribute to this (see tables 3.5 and 3.8). Furthermore, the experimentally determined commissure displacements show a clear dependency on frame size which is attributed to the smaller leaflet surface areas and lower commissure heights of the smaller valves. Finally, it is remarked that for the frame itself the frame top displacements are

independent on frame top while in the entire valve a remarkable difference is found. This difference in behaviour of frame and entire valve is caused by the different loadings. The frame tops were all loaded in the same way and with the same magnitude of the nodal force while the entire valve was loaded with a pressure load which leads to unequal loading of the 3 frame tops in magnitude (by the different leaflet surface areas) and in direction (by the different commissure heights).

The commissure displacements of 2 Hancock valves were also measured by Thomson and Barratt-Boyes (1977) whose results correlate quite well with our data. They found linear relationships between commissure displacement and pressure load, and they observed a remarkable difference between the displacements of the 3 frame tops of one valve (displacements ranged between 0.00 and 0.29 mm for the pressure load of 16 kPa).

3.5.3. The leaflet center displacement

For the leaflet center displacement a qualitative agreement between numerical prediction and experimental result is found. However, the numerical prediction is systematically 40% higher than experimentally found. This discrepancy is certainly related to the fact that the leaflet center displacement is dependent on nearly all geometry and material parameters of the valve as observed in the model sensitivity analysis in section 3.4.5. The most uncertainly defined parameters of those summarized in table 3.8 are fibre and membranes thicknesses. The experimental results indicate that they are probably underestimated in the numerical model. Besides, deviations between the material properties of the tissue strips analysed in section 2.3 and the present valve may also be present. Improving the numerical model may be possible by introducing inhomogeneous fibre and leaflet thickness. However, this probably leads to a very complex geometry description which is certainly not aimed at for the parameter variation study in the following chapter.

3.5.4. The stress distribution

From figure 3.21 it is observed that the maximum von Mises intensity in the membranes is found in the vicinity of point B and amounts to about 0.20 N/mm^2. The greatest negative values for the minimum

principal stress are found in the coaptation area near the leaflet suspension. It is remarked that only the presence of negative values is important because this indicates that the membranes may wrinkle. The absolute value however has to be interpreted with care due to the physical unrealistic constitutive equation used. The tensile fibre stress has a maximum in fibre 5 in the vicinity of the aortic ring and amounts to 0.64 N/mm^2. Finally, the shear force in node 36 and node 59 amounted to 0.005 and 0.012 N/mm^2 respectively. Christie and Medland (1982) calculated the stresses in a leaflet which was firmly attached to a rigid frame and found a maximum principal stress of 0.2 N/mm^2 in the leaflet center (at a pressure load of 16 kPa). Thubrikar et al. (1982) calculated stresses in the leaflet in circumferential and radial directions as membrane stresses in a cylinder. The radius of the leaflet was measured from a silicone mold of the valve prepared at the diastolic pressure gradient. They found a maximum stress in the leaflets of 0.33 N/mm^2 in circumferential direction at a pressure level of 13.3 kPa (100 mm Hg). The observed differences with our data are probably caused by differences between the underlying assumptions for the models.

In conclusion it is stated that the numerical model as described in this chapter yields a reliable picture of the mechanical behaviour of the Hancock bioprosthesis. In the next chapter this model will be used for a parameter variation study in order to formulate design specifications for a new leaflet valve prosthesis.

Chapter 4 Design specifications for a closed valve

4.1. Introduction

The goal of the present design study is to evaluate a valve prosthesis with artificial leaflets in which the main features of the natural aortic valve, like the fit to the natural sinuses, the fibre reinforced structure, the flexible leaflet suspension and the special viscoelastic material properties of the leaflets are retained. The most simple valve geometry and material properties of frame and artificial leaflets are aimed at to facilitate a cheap production process. To that end in the present study a leaflet valve prosthesis is considered in which the leaflets are directly connected to a flexible frame instead of using another material to suspend the leaflets to the frame. Furthermore, in the prosthesis aimed at, a fibre reinforced structure is taken in such a way that all fibres run almost parallel. Finally, the frame posts are chosen to be very narrow so that they do not disturb the gradual valve closing mechanism.

In this chapter the effects of the different geometry and material properties on the stress distribution in the leaflets of the valve prosthesis in closed position will be evaluated in order to specify its optimal design. The analysis will be focussed upon a 23 mm valve. For the determination of the stress distribution in the valve prosthesis, the numerical model of the Hancock valve described in chapter 3 is modified (section 4.2). Next, as a global survey, the geometry- and material parameters of the basic model are set to their outermost values one by one, leaving the others unchanged and the consequent changes in the stress distribution are analysed. From this global survey some parameters were chosen for a more detailed analysis in order to get insight in the effects of those parameters, including interactions, on the stresses in the valve (section 4.3). With this insight some design specifications are formulated for the closed valve (section 4.4).

4.2. The basic model

4.2.1. Description of the model

The valve prosthesis (a schematic view is given in figure 4.1) is modelled with a numerical model analogously to the numerical model of the Hancock valve described in chapter 3.

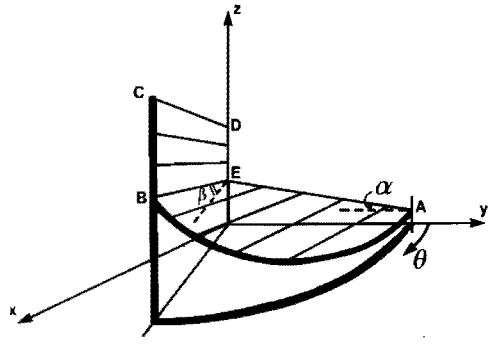

Fig. 4.1. A schematic view of the basic model of the leaflet valve prosthesis. ABE represents the free leaflet area; BCDE represents the coaptation area.

The mesh of the basic model is shown in figure 4.2. This figure illustrates that the fibres run almost parallel and that they are suspended directly to the frame.

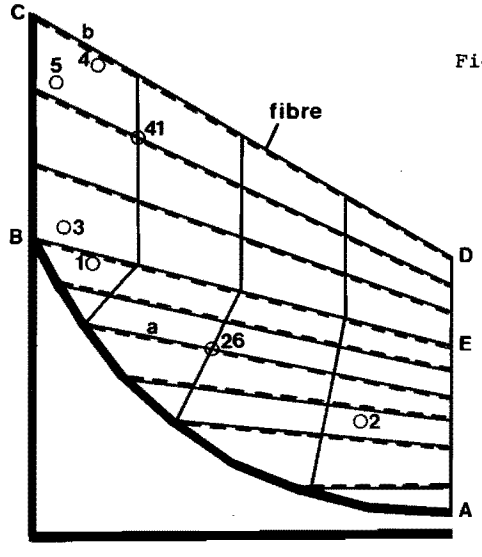

Fig.4.2. The mesh of the basic model of the leaflet valve prosthesis.

A uniform frame diameter of 1 mm is chosen, based on the framethickness of the Hancock valve (see chapter 2). For the description of the geometry of the basic model, the angle α, the angle β, the z-coordinate of point A (z(A)) and the length of the lines BC and DE (see figure 4.1) are taken from the 23 mm Hancock valve and amount 20^{o}, 15^{o}, 0.5 mm, 5.1 mm and 1.9 mm, respectively. With the assumptions that AE, BE, BC, CD and DE are straight lines and that AB may be represented by (see figure 4.1):

$$z = z(A) + C_1 (\bar{r}\ \theta)^2$$
$$x^2 + y^2 = \bar{r}^2 \qquad (4.1)$$

with

$$C_1 = \frac{z(B)-z(A)}{(\bar{r}\ \theta_B)^2} \ , \ \bar{r} = 10.82 \text{ mm}, \ z(A) = 0.5 \text{ mm}, \ \theta_B = \pi/3$$

the leaflet geometry is fully described. This description (4.1) for the line AB is chosen because with this relation the geometry of AB is fully described with one parameter (C_1), which is also uniquely related to the angle α. Besides, this representation is applicable for higher values of α than the description with the sphere used in case of the Hancock valve (see section 3.2.2). The material properties used are summarized in the first column of table 4.1. Besides, analogously to the Hancock valve, for the membrane thickness a value of 0.4 mm and for the membrane elastic modulus a value of 1.8 N/mm^2 were taken.

As a symmetrical valve geometry was aimed at, just only 1/6th part of the valve was modelled. The assumed symmetry conditions are the same as the ones described for the Hancock valve (see section 3.2), which also holds for the assumed geometry and material properties of the used elements. The valve was loaded with a pressure load of 12 kPa over the free leaflet area, realized in 10 msec. As elucidated in chapter 1 the following four stress parameters were analysed: i) the von Mises intensity in the membrane parts between fibres to characterise the membrane failure behaviour, ii) the tensile stress in the fibres corresponding to fibre break, iii) the

negative values of the minimum principal stress in the coaptation area, representing membrane wrinkling and iv) the magnitude of the shear force per unit length between fibre and membrane as a measure of the fibres tearing from the membrane. The latter shear force is calculated approximately from the difference between the two fibre directed components of the nodal forces from membranes and fibres respectively (see figure 3.6) and will be determined in two arbitrary nodes.

4.2.2. The stress situation in the basic model

In figure 4.3 a contourplot of the von Mises intensity in the membrane elements at a pressure load of 12 kPa is given.

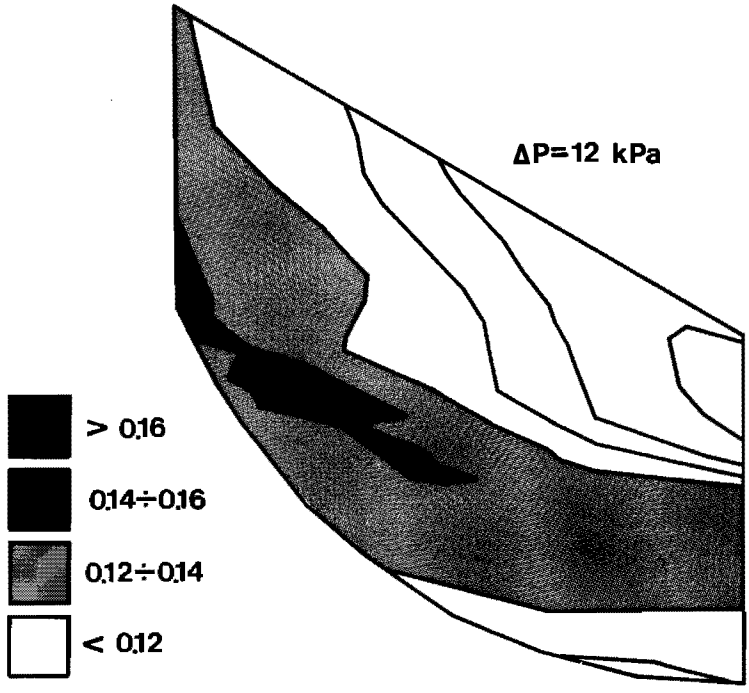

Fig. 4.3. A contourplot of the von Mises intensity in the membrane elements of the basic model.

This figure shows a projection of the leaflet in the plane of the coaptation area. It illustrates that the larger values for the von

Mises intensity are found in the vicinity of point B, along line BC and in the leaflet centre (from B to line AE). Figure 4.4 shows the tensile stress in the fibres. For the fibres in the coaptation area the maximum stress value is found at the frame attachment; it decreases in the direction of the valve center. In the fibres in the free leaflet area the stress is nearly constant over the whole fibre length. In figure 4.5 a contourplot of the minimum principal stress is given. This figure shows that the greatest negative principal stress is found along the leaflet attachment to the frame in the coaptation area. The shear force per unit length between fibre and membrane has been calculated for the arbitrary nodes 26 (in the free leaflet area) and 41 (in the coaptation area) and amounts 0.0006 and 0.021 N/mm respectively.

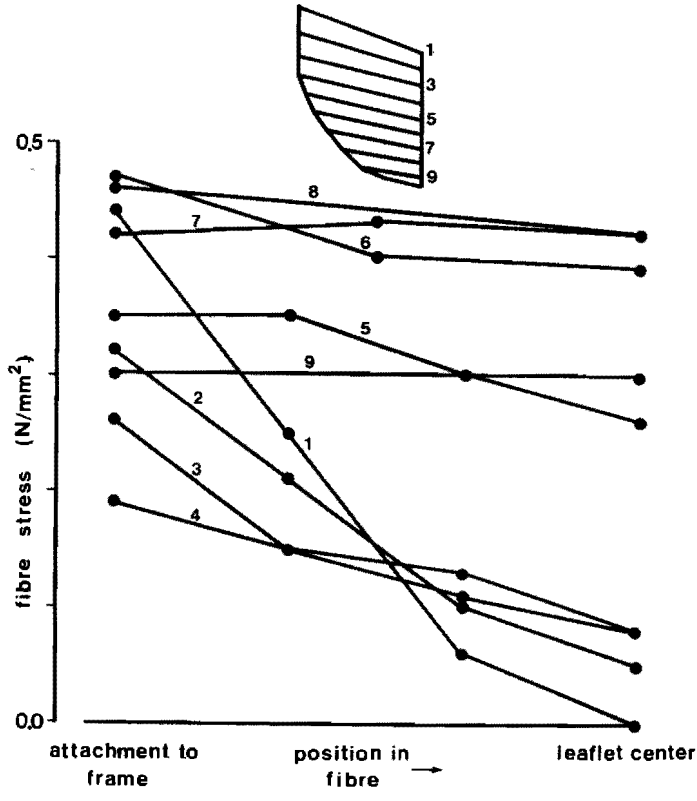

Fig. 4.4. The tensile stresses in the fibres of the basic model.

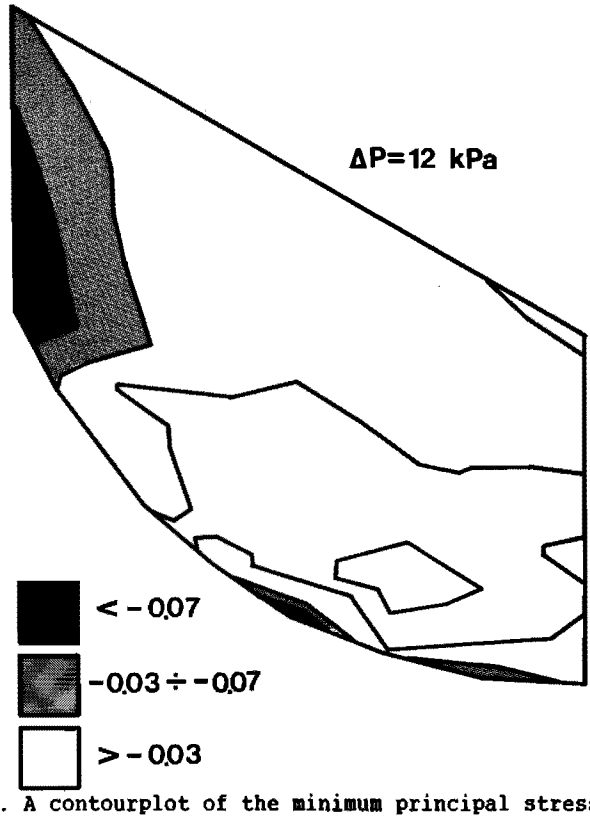

Fig. 4.5. A contourplot of the minimum principal stresses in the membrane elements of the basic model.

4.3. The parameter variations

4.3.1. A global survey

To get insight into the global influence of the design parameters on the stress distribution in the closed valve, firstly the geometry and material parameters are set one by one to their extreme values leaving the rest of the model unchanged. Here, no interactions were taken into account. The next parameters were varied:

i) the elastic modulus of the frame material: E_{FR}
ii) the thickness of the frame: d_{FR}
iii) the angle α, describing the free leaflet geometry
iv) the magnitude of the coaptation area: A_{coap}
v) the fibre thickness: d_f
vi) the elastic modulus of the fibre material: E_f
vii) the mean fibre distance: mfd

viii) the viscous properties of the frame material

ix) the viscous properties of the leaflet material

In table 4.1 the values of these parameters are given together with their outermost values in this global survey. Most of these values were chosen rather arbitrarily, but in such a way that differences in stresses were expected. To get a quantitative comparison of the stress situations for the different adjustments of the parameters, points were selected in the valve geometry where the worsest stress-distribution exists in the basic model. Hence, the von Mises intensity is determined for the points 1, 2, 3 and 4 (see figure 4.2). The tensile fibre stress is given for the fibre parts a and b (see figure 4.2) while the minimum principal stress is given for the points 3 and 5. The shear stress is calculated for the nodes 26 and 41.

symbol	parameter	basic value	minimum value	maximum value
E_{FR}	elastic modulus of the frame [N/mm^2]	1582	1000	200.000
d_{FR}	frame thickness [mm]	1	0.5	2.5
α	angle in free leaflet area [^{o}]	20	0	60
A_{coap}	magnitude of the coaptation area [mm^2]	38.2	19.1	76.4
d_f	fibre thickness [mm]	0.4	0.1	0.7
E	elastic modulus of fibre [N/mm^2]	23	2.3	230
mfd	mean fibre distance [mm]	1.4	1.4	no fibres

Table 4.1.: the varied parameters in the global survey.

Not varied in this analysis were the membrane thickness (0.4 mm) and elastic modulus of the membranes (1.8 N/mm^2) which are chosen so low to ensure low bending stresses in the membranes. This is thought to be of great importancy with regard to the opening and closing behaviour of the leaflets (see chapter 1). On the other hand a lower value of the membrane thickness is harmful due to the desired strength in closed position while the elastic modulus of the membranes for practical fabrication reasons (for example when polyurethanes are used) can not much be reduced. Hence, as applicable values of these parameters, the intervals $0.2 < d_m < 0.6$ mm and $1 < E_f < 5$ N/mm^2 will be taken. In future research, a more definite choice has to be made based on the analysis of the opening and closing behaviour of the leaflets (see chapter 5).

In table 4.2 the results of these calculations are given. From this table it can be seen that the highest value of the von Mises intensity in the membranes are always present in point 1 and somewhat less in point 3. The maximum fibre stress is not related to a certain fibre part. The magnitude of the (negative) minimum principal stress is mostly much lower than the von Mises intensities. The largest negative value is mostly found in point 3. The parameters which cause the greatest changes in the stress distribution are:

- the frame thickness: d_{FR}
- the angle α
- the fibre thickness: d_f
- the elastic modulus of the fibre material: E_f
- the mean fibre distance: mfd

The stress parameters are hardly influenced by the elastic modulus of the frame material, the magnitude of the coaptation area and the variation of the viscous properties of leaflet and frame material in the considered ranges. For example, when the magnitude of the coaptation area is changing with a factor 2, the von Mises intensity changes with 15% in the coaptation area but remains nearly constant ($\leq$ 5%) in the free leaflet area. The fibre stress also is only changing in the coaptation area.

The effect of the viscous properties of frame and leaflet is studied during a time varying pressure load (see figure 4.6a). During an upward or downward variation the stress distribution is calculated at three time-moments. In figure 4.6 the von Mises intensity in

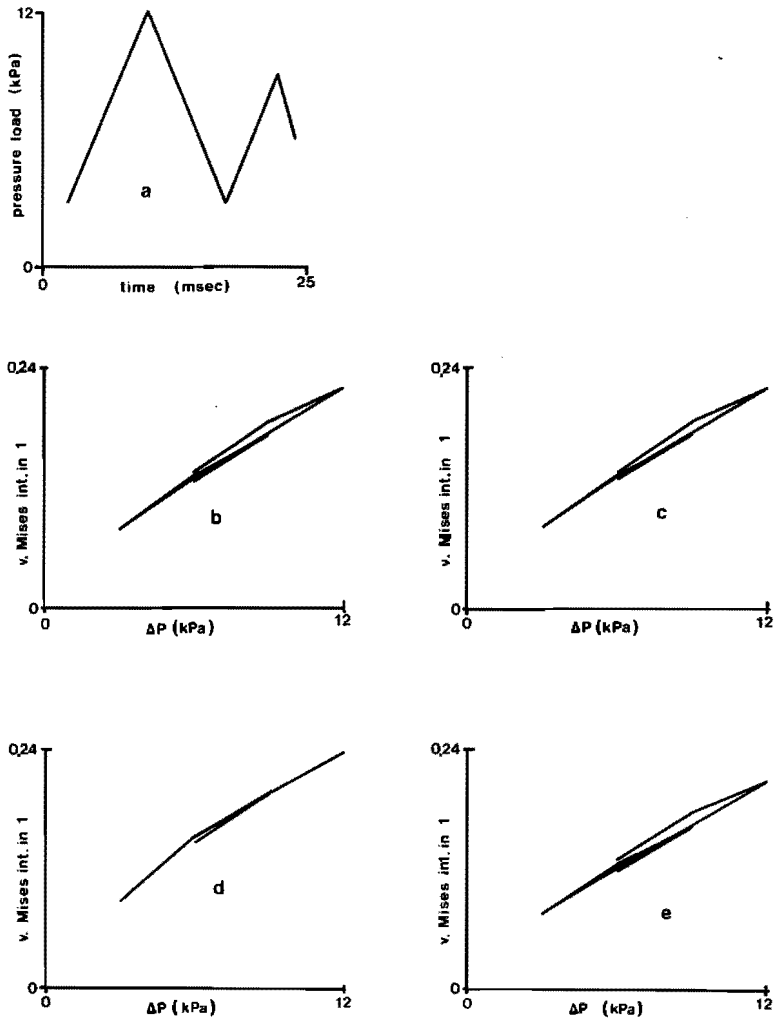

Fig. 4.6. Influence of the viscous parameters on the von Mises intensity in membrane point 1. (N/mm^2)

a. pressure load across the free leaflet area.
b. von Mises intensity for the basic model.
c. von Mises intensity in the case of the "viscous" frame.
d. von Mises intensity in the case of the "elastic" leaflet.
e. von Mises intensity in the case of the more viscous leaflet.

point 1 is given as a function of pressure load for the 4 cases: i) the basic model (b), ii) a "viscous" frame where the viscous properties of the frame material are adjusted to the viscous properties of the leaflet material (c), iii) elastic leaflet, in which the leaflets are purely elastic (d) and iv) "viscous" leaflet where the time constants were made 10 times smaller (e). From these figures it is seen that in comparison with the basic situation, the stress at 12 kPa increases when making the leaflet purely elastic and decreases slightly when the leaflet material is more viscous (see also values in table 4.2). Variation of the viscous property of the frame material has no effect on the von Mises intensity in point 1. The hysteresis loop remains constant for all cases except in the case of the purely elastic leaflet material, where no hysteresis is noticable.

In conclusion it is stated that for the stress distribution in the closed valve the 5 parameters d_{FR} α, d_f, E_f and mfd are of paramount importancy. Therefore, in the next section these 5 parameters will be studied in a more fundamental way. In this global survey it is also found that the viscous properties of frame and leaflets are of secondary importance during this part of the cardiac cycle. This also holds for the elastic modulus of the frame material and for the magnitude of the coaptation area. Therefore, in the next section these parameters will be left out of consideration, and for them and the thickness and elastic modulus of the membranes the values of the basic model will be taken.

	von Mises intensity (N/mm^2)				fibre stress (N/mm^2)		neg.values of min.pring. stress (N/mm^2)		shear force per unit length (N/mm)	
	1	2	3	4	a	b	3	5	26	41
basic model	0.222	0.147	0.158	0.113	0.47	0.44	0.096	0.049	0.0006	0.0206
E_{FR}= 1000 N/mm^2	0.227	0.151	0.157	0.106	0.48	0.41	0.097	0.050	0.0003	0.0211
E_{FR}= 200000 N/mm^2	0.210	0.141	0.161	0.128	0.45	0.51	0.092	0.046	0.0009	0.0192
d_{FR}= 0.5 mm	0.219	0.118	0.088	0.027	0.33	0.05	0.000	0.016	0.0134	0.0073
d_{FR}= 2.5 mm	0.211	0.141	0.161	0.128	0.46	0.51	0.092	0.046	0.0011	0.0193
α = 0 deg	0.162	0.142	0.170	0.134	0.40	0.54	0.106	0.047	0.0004	0.0185
α = 60 deg	0.296	0.101	0.151	0.158	0.66	0.73	0.164	0.010	0.0339	0.0058
A_{coap}=19 mm^2	0.230	0.149	0.181	0.161	0.50	0.58	0.101	0.067	0.0004	0.0295
A_{coap}=76 mm^2	0.212	0.145	0.134	0.055	0.45	0.22	0.079	0.023	0.0008	0.0088
d_f= 0.1 mm	0.270	0.186	0.208	0.202	0.66	0.87	0.099	0.034	0.0205	0.0028
d_f= 0.7 mm	0.177	0.121	0.123	0.069	0.30	0.20	0.087	0.053	0.0192	0.0242
E_f= 2.3 N/mm^2	0.267	0.184	0.204	0.195	0.07	0.08	0.099	0.036	0.0083	0.0073
E_f= 230 N/mm^2	0.133	0.136	0.097	0.049	1.37	0.66	0.076	0.052	0.0394	0.0207
mfd = ∞	0.275	0.177	0.214	0.215	-	-	0.099	0.032	-	-
"viscous frame"	0.224	0.148	0.158	0.110	0.47	0.43	0.097	0.050	0.0006	0.0205
"elastic leaflet"	0.237	0.166	0.169	0.117	0.49	0.45	0.105	0.054	0.0009	0.0220
"viscous leaflet"	0.214	0.141	0.153	0.111	0.46	0.44	0.091	0.047	0.0088	0.0198

Table 4.2. Stress quantities at a pressure load of 12 kPa, for the design parameters set to their outermost boundary values.

4.3.2. The parameter variation model

The remaining 5 parameters were varied separately in smaller steps to study the range of interest and to observe the global effects of these parameters on the stress quantities.

Figure 4.7 shows the dependencies of these design parameters on the von Mises intensity in the membranes (points 1, 2, 3 and 4). Figure 4.8 shows these dependencies on the tensile stress in the fibre parts a and b.

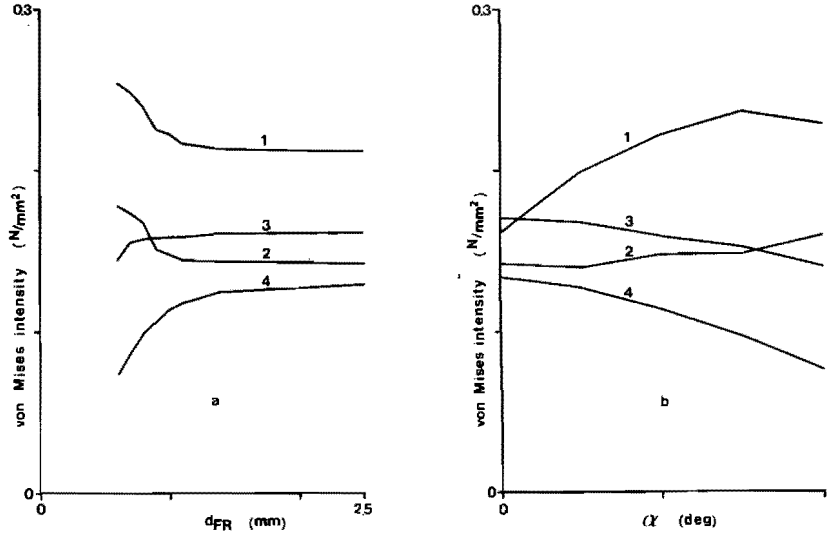

Fig. 4.7. Influence of the geometry and material parameters on the von Mises intensity in the membrane points 1, 2, 3 and 4.
a. influence of the frame thickness: d_{FR}
b. influence of the angle: α

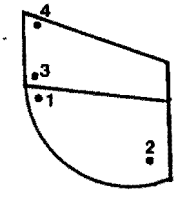

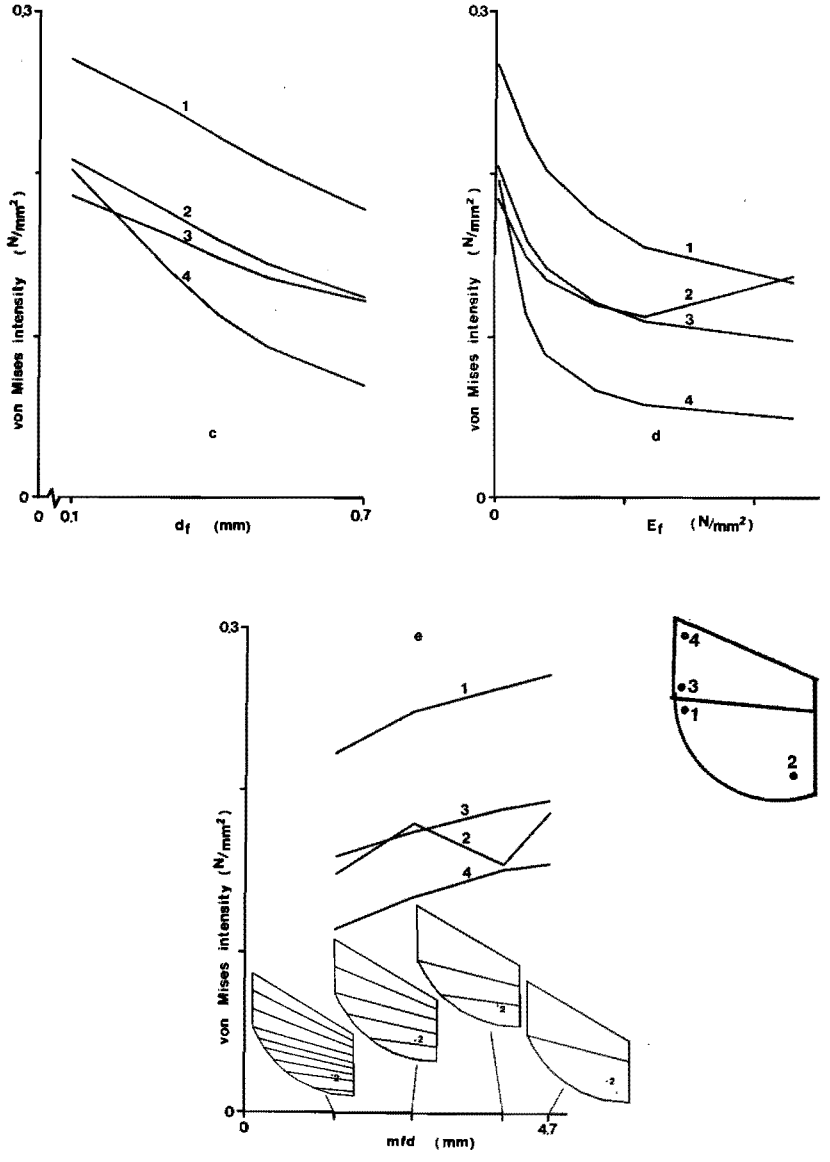

Fig. 4.7. Influence of the geometry and material parameters on the von Mises intensity in the membrane points 1, 2, 3 and 4.

c. influence of the fibre thickness: d_f
d. influence of the elastic modulus of the fibres: E_f
e. influence of the mean fibre distance: mfd

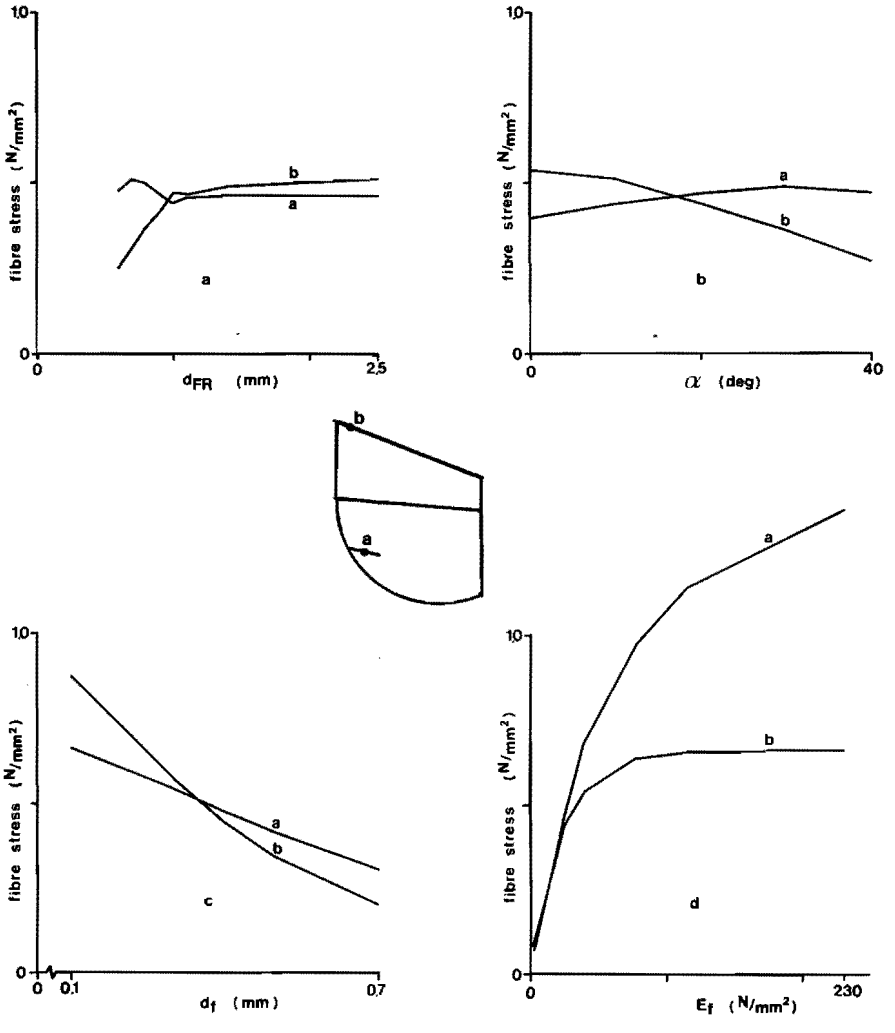

Fig. 4.8. Influence of the geometry and material parameters on the tensile stress in fibre parts a and b

a. frame thickness: d_{FR}
b. angle: α
c. fibre thickness: d_f
d. elastic modulus of fibres: E_f

From these figures it can be seen that the frame thickness, for the considered value of the elastic modulus of the frame, is only of interest when ranging between 0.6 and 1.4 mm. At a frame thickness greater than 1.4 mm no changes are observed for the stresses. At a frame thickness between 0.6 and 1.4 mm the stresses in the coaptation area (membrane points 3 and 4 and fibre part b) increase with increasing frame thickness. The fibre stress in the free leaflet area (part a) then remains constant while the membrane stresses in the free leaflet area (points 1 and 2) decrease. An increase of α leads to a decrease of the membrane and fibre stresses in the coaptation area while the changes in the free leaflet area are only marginal except for the von Mises intensity in point 1 which increases with increasing α. When the fibre thickness increases, the stresses in membranes and fibres become smaller over the whole leaflet. Stiffening of the fibres leads to an increase of the tensile fibre stresses and to a decrease of the von Mises intensity in the membranes. Finally, with an increase of the mean fibre distance, the membrane stresses show generally a slight increase. Only, for the von Mises intensity in membrane point 2, a rather discrete line is found as the smallest distance of point 2 to the nearest fibre is changing rather discretely. Therefore, this parameter later will be studied separately.

Figure 4.9 shows the dependencies of the design parameters on the (negative) minimum principal stresses in the points 3 and 5. In figure 4.10 these dependencies on the shear forces in the nodes 26 and 41 are given. From figure 4.9 it is observed that there is only a small influence of the design parameters on the negative principal stresses. Figure 4.10 shows that the angle α and the frame thickness have no influence on the shear stresses in the nodes 26 and 41 while variation of fibre stiffness and fibre thickness leads to a remarkable change of the considered shear stresses. The influence of the mean fibre distance on fibre stress and on shear stress is not given. Variation of this design parameter gives no comparable information on changes in fibre stresses and on changes in shear stresses as for the different calculated cases, the fibre structure is different (see figure 4.7e). Besides, the mean fibre distance is only allowed to have some discrete values. Due to these special difficulties the influence of this parameter will be studied separately.

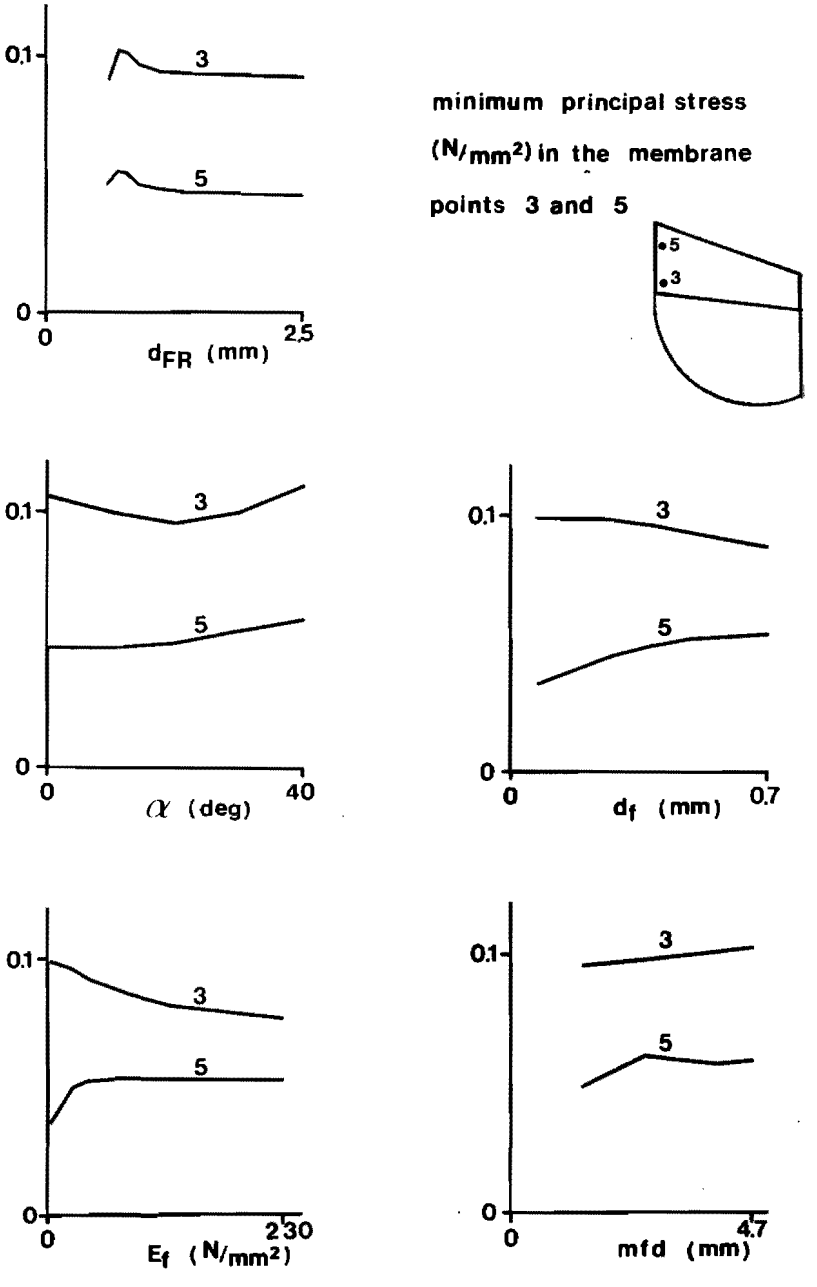

Fig. 4.9. Influence of the geometry and material parameters on the minimum principal stress in the membrane points 3 and 5.

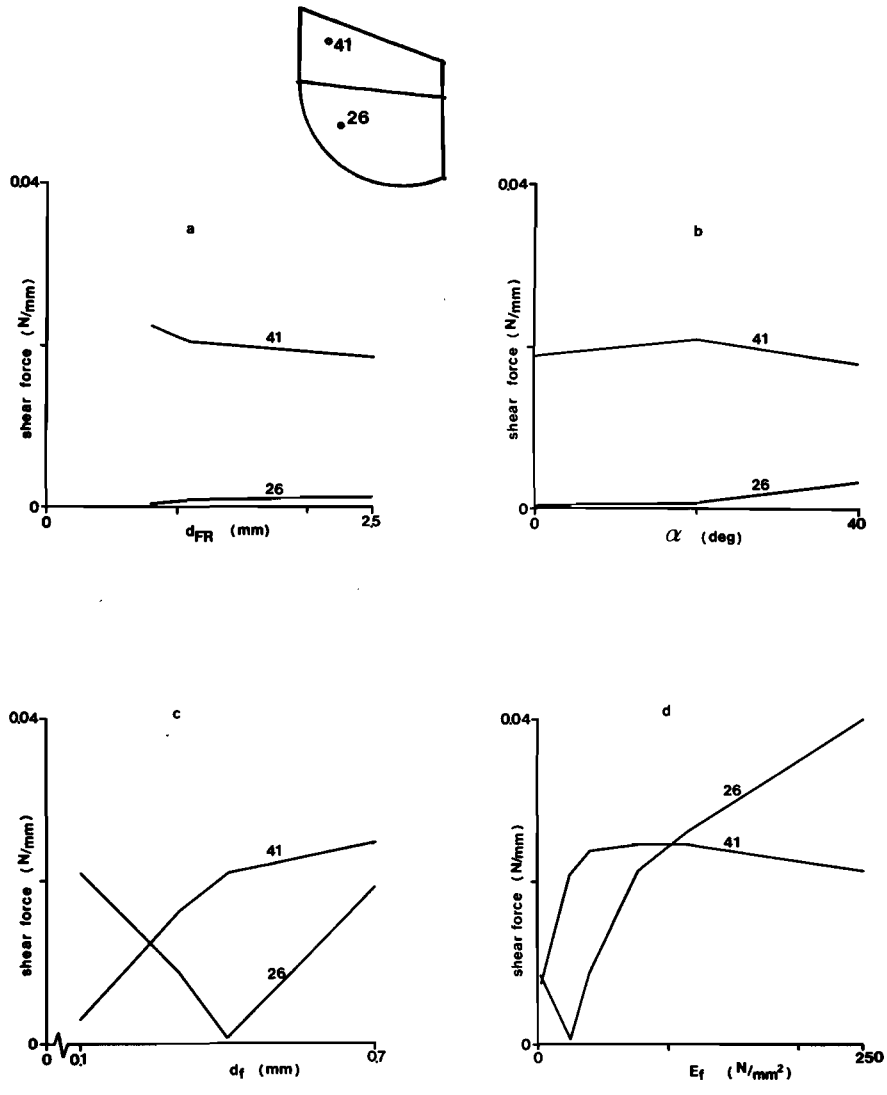

Fig. 4.10. Influence of the geometry and material parameters on the shear force per unit length in the nodes 26 and 41.

The parameter variation study was continued with the 4 parameters d_{FR}, α, d_f and E_f. For these parameters a statistical procedure was used to obtain a linear model (van Heck, 1984) in which linear interaction terms were incorporated. This procedure is here summarized and is explained into more detail by van Heck (1984). The following universal model was adopted for all stress parameters, based upon the relations shown in figures 4.7 ÷ 4.10:

$$\bar{y} = \beta_0 + \beta_1\xi_1 + \beta_2\xi_1^2 + \beta_3\xi_2 + \beta_4\xi_2^2 + \beta_5\xi_3 + \beta_6\xi_3^2 + \\ + \beta_7\xi_4 + \beta_8\xi_4^2 + \beta_9\xi_1\xi_2 + \beta_{10}\xi_1\xi_3 + \beta_{11}\xi_1\xi_4 + \\ + \beta_{12}\xi_2\xi_3 + \beta_{13}\xi_2\xi_4 + \beta_{14}\xi_3\xi_4 + \bar{e} \qquad (4.2)$$

with: $\bar{e}$ = model error

β_i = the unknown parameters

$\bar{y}$ = a stress parameter, made dimensionless by dividing the actual stress value by the unity value of 1 N/mm^2 (or 1 N/mm).

$\bar{y}_1$ = v. Mises intensity in point 1

$\bar{y}_2$ = v. Mises intensity in point 2

$\bar{y}_3$ = v. Mises intensity in point 3

$\bar{y}_4$ = v. Mises intensity in point 4

$\bar{y}_5$ = fibre stress in a

$\bar{y}_6$ = fibre stress in b

$\bar{y}_7$ = min. princ. stress in point 3

$\bar{y}_8$ = min. princ. stress in point 5

$\bar{y}_9$ = shear force per unit length in 26

$\bar{y}_{10}$ = shear force per unit length in 41

and:

$$\xi_1 = \left(\frac{\alpha-\alpha_0}{\Delta\alpha}\right) \qquad , \Delta\alpha = 10^{o}$$

$$\xi_2 = \frac{\left(\frac{1}{dFR^2}\right) - \left(\frac{1}{dFR_0^2}\right)}{\Delta\left(\frac{1}{d_{FR}^2}\right)} \qquad , \Delta\left(\frac{1}{d_{FR}^2}\right) = 0.4783 \text{ mm}^{-2}$$

$$\xi_3 = \frac{E_f - E_{f0}}{\Delta E_f} \quad , \Delta E_f = 10 \text{ N/mm}^2$$

$$\xi_4 = \left(\frac{d_f - d_{f0}}{\Delta d_f}\right) \quad , \Delta d_f = 0.2 \text{ mm}$$

The subscript $_0$ denotes here the value owing to the basic situation.

$\Delta\alpha$ is the distance between the α-levels.

For each calculation a deviation between the fitted model (4.2) and the actual stress value is found. This is denoted by $\bar{e}_i$. Contrarily to physical experiments this error has no a priori statistical meaning. However, to perform the variance analysis aimed at we assume that: i) the expected value of $\bar{e}_i$ is the same for each calculation and ii) is equal to σ_0^2, iii) $\bar{e}_i$ and $\bar{e}_j$ $(i \neq j)$ are statistically independent (see van Heck, 1984).
The 15 unknown parameters β_i for each stress parameter can then be estimated from (Chatfield, 1983; van Heck, 1984):

$$\hat{\underline{\beta}} = (\underline{X}^T\underline{X})^{-1}\,\underline{X}^T\,\underline{y} \qquad (4.3)$$

with $\underline{y}$: column matrix with the n observations of the considered stress parameter.

$\hat{\underline{\beta}}$: column matrix with the 15 estimated values for the unknown influence parameters.

$\underline{X}$: the n * (15) design matrix with the adjustments of the independent parameters for all n calculations.

The accuracy of the estimation procedure (4.3) and the coherence between the different design parameters is described by the variance-covariance matrix $\underline{V}_\beta$ and a correlation coefficient matrix ϱ. These matrices are estimated by (see van Heck, 1984):

$$\hat{\underline{V}}_\beta = (\underline{X}^T\underline{X})^{-1}\,\frac{KS_x}{(n-k-1)} \qquad (4.4)$$

and:

$$\hat{\varrho}_{ij} = \frac{\hat{V}_{\beta ij}}{\sqrt{\hat{V}_{\beta ii}\,\hat{V}_{\beta jj}}} \qquad (4.5)$$

with:

KS_r is the residual sum of squares

$\underline{KS}_r = (\underline{y} - X\hat{\underline{\beta}})^T (\underline{y} - X\hat{\underline{\beta}})$

To obtain a design matrix X in such a way that (X^TX) is not singular, ξ_1, ξ_2, ξ_3 and ξ_4 should normally have to be adjusted to 3 levels at least which leads to a complete calculation program involving all 3^3 = 81 possible combinations. Latin squares (Chatfield, 1983; van Heck, 1984) are used to reduce this calculation program. The reduced program is shown in table 4.3. Here the adjustments of the physical

calculation number	α_o ( )	d_{FR} (mm)	d_f (mm)	E_f (N/mm^2)
1	10	0.96	0.2	13
2	10	0.96	0.6	23
3	10	0.96	0.4	33
4	10	0.80	0.6	13
5	10	0.80	0.4	23
6	10	0.80	0.2	33
7	10	0.70	0.4	13
8	10	0.70	0.2	23
9	10	0.70	0.6	33
10	20	0.96	0.4	13
11	20	0.96	0.2	23
12	20	0.96	0.6	33
13	20	0.80	0.2	13
14	20	0.80	0.6	23
15	20	0.80	0.4	33
16	20	0.70	0.6	13
17	20	0.70	0.4	23
18	20	0.70	0.2	33
19	30	0.96	0.6	13
20	30	0.96	0.2	23
21	30	0.96	0.4	33
22	30	0.80	0.2	13
23	30	0.80	0.4	23
24	30	0.80	0.6	33
25	30	0.70	0.4	13
26	30	0.70	0.6	23
27	30	0.70	0.2	33

Table 4.3.: the calculation program.

parameters are given. This table shows that the calculation program contains only 27 combinations of levels for ξ_1, ξ_2, ξ_3 and ξ_4. To estimate the unknown influence parameters β_i at least 15 calculations are needed and the remaining 12 statistical degrees of freedom are used to estimate the variance of the model fit error.

4.3.3. Results

The calculations revealed that for all stress quantities the parameters β_4 and β_6 are not significantly different from zero. The estimated values for the remaining β's are given in table 4.4 together with their reliability intervals. These parameter values are given for each stress quantity. Also the residual sum of squares for each stress quantity is given here. The corresponding correlation coefficient matrix ϱ is shown in table 4.5 which illustrates that the calculation program is reasonable orthogonal.

Next, the values of β from table 4.4 are used to plot the fitted relation for each stress quantity as a function of the 4 design parameters. These functions are shown in figures 4.11 - 4.14. The basic values for the design parameters are $\alpha = 20^{o}$, $d_{FR} = 0.8$ mm, $E_f = 23$ N/mm^2 and df = 0.4 mm.

	1	2	3	4	5	6	7	8	9	10	11	12	13
1	1.0												
2		1.0											
3			1.0										
4				1.0								-.1	0.2
5					1.0							0.2	-.1
6						1.0	-.1				0.2		
7						-.1	1.0				-.4		
8								1.0					
9									1.0				
10										1.0			
11						0.2	-.4				1.0	0.1	0.1
12				-.1	0.2						0.1	1.0	-.3
13				0.2	-.1						0.1	-.3	1.0

Table 4.5. The correlation coefficient matrix for the used calculation program (β_4 and β_6 are not taken into account)

	v.M.1	v.M.2	v.M.3	v.M.4	f.s. a	f.s. b	m.p.s.3	m.p.s.5	s.f.26	s.f.41
β_0	240 ± 3	165 ± 3	159 ± 3	101 ± 4	485 ± 13	350 ± 32	100 ± 3	53 ± 2	4 ± 3	21 ± 1
β_1	28 ± 1	8 ± 1	-3 ± 1	-15 ± 2	13 ± 7	-70 ± 17	11 ± 1	9 ± 1	4 ± 3	2 ± 1
β_2	-5 ± 2	-8 ± 3	NS	NS	-12 ±11	64 ± 29	5 ± 2	NS	2 ± 1	NS
β_3	14 ± 1	13 ± 1	NS	-10 ± 2	20 ± 7	-47 ± 17	3 ± 1	2 ± 1	3 ± 2	1 ± 1
β_4	---	---	---	---	---	---	---	---	---	---
β_5	-14 ± 1	-10 ± 1	-11 ± 1	-16 ± 2	161 ± 7	101 ± 17	NS	NS	NS	4 ± 1
β_6	---	---	---	---	---	---	---	---	---	---
β_7	-32 ± 1	-22 ± 1	-26 ± 1	-40 ± 2	-140 ±7	-207 ±17	-3 ± 1	6 ± 1	-11 ±3	-1 ± 1
β_8	NS	NS	NS	12 ± 4	NS	60 ±31	-3 ± 1	-4 ± 2	18 ±5	-3 ± 1
β_9	-7 ± 2	NS	5 ± 2	NS	-11 ±9	NS	10 ± 2	4 ± 1	NS	NS
β_{10}	NS	NS	NS	NS	NS	NS	NS	NS	NS	NS
β_{11}	NS	NS	6 ± 2	10 ± 3	NS	39 ± 21	3 ± 2	NS	NS	NS
β_{12}	NS	NS	NS	NS	NS	NS	NS	NS	NS	NS
β_{13}	NS	NS	NS	5 ± 3	-12 ±9	NS	NS	NS	NS	NS
β_{14}	-6 ± 2	NS	NS	NS	-75 ±9	-96 ± 22	NS	NS	7 ±3	-3 ± 1
KS_r	0.11	0.12	0.10	0.26	2.7	16	0.10	0.06	0.40	0.01

Table 4.4. The estimated β-values together with their 95 % reliability intervals,and the reduced sum of squares for the different stress quantities. v.M. : von Mises intensity, f.s. : fibre stress, m.p.s. : minimum principal stress, s.f. : shear force per unit length. NS means Not Significant. All values have to be multiplied by 10^{-3}.

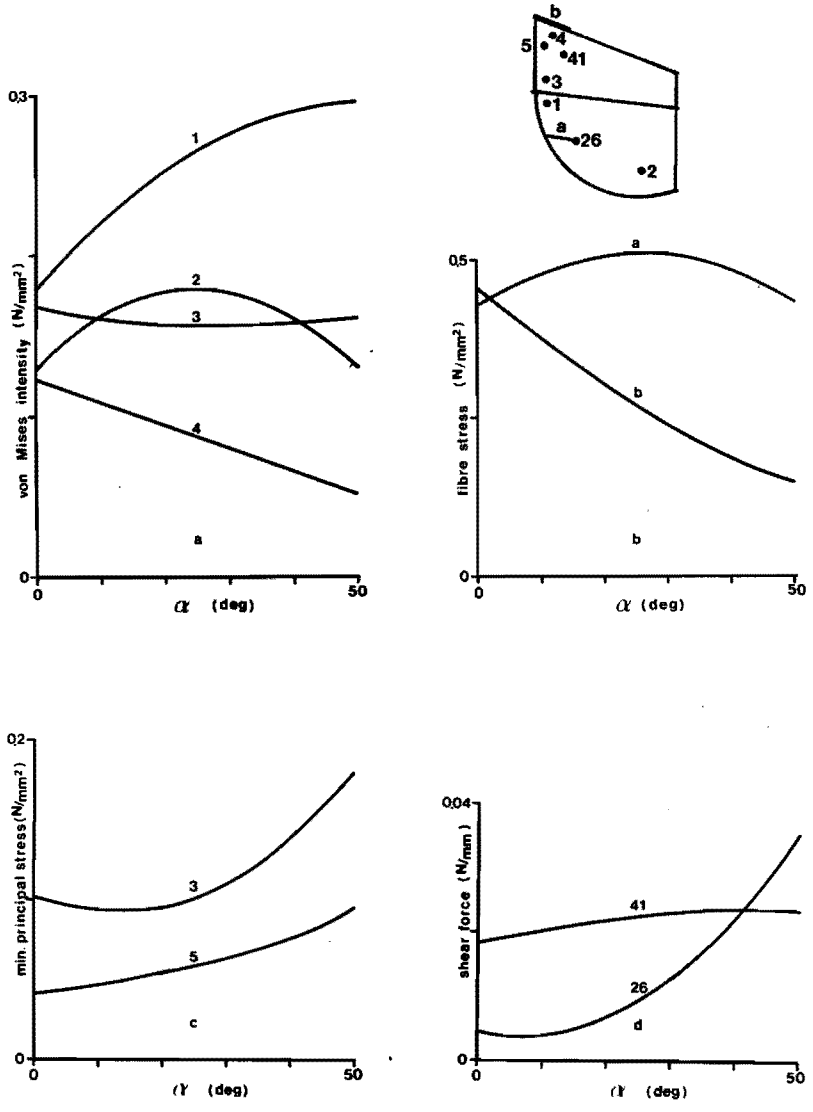

Fig. 4.11. Influence of the angle α.
basic values: α = 20 , d_{FR} = 0.8 mm, E_f = 23 N/mm^2, d_f = 0.4 mm.

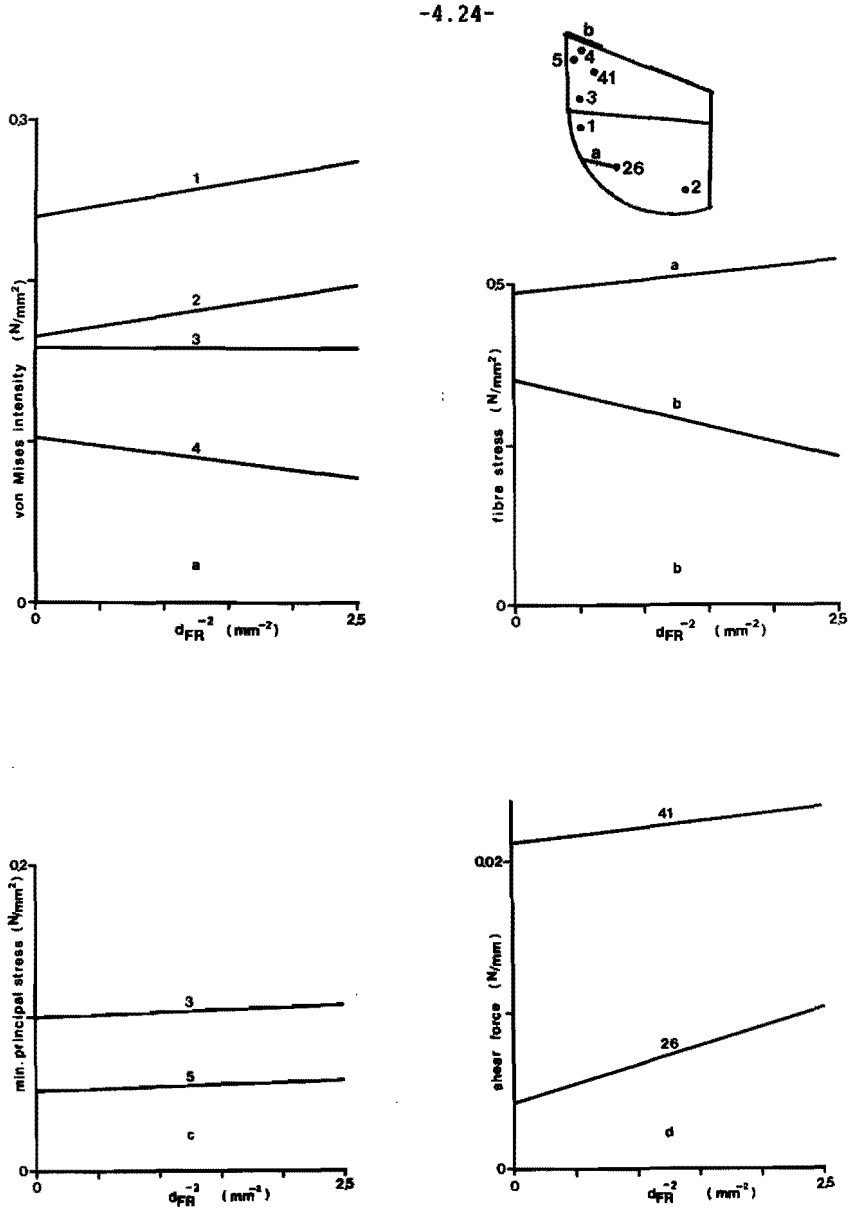

Fig. 4.12. Influence of $\left(\frac{1}{d_{FR}^2}\right)$.
basic values: $\alpha = 20$, $d_{FR} = 0.8$ mm, $E_f = 23$ N/mm^2, $d_f = 0.4$ mm.

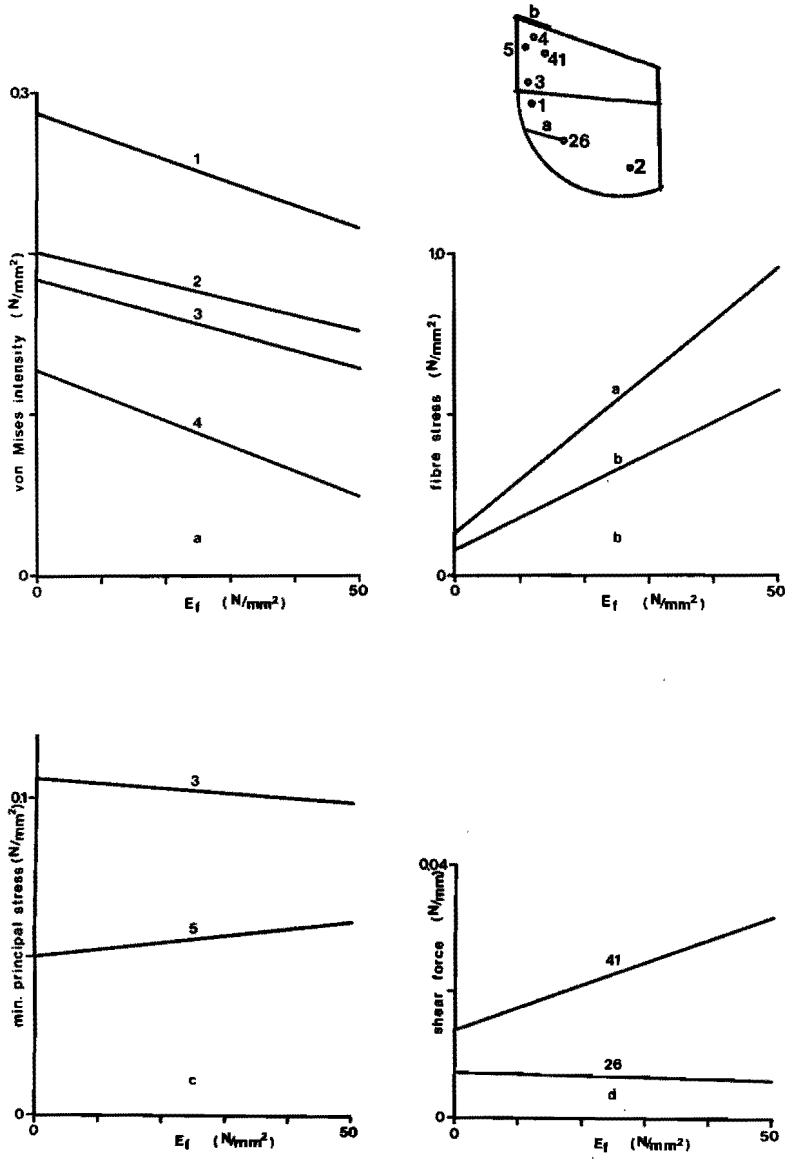

Fig. 4.13. Influence of the elastic modulus of the fibre material (α = 20 , d_{FR} = 0.8 mm, E_f = 23 N/mm^2, d_f = 0.4 mm).

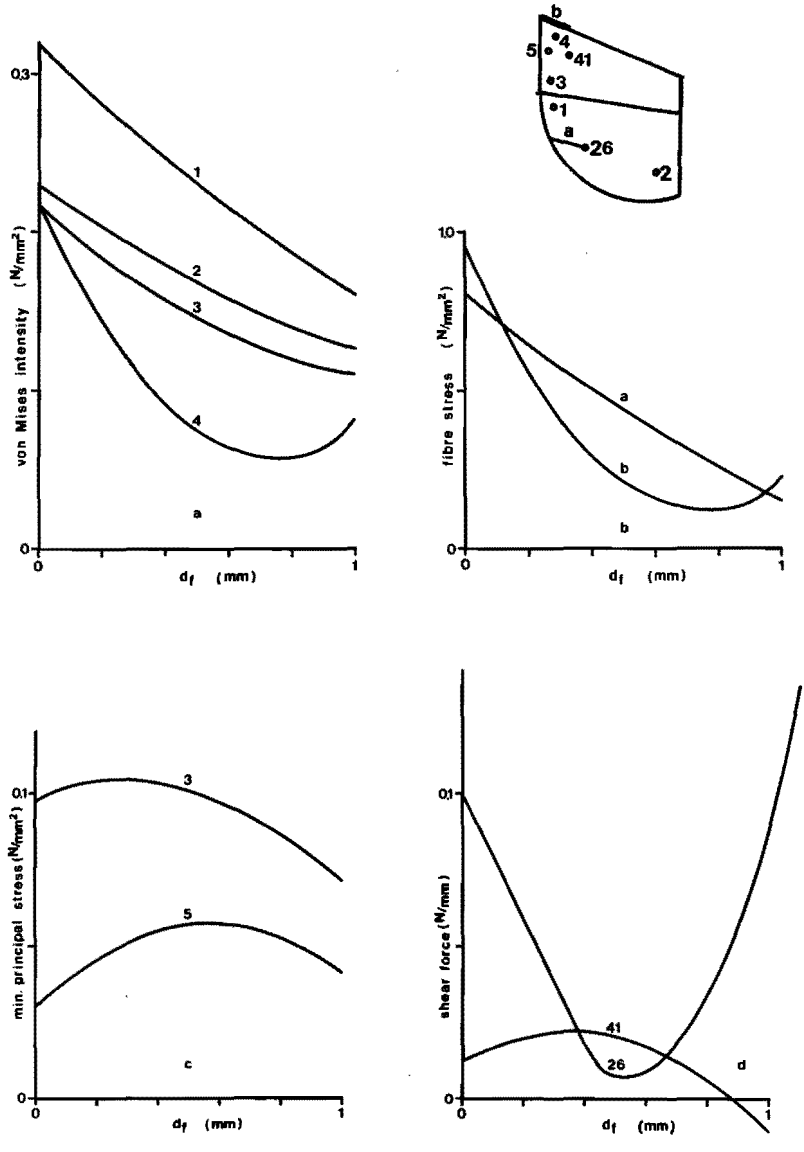

Fig. 4.14. Influence of the fibre thickness d_f ($\alpha = 20^0$, $d_{FR} = 0.8$ mm, $E_f = 23$ N/mm^2, $d_f = 0.4$ mm).

For the parameter α (figure 4.11) all stress quantities appear to become smaller for decreasing values of α, except the von Mises intensity in the points 3 and 4 and the fibre stress in b. The latter quantities, however, are considerably smaller than comparable stress quantities in other points of the valve. Hence, for point 3 the value of the minimum principal stress is regarded to be a more relevant design criterium than the von Mises intensity there. As applicable range for α the interval $0^{o} < \alpha < 20^{o}$ is chosen. With regard to the actual valve design very small values of α need to be avoided to prevent leaflet collapsing in the closed position. Therefore, for the design the rather arbitrary value of $\alpha = 10^{o}$ has been chosen.

For the quantity $(1/d_{FR}^{2})$ linear relationships are found (see figure 4.12) as the second order term of $(1/d_{FR}^{2})$ did not contribute significantly to the linear model (4.2). Most stresses show a minimum for $(1/d_{FR}^{2}) \rightarrow 0$, which corresponds to a stiff frame. Here, again the von Mises intensity in the points 3 and 4 and the fibre stress in b show an opposite behaviour. However, for a stiff frame, the values of those stress quantities are again considerably lower than the comparable stress quantities in the other points of the valve.

For the elastic modulus of the fibre material linear relationships are found also as the second order term did not contribute significantly to the linear model (4.2). As shown in figure 4.13, a completely different behaviour of the 10 stress quantities is found, which makes the choice of an optimum very difficult. Figure 4.14 illustrates that most of the stress quantities and especially the shear force per unit length in node 26 have an irregular relationship to the fibre thickness.

To specify the fibre design specifications into more detail, the 10 stress quantities are also plotted in figure 4.15 but now with d_{f} and E_{f} as simultaneous varying parameters. Here, α and $(1/d_{FR}^{2})$ are set at a constant value of 10^{o} and 0 mm^{-2}, respectively. The plots reveal that the von Mises intensity in the membranes can be reduced by using a higher fibre stiffness. In that case the fibre stress shows a considerable increase. The largest negative values of the minimum principal stress are found in point 3. An increase of the fibre stiffness leads to a decrease of that stress quantity, although the variation is relatively small.

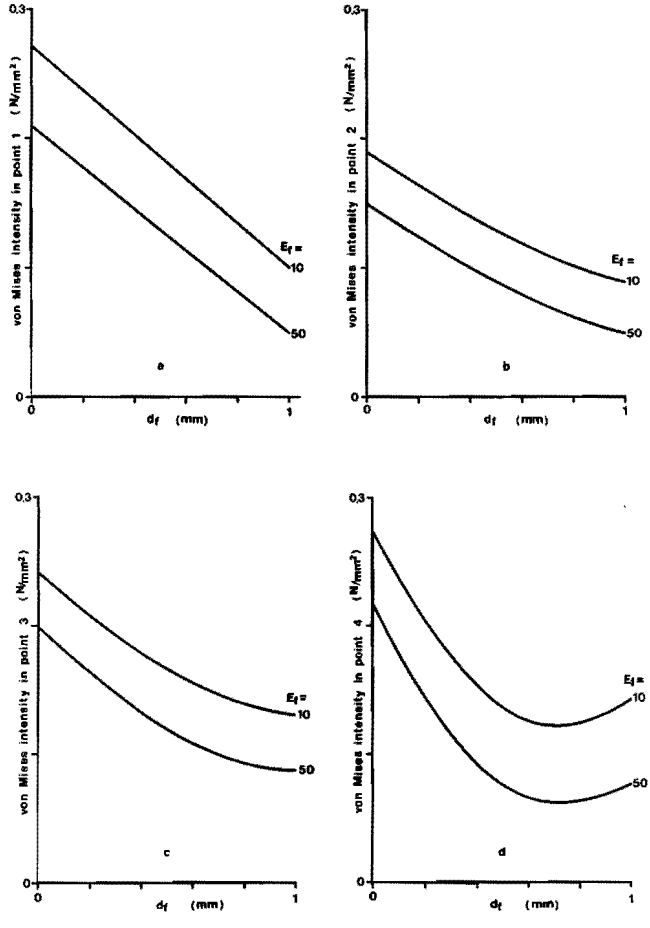

Fig. 4.15. Influences of the fibre thickness and fibre elastic modulus (α = 10 , stiff frame).

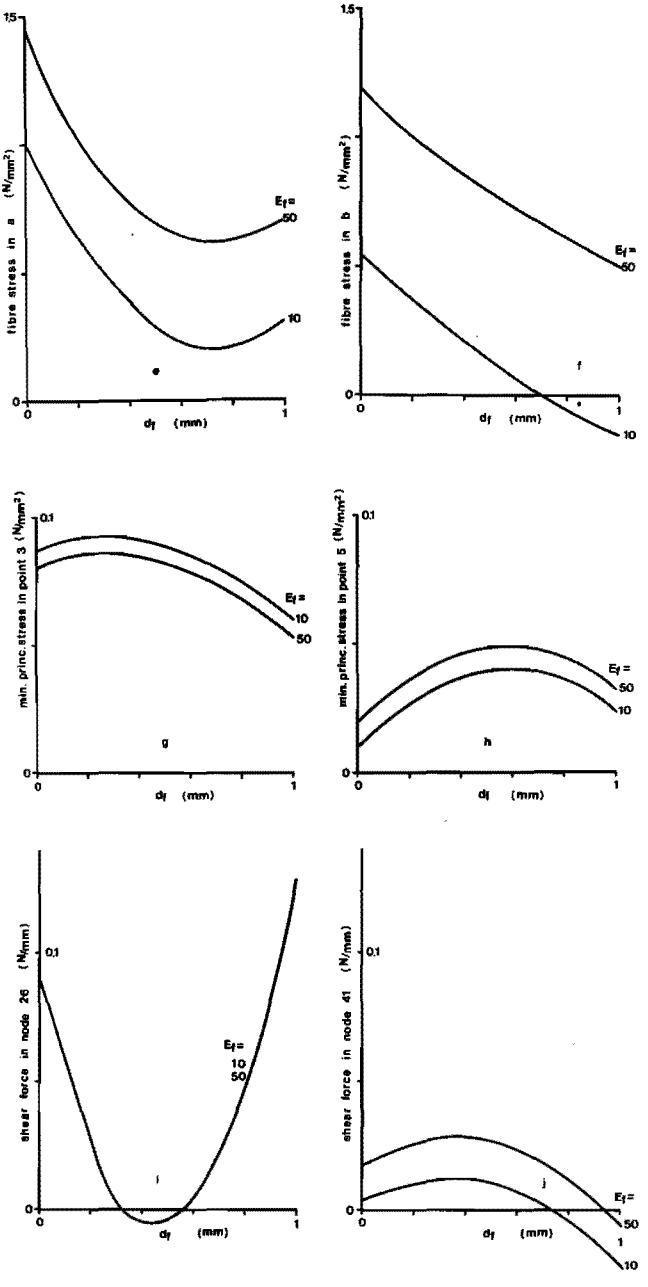
fibre stress in a (N/mm²)
15
Ef=
50
10
e
0
0
df (mm)
1
fibre stress in b (N/mm²)
1.5
Ef=
50
10
f
min. princ.stress in point 3 (N/mm²)
0.1
Ef=
10
50
g
min. princ.stress in point 5 (N/mm²)
0.1
Ef=
50
10
h
shear force in node 26 (N/mm)
0.1
Ef=
10
50
i
shear force in node 41 (N/mm)
0.1
j
Ef=
50
1
10

The shear force in node 26 is quite high in comparison with node 41 and almost independing on the fibre stiffness. The shear force in node 41 remains small when E_f ranges between 10 and 50 N/mm^2. Therefore, the value of E_f for the design has to be chosen primarily upon its influence on the von Mises intensities in membranes and fibre stresses. As it is expected that low membrane stresses are more important with regard to the prevention of valve failure than low fibre stress values, higher values of E_f are prefered here. Hence, as applicable range for E_f the interval $10 < E_f < 50$ N/mm^2 may be taken, whereby $E_f = 50$ N/mm^2 will be used for the actual design. With regard to the choice for the fibre thickness, the applicable values are restricted to values lower than the matrix thickness (0.4 mm). The reason for this is that a thicker leaflet in the fibre region than in between those fibres is probably disadvantageous to the calcification process as described in chapter 1. Besides, it is not advisable to increase the value of membrane thickness due to the bending strains acting during opening and closing (see chapter 5). On the other hand very low values lead to high values of nearly all stress quantities. Therefore, in case of $d_m = 0.4$ mm, as applicable range, the interval $0.2 < d_f < 0.3$ mm has been chosen. As design specification the arbitrary value of 0.25 mm will be taken.

Finally, for the specific design situation ($\alpha = 10^o$, stiff frame, $d_f = 0.25$ mm, $E_f = 50$ N/mm^2) the influence of the fibre-structure on the stress distribution is analysed for various values of the mean fibre distance. The results are tabulated in table 4.6.

	von Mises intensity (N/mm^2)				fibre stress (N/mm^2)		mfd (mm)
	1	2	3	4	a	b	
situation 1	0.200	0.140	0.179	0.150	0.94	1.34	1.5
situation 2	0.219	0.157	0.194	0.170	1.04	1.51	2.7
situation 3	0.244	0.172	0.238	0.261	-	-	∞

	neg.values min. princ.stress (N/mm^2)		shear force/ unit length (N/mm)		mfd (mm)
	3	5	26	41	
situation 1	0.108	0.049	0.0033	0.0240	1.5
situation 2	0.111	0.062	0.0040	0.0263	2.7
situation 3	0.123	0.034	--	--	∞

Table 4.6. Influence of the mean fibre distance

The difference between the fibre-reinforced basic situation (situation 1) and the situation without fibres (situation 3) amounts for all membrane stresses in the range of 20-75%. However, decreasing the mean fibre distance in case of fibre reinforcements (compare situations 1 and 2) leads to much lower values of changes in all stress quantities (< 15%). Hence, the mean fibre distance itself is not very critical, which is also seen from figure 4.7.e. As applicable range the interval 0.8 < mfd < 2.7 mm is chosen. For the design of the valve the value of 1.5 mm will be taken.

4.4. Discussion

From this parameter variation study some design specifications are obtained for a 23 mm leaflet valve prosthesis in closed position. In table 4.7 the intervals for the parameter values, together with the chosen values for the design are listed. An acceptable compromise at this moment is found for the following parameter values: $\alpha = 10^{o}$, a stiff frame, elastic modulus of fibre material $E_f = 50$ N/mm^2, fibre thickness $d_f = 0.25$ mm and a mean fibre distance mfd = 1.5 mm.

	applicable range of parameter values	chosen value for design
E_{FR}	1000-stiff frame	stiff
d_{FR}	0.5-1.5 mm	frame
α	0-20 deg	10 deg
A_{coap}	19-76 mm^2	38 mm^2
d_f	0.2-0.3 mm	0.25 mm
E_f	10-100 N/mm^2	50 N/mm^2
mfd	0.8-2.7 mm	1.5 mm
d_m	0.2-0.6 mm	0.4 mm
E_m	1-5 N/mm^2	1.8 N/mm^2

Table 4.7. Parameter values for the design

For the membranes an elastic modulus of $E_m = 1.8$ N/mm^2 and a thickness of $d_m = 0.4$ mm is chosen, while for the magnitude of the coaptation area a value of 38 mm^2 is taken.

These parameter values lead to a valve design which exhibits several great advantages. Firstly, due to the low α-value, the valve is relatively low. This has the great advantage that the valve implanted in the aortic position fits to the sinusses which is important for the closing behaviour. Furthermore, the valve may also be used in the mitral position where a low profile is sometimes needed due to lack of space in a small left ventricle. However, it has to be remarked that the hydrodynamics in the mitral position is totally different from the aortic position. The natural human mitral valve is a bi-leaflet valve in contrary to the aortic valve which has three leaflets. Therefore, for a mitral valve prosthesis probably a bi-leaflet prosthesis has to be developed. A great advantage of a stiff frame is that steel can be used as frame material; problems of polymer creep of a flexible frame are then overcome. When the frame of steel is covered with the same material as used for the leaflets (polyurethane), the leaflets may be glued to the frame which gives a solid attachment. The chosen ratio of fibre stiffness and membrane stiffness is about 25 with a fibre elastic modulus of 50 N/mm^2. The values are within the range of the material parameter values of polyurethanes which can be produced with standard synthesis techniques. Due to the use of the same material for fibres and membranes, glueing between both components will ensure a strong fibre-matrix connection. The fibres with a diameter of 0.25 mm can be fabricated by spinning techniques, while the leaflets can be made from prefabricated sheats in which fibres lay almost parallel with a fibre distance of about 1.5 mm. In conclusion, it is summarized that the valve aimed at is of a relatively simple design, will be easy to produce and will be applicable for both the aortic and the mitral position because of its small height.

In this analysis, fixed values for the membrane thickness (0.4 mm) and the membrane elastic modulus (1.8 N/mm^2) were assumed, based upon the values for the Hancock valve. For other values the determined ranges for the design parameter values may change. Besides, the above mentioned design is based upon quite arbitrary values within applicable intervals of each parameter. Hence, the present design study based upon the analysis of the leaflet valve in closed position is not conclusive. A more restrective choice has to be based upon an analysis of the opening and closing behaviour (see chapter 5).

Chapter 5 The desired follow-up study: the analysis of the valve during opening and closing

5.1. Introduction

Until now the design study was concerned with valve failure due to the stress situation in the closed loaded leaflet valve prosthesis. In chapter 1 it was stated that another very important unfavourable situation occurs when the valve is opening and closing. During this opening and closing phase the leaflets are bended and wrinkled, so that high bending strains arise. This may cause microtears in the leaflet in combination with leaflet calcification. In the future research, the main item is firstly to answer the question whether the varying bending strains are responsible for leaflet failure and calcification. When the bending strains are indeed related to tissue failure and calcification, the analysis of the mechanical behaviour of the valve prosthesis during opening and closing has to be performed. This can be done by developing a numerical model which predicts the bending strains in a leaflet valve prosthesis during that situation. The results of that model need to be verified by experiments. Finally, also for the opening and closing phase design specifications have to be formulated and combined with those of the closed valve.

In this chapter a preparatory study is described with regard to the possible relation between varying bending strain and calcification. A bending loading system and experimental method together with the preliminary results on polyurethane material strips are described in section 5.2. In section 5.3 some recommendations are made for the follow-up study of the mechanical behaviour of the leaflet valve prosthesis in opened position.

5.2. Bending equipment and preliminary results

5.2.1. Experimental equipment

One hypothesis states that one of the possible phenomena responsible for leaflet calcification is the appearance of varying bending strains in the material, which may introduce microtears in the leaflet surface where calcification then starts. To verify this

hypothesis an equipment has been designed in which (polyurethane) material strips are loaded with a well determined varying bending strain. This equipment (see figure 5.1) is constructed around a transparant lucite reservoir filled with a meta-stable calcium phosphate solution (buffered with barbital sodium, pH = 7.4, temp. = 37°C). In this equipment 4 lucite plates are present which are driven by a small electrical motor (Engel, GNM2130), a gear wheel transmission (Engel, G4) and a construction to transform the rotational movement into a translational one, (see figure 5.1). The outer two plates move 180° out of phase with the inner two, to eliminate the fluid mass inertia effects. Between those plates the polyurethane test specimens are clamped and they are submitted to a bending movement by which a specimen lays straight against one plate during one part of the loading cycle and which is curved circularly during another part of that cycle (see figure 5.2). This results in a varying bending strain in the specimen. The magnitude of the maximum bending strain in the circularly curved part of the specimen may be roughly estimated by:

$$\varepsilon_b = \frac{d}{D-d}$$

in which: d = specimen thickness

D = distance between two plates

while the bending strain in the straight part of the specimen equals zero. The thickness d of the polyurethane specimens (Biomer) is controlled during the fabrication process in our laboratory and is adjustable between 0.1 and 0.6 mm. The plate distance D can be adjusted in a range from 5 to 25 mm. The maximum bending strain in the specimens ranges then from about 1% to 14%. This is in agreement with the order of magnitude of bending strains found in leaflet valve prostheses by Thubrikar et al. (1982). They found in porcine leaflet valve prostheses bending strains in the leaflets of 5-6% in circumferential direction and of 10-12% in radial direction. The moving plates can be positioned slantingly to each other so that the test specimens between two plates have a different radius of curvature during the curved phase of the loading cycle, resulting in

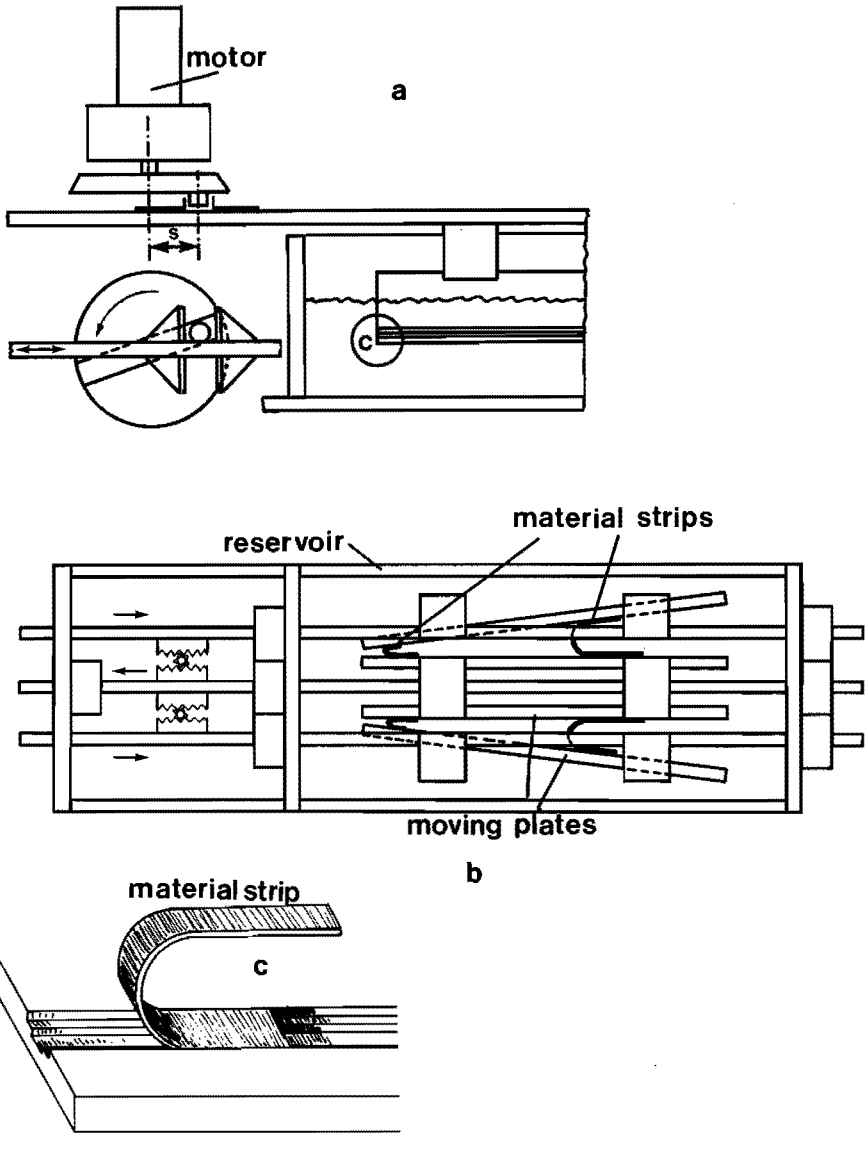

Fig. 5.1. bending equipment for polymer or biological material strips.
a. side view, showing the driving system.
b. upper view (the driving system is not drawn).
c. a schematic outline of the material strip positioned between the plates.

bending strains of different magnitude. In the moving plates grooves are present so that when the leaflet strip lays against the plate a certain part of the material strip is in contact with the fluid (see figure 5.2). The loading frequency is adjustable between 0 and 8 Hz and the amplitude of the sinusoidal movement (the strike s, see figure 5.1 and 5.2) between 0 and 40 mm. Furthermore, a temperature control and a pH-control are present. The number of cycles during an experiment is recorded with a mechanical counter. The test specimens are 10 mm wide and have a minimum length according to (see figure 5.2):

$$l_{sp} = 2\ s + \frac{1}{2}\pi D + 2l_{cl}$$

with s = strike of the moving plates
D = plate distance
l_{cl} = clamp length

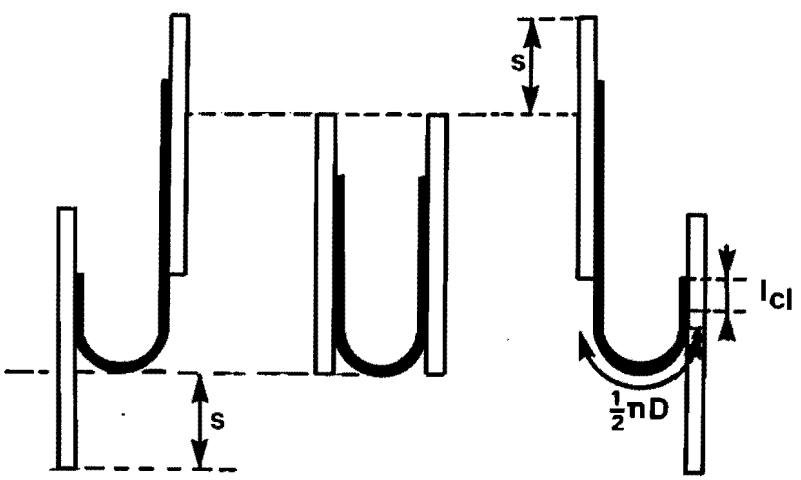

Fig. 5.2. the movement of the plates and the deformations of the material strips.

12 material strips were loaded with 1.5 million bending cycles (frequency 8 Hz), the maximum bending strain in the strips varying between 3 and 9%. During the loading cycles, the temperature and pH remained at a constant value (37^{o}C and 7.4 respectively). As a reference, 2 unloaded material strips were positioned in the reservoir.

They were positioned at the same height in the reservoir as the loaded strips; in such a way that the total strip surfaces were surrounded with the calcium solution. After loading, one half of the strips were analysed quantitatively by measuring the amount of phosphate present in the deposition at the central parts of the strips after dissolving the deposits. To that end 2 compounds were added to the deposit (molybdate and vanadate). The phosphate which is a main component in the deposit reacts with both, forming mixed hetero polyacid. This compound adsorbs light of a certain wavelength (400 nm). The light adsorbtion is measured with a UV-spectrofotometer which is a measure for the phosphate-concentration (Boltz and Howell, 1977). For completeness it is remarked that before quantitative analysis, from each strip 10 mm of both ends were cut off, to eliminate the clamp effects. The other half of the material strips were analysed qualitatively. The mineralogic composition was determined by X-ray fluorescence and X-ray diffraction while for a loaded and an unloaded strip scanning electron microscopical photographs of the material surface were made.

5.2.2. Results

Table 5.1 shows the amount of phosphate per unit area deposited on the surfaces of the strips. The unloaded specimens show hardly any calcium deposits, while the loaded strips all show a considerable amount of calcification. However, there is no clear relationship between the amount of calcium deposits and the magnitude of the varying bending strain.

bending strain [%]	deposit of PO_4 [$\mu g/mm^2$]
0	0.0006
3.8	0.016
4.8	0.008
5.5	0.014
6.5	0.014
8.4	0.016

Table 5.1. Phosphate deposits per unit area on the different material strips. The standard deviation amounts to 0.0015 $\mu g/mm^2$.

From the mineralogic analyses it was concluded that the calcium deposits are amorphous calcium (ortho) phosphate ($Ca_3(PO_4)_2$). In figure 5.3 the scanning electron microscopical photograph of the surface of a loaded and an unloaded strip are given, showing that the calcium deposits exist out of reasonable big plaques with cracks and tears and that the plaques are distributed at random over the whole surface. Furthermore, a clear difference is observed between the calcium depositions on the loaded and the unloaded strip, which is in agreement with the quantitative results.

5.2.3. Discussion

From these in-vitro experiments the conclusion is drawn that varying bending strains may lead to leaflet calcification. Further research has to be performed to investigate the relation between the amount of calcification and the magnitude of the varying bending strain; in the studied range of bending strains (3-9%) no such relation was observed. From literature it is known that the calcification process is also dependent on many other phenomena. For example, in-vivo calcification is influenced by surface condition (Merrill, 1977), surface loading (Coleman, 1981), chemical structure of the material (Long and Urry, 1981) and the local hemodynamic situation (Coleman, 1981). Hence, a further study of the calcification process is desired. However, from the present preliminary study it is postulated that for the design of a valve prosthesis it is also important to minimize the bending strain during a cardiac cycle. This may lead to adjustments of the design specifications for the closed valve.

5.3. Discussion, some recommendations

On the base of this preparatory study it is hypothesized that the closing and opening phase of the cardiac cycle causes an unfavourable situation for the leaflet valve prostheses. Especially the leaflet calcification, which is shown to be present in case of a time-varying bending strain, is a very annoying problem. Hence, it is necessary to determine the bending strains in a valve prosthesis during opening and closing. More precisely, to understand the important phenomena on the stresses during the opening and closing phase a numerical model is desired in which a parameter variation can be performed in a similar way as in the model of the closed valve (chapter 4). The bending strains could be determined for example by replacing the membrane and cable elements of the numerical model for the closed valve by shell and beam elements respectively.
The problems in this approach are:

- The valve loading during the opening and closing phase, which consists of a 3 dimensional instationary flow field around the valve.
- Knowing the load, the leaflet geometry has to be calculated, starting from a certain reference situation (for example the closed situation).

As an alternative, a pure kinematical model may be designed in which the leaflets are substituted by a fibre network. In that case the loading is not relevant and only a numerical method has to be developed to describe the kinematics of the leaflet movements.

Furthermore, the relation between leaflet calcification and the magnitude of varying bending strain has to be verified for total leaflet valve prostheses. For this purpose, an equipment has been designed (Rousseau et al., 1984) in which a total leaflet valve prostheses can be loaded physiologically in an accelerated way up to a frequency of 10 Hz. Finally with the obtained model for prediction of the bending strain, the design parameters of the closed valve need to be adjusted to also minimize the bending strains in the opened valve.

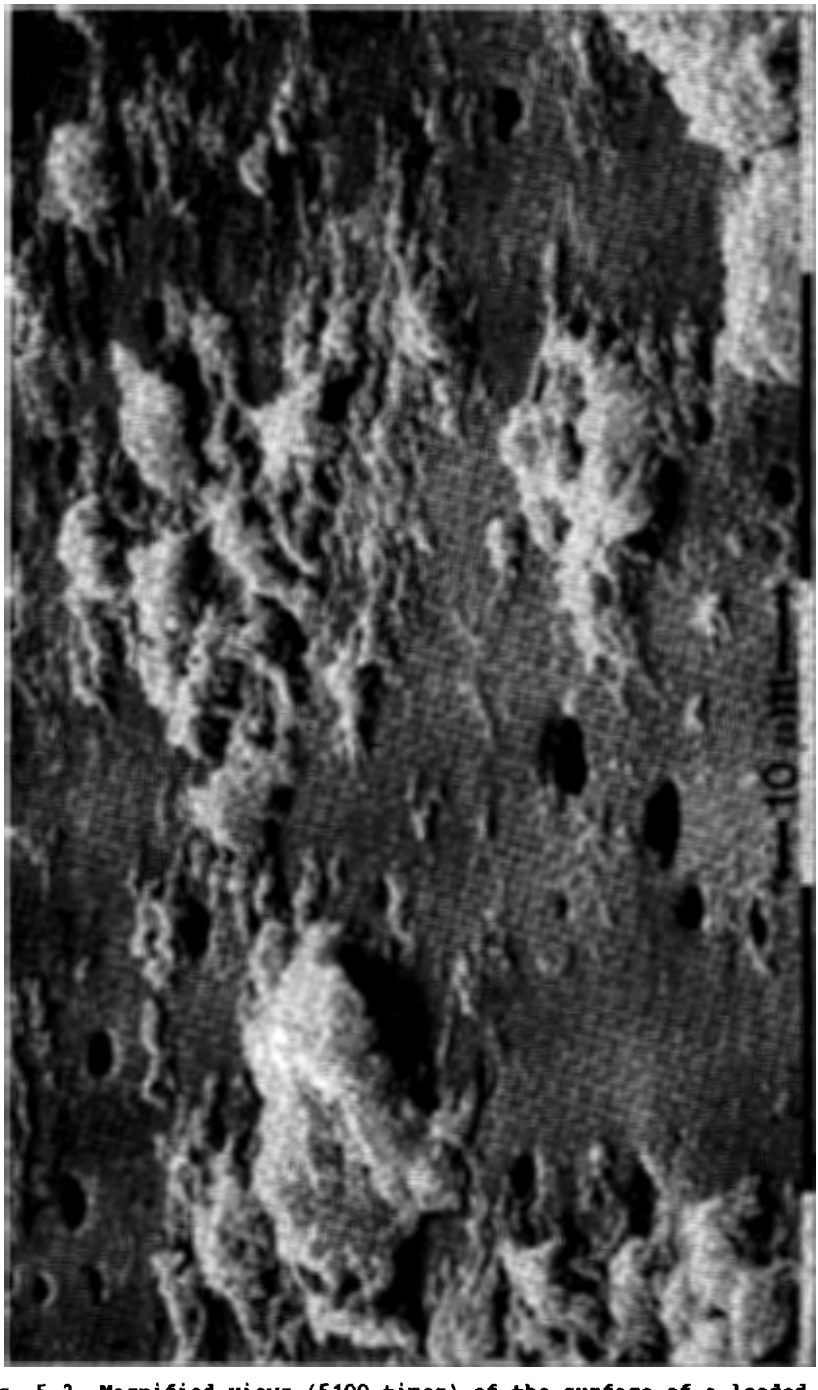

Fig. 5.3. Magnified views (5100 times) of the surface of a loaded material strip (a) and an unloaded strip (b).

b: unloaded strip

Chapter 6 Summary and conclusions

The investigations described in this thesis were intended to formulate mechanical specifications for the design of an artificial leaflet valve prosthesis. This research is part of a larger project founded upon the opinion that a detailed analysis of the behaviour of the natural aortic valve may lead to a better understanding of the relevant design parameters of such a valve. To that end in earlier studies, the hydrodynamical, the mechanical and the kinematical aspects of the natural aortic valve behaviour were studied. Because of the stress reducing mechanisms found to be present in the natural aortic valve, a leaflet valve prosthesis is pursued which exhibits the main characteristics of the natural aortic valve. However, for clinical practice some design restrictions had to be made and therefore we focus in this study upon a leaflet valve prosthesis in which 3 fibre reinforced artificial leaflets are suspended to a frame which is allowed to be flexible to ensure commissure displacements. The geometry of the frame and the leaflets has to be such that it fits optimally to the sinuses to provide a gradual valve closure.

Firstly, the failure phenomena of leaflet valve prostheses are summarized from literature. This revealed that these phenomena basically may be divided in three types: i) tears and perforations into the central portions of the leaflets, ii) tears in the leaflet in the vicinity of the commissures and iii) calcification of the leaflets, the plaques are localized in central regions and at the base along the leaflet attachment. The stress- and strain distribution in two phases of the cardiac cycle are thought to be at least in part responsible for those failure mechanisms: the closed loaded situation and the closing- and opening behaviour of the leaflets. It is plausible that the tears and perforations in the leaflets near the commissures are caused by high tensile stresses during the closed loaded phase. The fact that tears may grow perpendicular to the free edge may indicate that in that region, besides rupture of the membrane parts also fibre break occurs due to high tensile stresses in the fibres. Besides, as a consequence of the fibre network, it may not be excluded that the membraneous parts between the fibres wrinkle in parts of the coaptation area which are not loaded. Finally tearing of the fibres from the matrix may occur by high shear forces per unit

length between fibre and matrix. In the opened valve situation it is hypothesized that the tears and perforations in the central part of the leaflet in the vicinity of the leaflet attachment are caused by high bending strains. In these regions leaflet calcification was also observed.

In this thesis the main attention is focussed upon the first of the postulated two unfavourable valve loading situations during the cardiac cycle, being the closed situation. For this situation, a numerical model was made to predict stresses and strains in a leaflet valve prosthesis, which model was verified experimentally for a Hancock bioprosthesis. To that end, the geometry and material parameters of the Hancock valve had to be accurately known. The frame geometry was exactly known by the Hancock designs. The leaflet geometry was characterized by the leaflet surface areas, the commissure heights and the suspension angle. A remarkable difference between the geometry of the 3 valve parts was found. The elastic and viscoelastic material properties of the Hancock leaflet tissue, the fresh and glutaraldehyde treated porcine aortic valve leaflets and the frame were determined in uniaxial tensile experiments. The specimens were stretched with constant strain rates and subsequently kept at a constant stretched length. As a result of the glutaraldehyde treatment, the stress-strain curve for the leaflet tissue shifts towards the stress-axis with respect to the curve obtained in the fresh state. From the relaxation functions it was observed that the fresh leaflet tissue shows much more relaxation than the treated one and remarkably more than the Hancock leaflet tissue. The viscoelastic material behaviour of the different materials could be well described using the model of Fung.

The mechanical behaviour of the closed Hancock valve was examined using a non-linear finite element program. For sake of reduction of calculation time, the numerical model was restricted to 1/6 part of the valve. First, the separate frame was analysed numerically. The frame was loaded and unloaded by prescribing a radial frame top displacement. The force-displacement relation of the frame top was determined for some values of loading velocity and for some different valve sizes. These relations were also obtained experimentally by loading and unloading several frames and recording the force and the

displacement signals. The numerical predicted force-displacement relations appeared to be in accordance with the experimental results. Experimentally, the slope of the ascending line (α) and the amount of hysteresis (β) are not statistically significantly dependent on frame top number, frame size or loading velocity. On the contrary, the numerical predicted value of α shows a slight increase with increasing frame size. Furthermore the experimental results verify the model assumption that the influence of the a-symmetry of the frame itself on its force-displacement relation is negligible. Finally, the experiments revealed that the clothed frames are stiffer than the non-clothed ones.

Next, the entire valve was analysed numerically. The valve model was built up by 75 nodes and 136 elements. The valve was assumed to be fixed rigidly at the base and was loaded incrementally with two different time varying uniform pressure loads: i) a linear with time increasing load followed by a decreasing load with the same velocity, and ii) a physiological loading. The following stress quantities were determined: i) the von Mises intensity in the membrane parts which has a maximum in the vicinity of the commissure and amounts to about 0.20 N/mm^2 at a pressure load of 12 kPa, ii) the tensile fibre stress which has a maximum value of 0.64 N/mm^2 in a fibre in the coaptation area near the aortic ring, iii) the negative values for the minimum principal stress in the membranes between the fibres which are concentrated in the coaptation area in the vicinity of the leaflet suspension ($\sim$ 0.1 N/mm^2), and iv) the shear force per unit length between fibre and matrix in two arbitrary nodes (0.005 and 0.012 N/mm respectively). Furthermore, for experimental verification the next displacements in the valve were calculated: i) the radial commissure displacement and ii) the axial displacement of the leaflet center.

The commissure displacements of the entire valve were measured using an inductive measuring technique which consists essentially of 2 small electrical coils. One coil was sutured at the commissure whereas the other coil was glued to the nearest opposite wall of the valve housing. The time varying current through the coil on the valve housing induced a voltage in the coil on the commissure from which the distance between the 2 coils was derived. The measured commissure displacements were compared with the numerical results for the two different load patterns: linear with time loading and unloading and

the physiological load pattern. It was observed that in both the numerical and experimental case, the relation between commissure displacement and pressure load is linear and that this relation is independent of the loading type. The amount of hysteresis is negligible except for very low loading velocities; then a remarkable hysteresis loop was found. Experimentally a remarkable difference was observed between the commissure displacements of the 3 commissures of one valve. To analyse numerically the influence of the a-symmetry of the valve upon the displacements of leaflet center and commissures, a simplified numerical model was designed of the total valve. Here, linear elastic material behaviour and a linear relationship between strain and elongation was assumed. With this simplified a-symmetrical model the differences between the commissure displacements of the 3 frame tops could be quite well predicted.

The leaflet center displacement was measured cinematographically for the quasi-static loading case. For the physiological loading case this quantity was calculated by integrating the leaflet center velocity measured with an adjusted ultrasonic Doppler device. The position of the probe was such that only the axial component of the leaflet velocity was measured. Numerically as well as experimentally, the relation between leaflet center displacement and the pressure load appeared to be non-linear and shows an amount of hysteresis. However, the numerical predictions of the leaflet center displacement are systematically about 40% higher than the measured leaflet displacements which is certainly related to the fact that the leaflet center displacement is dependent on nearly all geometry- and material parameters of the valve as observed from the model sensitivity analysis. From these results it is stated that the numerical model of the Hancock valve yields a reliable picture of the mechanical behaviour of that valve.

Next, the numerical model was used for a parameter variation study to formulate design specifications for a new leaflet valve prosthesis. A symmetrical leaflet valve prosthesis is analysed in which the leaflets are directly connected to a flexible frame. The fibre reinforced structure is designed so that all fibres run almost parallel and that all fibres are directly suspended to the frame. The frame posts are very narrow so that they fit the natural sinuses. This valve is modelled analogously to the numerical model of the

Hancock valve. The valve was loaded with a pressure load of 12 kPa realized in 10 ms. In this parameter variation study 9 geometry and material parameters were chosen as the independent parameters. As dependent parameters 10 stress quantities were chosen: the von Mises intensity in 4 discrete membrane points, the tensile fibre stress for 2 fibre points, the negative value of the minimum principal stress in 2 membrane points in the coaptation area and finally the shear force per unit length between fibre and matrix in 2 nodes. Firstly, the global influence of the 9 design parameters on the 10 stress parameters were studied by setting the design parameters to their outermost values and observing the changes in the stress parameters. From this global survey it was concluded that just 5 parameters are of real importance for the stresses in the closed loaded valve. These are: i) the angle α between the leaflet middle line and the horizontal plane (see fig. 4.1), ii) the frame thickness d_{FR}, iii) the fibre thickness d_f, iv) the elastic modulus of the fibres E_f and v) the mean fibre distance mfd. In a further analysis these 5 parameters were varied separately in smaller steps to study the range of interest and to observe the global relationships between the stress quantities and the design parameters. These approximated relationships were used in a statistical analysis in which linear models were used to describe the relation between stress- and design parameters. For this purpose 27 calculations were performed with different adjustments for the design parameters. As a result, all stress quantities were plotted against the design parameters. From these plots it was observed that for small values of α ($\alpha \approx 10^{o}$) a favourable stress distribution is found. Furthermore, it was observed that for the most stress quantities a stiff frame ($1/d_{FR}^2 \approx 0$) leads to small stress values. For the elastic modulus of the fibre material and fibre thickness a compromise had to be made. Values of 50 N/mm^2 and 0.25 mm were chosen. For the membranes these values are equal to 1.8 N/mm^2 and 0.4 mm respectively. Finally, using these values for the design parameters the mean fibre distance mfd was studied separately. From this separate study it was found that an applicable mean fibre distance amounts to 1.5 mm.

In future research the mechanical behaviour of the leaflet valve prosthesis during the opening and closing phase has to be evaluated in order to formulate additional specifications for the valve in the

opening and closing phase. During that phase the leaflets are bended and wrinkled so that high bending strains occur. This may introduce microtears in the leaflet in combination with leaflet calcification. From a preparatory in-vitro study the conclusion was drawn that varying bending strains indeed lead to calcification, although the amount of calcification could not yet be related to the magnitude of the varying bending strain. This study has also to be pursued in the future.

References

- Akutsu, T., Dreyer, B. and Kolff, W.J.:
  Polyurethane artificial heart valves in animals,
  J. Applied Physiology, 14, pp 1045-1048, 1959.

- Arts, T. and Reneman, R.S.:
  Measurement of deformation of canine epicardium in vivo during cardiac cycle,
  Am. J. Physiol., 239, pp 432-437, 1980.

- Austen, W.G. and Hutter, A.M.:
  Acquired mitral and tricuspid valvular disease,
  Chapter 58 in: "Textbook of surgery" (ed. by Sabiston, D.C.),
  Philadelphia, W.B. Saunders Company, 1977.

- Björk, V.O.:
  A new tilting disc valve prosthesis,
  Scand. J. Thorac. Cardiovasc. Surg., 3, pp 1-10, 1969.

- Bodnar, A. and Ross, D.N.:
  Mode of failure in 226 explanted biologic and bioprosthetic valves, chapter 35 from: "Cardiac bioprostheses, proceedings of the second international symposium" edited by L.H. Cohn and V. Gallucci;
  New York, York Medical Books, 1982.

- Boltz, D.F. and Howell, J.A.:
  chapter 9 in: "Colorimetric determination of nonmetals, Chemical analysis, vol. 8"
  New York, John Wiley & Sons, 1977.

- Boretos, J.W.:
  Past, present and future role of polyurethanes for surgical implants,
  Pure and Applied Chemistry, 52, pp 1851-1855, 1981.

- Borkon, A.M., McIntosh, C.L., Jones, M., Roberts, W.C. and Morrow, A.G.:
  Inward stent-post bending of a porcine bioprosthesis in the mitral position; cause of bioprosthetic dysfunction,
  J. Thorac. Cardiovasc. Surg., 83, pp 105-107, 1982.

- Braunwald, N.S. and Morrow, A.G.:
  A late evaluation of flexible Teflon prostheses utilized for total aortic valve replacement; postoperative clinical, hemodynamic and pathological assessments,
  J. Thorac. Cardiovasc. Surg., 49, pp 485-496, 1965.

- Brawley, R.K., Donahoo, J.S. and Gott, V.L.:
  Current status of the Beall, Björk-Shiley, Braunwald-Cutter, Lillehei-Kaster and Smeloff-Culter cardiac valve prostheses,
  Am. J. Cardiol., 35, pp 855-865, 1975.

- Broom, N.D.:
  Fatigue-induced damage in glutaraldehyde-preserved heart valve tissue,
  J. Thorac. Cardiovasc. Surg., 76, pp 202-211, 1978.

- Broom, N.D. and Thomson, F.J.:
  Influence of fixation conditions on the performance of glutaraldehyde-treated porcine aortic valves: towards a more scientific basis,
  Thorax, 34, pp 166-176, 1979.

- Brown, J.W., Dunn, J.M., Spooner, E. and Kirsch, M.M.:
  Late spontaneous disruption of a porcine xenograft mitral valve; Clinical, hemodynamic, echocardiographic and pathological findings,
  J. Thorac. Cardiovasc. Surg., 75, pp 606-611, 1978.

- Bruck, S.D.:
  Possible causes for the calcification of glutaraldehyde-treated tissue heart valves and blood contacting elastomers during prolonged use in medical devices: a physico-chemical view,
  Biomaterials, 2, pp 14-18, 1981.

- Carpentier, A., Deloche, A., Relland, J., Fabian, J.N., Forman, J., Camilleri, J.P., Soyer, R. and Dubost, Ch.:
  Six year follow-up of glutaraldehyde-preserved heterografts; with particular reference to the treatment of congenital valve malformations,
  J. Thorac. Cardiovasc. Surg., 68, pp 771-782, 1974.

- Carpentier, A. and Dubost, C.:
  From xenograft to bioprosthesis: evolution of concepts and techniques of valvular xenografts, chapter 22 in "Biological tissue in heart valve replacement" (edited by Ionescu, M.I., Ross, D.N., Wooler, G.H.), pp 515-541, London, Butterworths, 1972.

- Chatfield, C.:
  Statistics for technology; a course in applied statistics,
  London/New York, Chapman and Hall, 1983.

- Chetta, G.E. and Lloyd, J.R.:
  The design, fabrication and evaluation of a trileaflet prosthetic heart valve,
  J. Biomech. Engng., 102, pp 34-41, 1980.

- Coleman, D.L.:
  Mineralization of blood pump bladders,
  Trans. Am. Soc. Artif. Intern. Organs, 27, pp 708-713, 1981.

- Coleman, D.L., Lim, D., Kessler, T. and Andrade, J.D.:
  Calcification of nontextured blood pumps,
  Trans. Am. Soc. Artif. Intern. Organs, 27, pp 97-103, 1981.

- Christie, G.W. and Medland, I.C.:
  A non-linear finite element stress analysis of bioprosthetic heart valves.
  Chapter 9 in: "Finite elements in biomechanics", (edited by R.H. Gallagher, B.R. Simon, P.C. Johnson and J.F. Gross),
  New York, John Wiley & Sons Ltd., 1982.

- Clark, R.E. and Swanson, W.M.:
  In-vitro durability of Hancock model 242 porcine heart valve,
  J. Thorac. Cardiovasc. Surg., 78, pp 277-280, 1979.

- Cohn, L.H. and Collins, J.J.:
  The glutaraldehyde stabilized porcine xenograft valve, Chapter 5 in: "Tissue heart valves" (ed. by Ionescu, M.),
  London, Butterworths, 1979.

- Cooley, D.A.:
  The quest for the perfect prosthetic heart valve,
  Med. Instrument, 11, pp 82-84, 1977.

- Crissman, J.M. and Zapas, L.J.:
  Mechanical behaviour of isotactic polypropene subjected to various strain histories in uniaxial extension,
  Polymer, 24, pp 351-358, 1983.

- Dale, J.:
  Arterial thromboembolic complications in patients with Björk-Shiley and Lillehei-Kaster aortic disc valve prostheses,
  Am. Heart J., 93, pp 715-722, 1977.

- Davies, M.J.:
  The pathology of valve surgery, chapter 6 in "Pathology of cardiac valves", pp 153-172,
  Butterworths, London-Boston, 1980.

- Dortmans, L.J.M.G., Sauren, A.A.H.J. and Rousseau, E.P.M.:
  Parameter estimation using the quasi-linear viscoelastic model proposed by Fung,
  J. Biomech. Engng., pp 198-203, 106, 1984.

- Drury, P.J., Bodnar, E. and Ross, D.N.:
  Flexibility measurements in cardiac valve support frames,
  Art. Org., 5 (suppl), pp 556-559, 1981.

- D.S.M. information, Stamylan P, 1977.

- Emery, R.W., Palmquist, W.E., Mettler, E. and Nicoloff, D.M.:
  A new cardiac valve prosthesis: In-vitro results,
  Trans. Am. Soc. Artif. Intern. Organs, 24, pp 550-555, 1978.

- Eyster, E., Rothchild, J. and Mychajliw, A.A.S.:
  Chronic intravascular hemolysis after aortic valve replacement,
  Circulation, 44, pp 657-665, 1971.

- Figliola, R.S. and Mueller, T.J.:
  Fluid stresses in the vicinity of disc, ball and tilting disc prosthetic heart valves from in-vitro measurements,
  J. Biomech. Engng., 99, pp 173-177, 1977.

- Figliola, R.S. and Mueller, T.J.:
  On the hemolytic and thrombogenic potential of occluder prosthetic heart valves from in-vitro measurements.
  J. Biomech. Engng., 103, pp 83-90, 1981.

- Fung, Y.C.B.:
  Stress-strain history relations of soft tissues in simple elongation, chapter 7 in "Biomechanics, its foundations and objectives" (edited by Fung, Y.C.B., Perrone, N. and Anliker, M.), pp 181-208,
  Englewood Cliffs, N.J., Prentice Hall, 1972.

- Gerring, E.L., Bellhouse, B.J., Bellhouse, F.H. and Haworth, W.S.:
  Long term animal trials of the Oxford aortic/pulmonary valve prosthesis without anticoagluants,
  Trans. Am. Soc. Artif. Intern. Organs, 20, pp 703-708, 1974.

- Gilding, D.K., Reed, A.M., Askill, I.N., Briana, S. and Jones, R.D.:
  A new polyether urethane for critical medical applications,
  pp 1-16,
  Transactions 2nd World Congres for Biomaterials, Washington D.C., 1984.

- Ghista, D.N. and Reul, H.:
  Optimal prosthetic aortic leaflet valve: design parametric and longevity analyses; development of the Avcothane-51 leaflet valve based on the optimum design analyses,
  J. Biomechanics, 10, pp 313-323, 1977.

- Haüssinger, G. and Reul, H.:
  In-vitro fatigue test results and hemolysis of a flexible leaflet valve,
  Biomed. Technik, 26, pp 40-43, 1981.

- Haworth, W.S., Lewis, R.W.H., Bellhouse, B.J. and Bellhouse, F.H.:
  Design and use of a new machine for accelerated fatigue testing of prosthetic heart valves,
  Trans. Am. Soc. Artif. Intern. Organs, 1, pp 138-142, 1978.

- van Heck, J.G.A.M.:
  On the dynamic characteristics of slideways,
  Ph D. Thesis, University of Technology, Eindhoven, The Netherlands, 1984.

- Hennig, E., Keilbach, H., Hoder, D. and Bücherl, E.S.:
  Calcification of artificial heart valves and artificial hearts,
  Abstract Trans. Am. Soc. Artif. Intern. Organs, pp 10-27, 1981.

- Housman, L.B., Pitt, W.A., Mazur, J.H., Litchford, B. and Gross, S.A.:
  Mechanical failure (leaflet disruption) of a porcine aortic heterograft; rare cause of acute aortic insufficiency,
  J. Thorac. Cardiovasc. Surg., 78, pp 212-213, 1978.

- Ionescu, M.I. and Ross, D.N.:
  Heart valve replacement with autologous fascia lata,
  Lancet, pp 335-338, 1969.

- Ishihara, T., Ferrans, V.J., Boyce, S.W., Jones, M. and Roberts, W.C.:
  Structure and classification of cuspal tears and perforations in porcine bioprosthetic cardiac valves implanted in patients, chapter 33 in: "Cardiac Bioprostheses", (ed. by Cohn, L.H. and Gallucci, V.),
  New York, York Medical Books, 1982.

- Kiraly, R.J., Hillegass, D.V., Snow, J.L. and Nosè, Y.:
  Hexsyn leaflet valve,
  Artif. Organs, 5 (suppl.), pp 323-326, 1981.

- Lefemine, A.A., Miller, M. and Pinter, G.C.:
  Chronic hemolysis produced by cloth clovered valves,
  J. Thorac. Cardiovasc. Sur., 67, pp 857-862, 1974.

- Lefrak, E.A. and Starr, A.:
  Porcine aortic valve xenograft, chapter 15 in "Cardiac valve prostheses", pp 301-329,
  New York, Appleton Century Crofts, 1979.

- Leliveld, W.H.:
  The design of a mock circulation system,
  Report Eindhoven University of Technology, no. 74-E-47, 1974.

- Lennox, S.C.:
  Valve replacement,
  Chapter 16 in: "Recent advances in cardiology" (ed. by Hamer. J.),
  Edinburgh, Churchill Livingstone, 1973.

- Liotta, D., Messmer, B.J., Hallman, G.L., Hall, R.J., Martin, C., Chafizadeh, G.N. and Cooley, D.A.:
  Prosthetic and fascia lata valves: hydrodynamics and clinical results,
  Trans. Am. Soc. Artif. Intern. Organs, 16, pp 244-251, 1970.

- Long, M.M. and Urry, D.W.:
  On the molecular mechanism of elastic fiber calcification,
  Trans. Am. Soc. Artif. Intern. Organs, 27, pp 690-696, 1981.

- Magilligan, D.J., Fischer, E. and Alam, M.:
  Hemolytic anemia with porcine xenograft aortic and mitral valves,
  J. Thorac. Cardiovasc. Surg., 79, pp 628-631, 1980.

- MARC Analysis Research Corporation, User manual, 1983.

- McAlpine, W.A.: Heart and coronary arteries.
  Berlin, Springer Verlag, 1975.

- McIntosh, C.L., Michaelis, L.L., Morrow, A.G., Itscoitz, S.B., Redwood, D.R. and Epstein, S.E.:
  Atrioventricular valve replacement with the Hancock porcine xenograft: A five year clinical experience,
  Surgery, 78, pp 768-775, 1975.

- McMillen, C.R.:
  Physical testing of elastomers for cardiovascular applications,
  Art. Org., 7, pp 78-91, 1983.

- Merrill, E.W.:
  Properties of materials affecting the behavior of blood at their surfaces, In: "The behavior of blood and its components at interfaces" eds L. Vroman and E.F. Leonard, Annals of the New York Academy of Sciences, pp 6-17, vol. 283,
  New York, New York Acad. of Sciences, 1977.

- Missirlis, Y.F. and Chong, M.:
  Aortic valve mechanics. Part I: Material properties of natural porcine aortic valves,
  J. Bioengng., 2, pp 287-300, 1978.

- Mohri, H., Hessel, E.A., Nelson, R.J., Anderson, H.N., Dillard, D.H. and Merendino, K.A.:
  Design and durability test of Silastic trileaflet aortic valve prostheses,
  J. Thorac. Cardiovasc. Surg., 65, pp 576-582, 1973.

- Mueller, T.J., Underwood, F.N., Lloyd, J.R. and MacDonell, E.H.:
  Numerical and experimental fluid dynamics studies related to prosthetic heart valve thrombus formation and erythrocyte damage,
  Paper Euromech., 67, Resp. Cardiovasc. Mech., Aachen, 1975.

- Muller, W.H. and Nolan, S.P.:
  Acquired disorders of the aortic valve,
  Chapter 58 in: "Textbook of surgery" (ed. by Sabiston, D.C.),
  Philadelphia, W.B. Saunders Company, 1977.

- Munro, M. and Beaumont, P.W.R.:
  Fracture mechanisms and toughening of fibre composites,
  ICM, 3, pp 253-261, 1979.

- Nosé, Y., Harasaki, H. and Murray, J.:
  Mineralization of artificial surfaces that contact blood,
  Trans. Am. Soc. Artif. Intern. Organs, 27, pp 714-719, 1981.

- Pohlner, P.G., Thomson, F.J., Hjelms, E. and Barratt-Boyes, B.G.:
  Experimental evaluation of aortic homograft valves mounted on flexible support frames and comparison with glutaraldehyde-treated porcine valves,
  J. Thorac. Cardiovasc. Surg., 77, pp 287-293, 1979.

- van Renterghem, R.J.:
  Aortic valve geometry during the cardiac cycle,
  Thesis University of Limburg, The Netherlands, 1983.

- Reul, H., Hennig, E., Tillmann, W., Herold, M. and Bücherl, E.:
  In-vitro and in-vivo studies at two newly developed prosthetic heart valves,
  Proc. Eur. Soc. Artif. Organs, 7, pp 327-331, 1980.

- Roff, W.J., Scott, J.R. and Pacitti, J.:
  Fibres, films, plastics and rubbers; handbook of common polymers.
  Butterworth, London, 1971.

- Rousseau, E.P.M., Sauren, A.A.H.J., van Hout, M.C. and van Steenhoven, A.A.:
  Comparative tensile and relaxation experiments on fresh and glutaraldehyde treated porcine aortic valve tissue,
  Zeitschrift Biomed. Technik, 26, pp 98, 1981.

- Rousseau, E.P.M., Sauren, A.A.H.J., van Hout, M.C. and van Steenhoven, A.A.:
  Elastic and viscoelastic materialbehaviour of fresh and glutaraldehyde treated porcine aortic valve tissue,
  J. Biomechanics, 16, pp 399-348, 1983a.

- Rousseau, E.P.M., van Steenhoven, A.A., Sauren, A.A.H.J. and van Renterghem, R.J.:
  A numerical model for the analysis of the mechanical behaviour of a leaflet valve prosthesis,
  pp 217-220 in: "1983 Biomechanics Symposium", (ed. by Woo, S.L. and Mates, R.E.), New York, ASME, 1983b.

- Rousseau, E.P.M., van de Ven, A.P.C., van Steenhoven, A.A. and Seroo, J.M.:
  Design of a system for the accelerated loading of heart valve prostheses,
  J. Biomechanics, 17, pp 145-153, 1984.

- Russell, F.B., Lederman, D.M., Singh, P.I., Cumming, R.D., Morgan, R.A., Levine, F.H., Austen, W.G. and Buckley, M.J.:
  Development of seamless tri-leaflet valves,
  Trans. Am. Soc. Artif. Intern. Organs, 26, pp 66-71, 1980.

- Salomon, N.W., Copeland, J.G., Goldman, S. and Larson, D.F.:
  Unusual complication of the Hancock porcine heterograft; Strut compression in the aortic root,
  J. Thorac. Cardiovasc. Surg., 77, pp 294-296, 1979.

- Sauren, A.A.H.J., Kuypers, W., van Steenhoven, A.A. and Veldpaus, F.E.:
  Aortic valve histology and its relation with mechanics,
  J. Biomechanics, 13, pp 97-104, 1980.

- Sauren, A.A.H.J.:
  The mechanical behaviour of the aortic valve,
  Thesis University of Technology Eindhoven, The Netherlands, 1981.

- Sauren, A.A.H.J., van Hout, M.C., van Steenhoven, A.A., Veldpaus, F.E. and Janssen, J.D.:
  The mechanical properties of porcine aortic valve tissues,
  J. Biomechanics, 16, pp 327-337, 1983.

- Sauren, A.A.H.J. and Rousseau, E.P.M.:
  A concise sensitivity analysis of the quasi-linear viscoelastic model proposed by Fung,
  J. Biomech. Engng., 105, pp 92-95, 1983.

- Schoen, F.J., Titus, J.L. and Lawrie, G.M.:
  Bioengineering aspects of heart valve replacement
  Annals Biomech. Engng., 10, pp 97-128, 1982.

- Senning, A.:
  Fascia lata replacement of aortic valves,
  J. Thorac. Cardiovasc. Surg., 54, pp 465-470, 1967.

- Smith, A. and Bruton, J.:
  in: "Color atlas of histological staining techniques".
  Chicago, Med. Publ. Inc., 1977.

- Starr, A.:
  Total mitral valve replacement: fixation and thrombosis,
  Surgic. Forum, 11, pp 258-260, 1960.

- van Steenhoven, A.A.:
  The closing behaviour of the aortic valve,
  Thesis University of Technology, Eindhoven, The Netherlands, 1979.

- van Steenhoven, A.A. and van Dongen, M.E.H.:
  Model studies of the closing behaviour of the aortic valve,
  J. Fluid Mech., 90, pp 21-36, 1979.

- van Steenhoven, A.A., Verlaan, C.W.J., Veenstra, P.C. and Reneman, R.S.:
  The closing behaviour of the natural aortic valve, in: "Basic and clinical aspects of cardiac dynamics" (edited by Baan, J., Arntzenius, A.C. and Yellin, E.L.),
  The Hague, Martinus Nijhoff Publ. 477-488, 1980).

- van Steenhoven, A.A. and van Dongen, M.E.H.:
  The role of the trapped sinus vortex in aortic valve closure.
  In: "Biofluid mechanics 2" (edited by Schneck, D.J.),
  New York, Plenum Publ. Corp., pp 317-325, 1980.

- van Steenhoven, A.A., Verlaan, C.W.J., Veenstra, P.C. and Reneman, R.S.:
  An in-vivo cinematographic analysis of the behaviour of the aortic valve.
  Am J. Physiol., 240, pp 286-292, 1981.

- van Steenhoven, A.A., van Duppen, Th.J.A.G., Cauwenberg, J.W.G. and van Renterghem, R.J.:
  In vitro closing behaviour of Björk-Shiley, St. Jude and Hancock heart valve prostheses in relation to the in vivo recorded aortic valve closure,
  J. Biomechanics, 15, pp 841-848, 1982a.

- van Steenhoven, A.A., Veenstra, P.C. and Reneman, R.S.:
  The effect of some hemodynamic factors on the behaviour of the aortic valve,
  J. Biomechanics, 15, pp 941-950, 1982b.

- Steinmetz, G.P., May, K.J., Mueller, V., Anderson, H.N. and Merendino, K.A.:
  An improved accelerated fatigue machine and pulse simulation for testing and developing prosthetic cardiac valves,
  J. Thorac. Cardiovasc. Surg., 47, pp 186-198, 1964.

- Stevenson, D.M., Yoganathan, A.P. and Franch, R.H.:
  The Björk-Shiley heart valve prosthesis,
  Scand. J. Thor. Cardiovasc. Surg., 16, pp 1-7, 1982.

- Stinson, E.B., Griepp, R.B., Oyer, P.E. and Shumway, N.E.:
  Long-term experience with porcine aortic valve xenografts,
  J. Thorac. Cardiovasc. Surg., 73, pp. 54-63, 1977.

- Tandon, A.P., Smith, D.R., Whitaker, W. and Ionescu, M.I.:
  Long-term haemodynamic evaluation of aortic pericardial xenograft,
  British Heart J., 40, pp 602-607, 1978.

- Thomson, F.J. and Barratt-Boyes, B.G.:
  The glutaraldehyde-treated heterograft valve; some engineering observations,
  J. Thorac. Cardiovasc. Surg., 74, pp 317-321, 1977.

- Thubrikar, M.J., Skinner, J.R., Eppink, R.T. and Nolan, S.P.:
  Stress analysis of porcine bioprosthetic heart valves in-vivo,
  J. Biomed. Mater. Res., 16, pp 811-826, 1982.

- Thubrikar, M.J., Deck, J.D., Aouad, J. and Nolan, S.P.:
  Role of mechanical stress in calcification of aortic bioprosthetic valves,
  J. Thorac. Cardiovasc. Surg., 86, pp 115-125, 1983.

- Wallace, R.B.:
  Tissue valves,
  Am. J. Cardiol., 35, pp 866-871, 1975.

- Westerhof, N., Elzinga, G. and Sipkema, P.:
  An artificial arterial system for pumping hearts,
  J. Appl. Physiol., 31, pp 776-781, 1971.

- Williams, J.C., Vernon, C.R., Daicoff, G.R., Bartley, T.D., Wheat, M.W. and Ramsey, H.W.:
  Hemolysis following mitral valve replacement with the Beall prosthesis,
  J. Thorac. Cardiovasc. Surg., 61, pp 393-396, 1971.

- Wisman, C.B., Pierce, W.S., Donachy, J.H., Pae, W.E., Myers, J.L. and Prophet, G.A.:
  A polyurethane trileaflet cardiac valve prosthesis: in-vitro and in-vivo studies,
  Trans. Am. Soc. Artif. Intern. Organs, 28, pp 164-168, 1982.

- Wright, J.T.M.:
  The heart, its valves and their replacement,
  Bio. Med. Engng., 7, pp 26-33, 1972.

- Wright, J.T.M., Eberhardt, C.E., Gibbs, M.L., Saul, T., Gilpin, C.B.:
  Hancock II - An improved bioprosthesis,
  chapter 37 from: "Cardiac bioprostheses, proceedings of the second international symposium", edited by L.H. Cohn and V. Gallucci;
  New York, York Medical Books, 1982.

- Yoganathan, A.P., Corcoran, W.H. and Harrison, E.C.:
  Wall shear stress measurements in the near vicinity of prosthetic aortic heart valves,
  J. Bioengng., 2, pp 369-379, 1978.

- Yoganathan, A.P., Chaux, A., Gray, R.J., De Robertis, M. and Matloff, J.M.:
  Flow characteristics of the St. Jude prosthetic valve: an in vitro and in vivo study.
  Artif. Organs, 6, pp 288-294, 1982.

- Zerbini, E.J.:
  Results of replacement of cardiac valves by homologous Dura mater valves,
  Chest, 67, pp 706-710, 1975.

- Zimmerman, J.: The functional and surgical anatomy of the aortic valve.
  Am. J. Med. Sciences, 5, pp 862-866, 1969.

Appendix I

Some characteristics for a continuous relaxation spectrum

In this appendix two important material characteristics are derived for the continuous relaxation spectrum $S(\tau)$:

$$S(\tau) = \frac{K}{\tau} + S_0 \qquad \theta_1 \leq \tau \leq \theta_2 \tag{I.1}$$
$$= 0 \qquad\qquad \tau\ ,\ \theta_1\ ,\ \tau > \theta_2$$

The considered characteristics are i) the normalized relaxation function H(t) and ii) the loss modulus $E_1(\omega)$. The differences in these characteristics for the cases $S_0 = 0$ and $S_0 \neq 0$ are denoted.
The normalized relaxation function of the frame material (polypropene) showed a non-linear relationship with ln(t). In this appendix it is showed that this non-linearity can be obtained by introducing a $S_0 \neq 0$ in the continuous relaxation spectrum. Furthermore, to obtain values of the loss modulus for the frame and the leaflet material the loss modulus is derived in terms of the model of Fung.

The normalized relaxation function H(t)

Consider the relation (2.3):

$$H(t) = \frac{G(t) - G(\infty)}{1 - G(\infty)} \tag{2.3}$$

After substitution of (2.4):

$$G(t) = \frac{1 + S_0 \int_{\theta_1}^{\theta_2} e^{-t/\tau} d\tau + K \int_{\theta_1}^{\theta_2} \frac{1}{\tau} e^{-t/\tau} d\tau}{1 + S_0(\theta_2 - \theta_1) + K \ln(\theta_2/\theta_1)} \tag{2.4}$$

and

$$G(\infty) = [1 + S_0(\theta_2 - \theta_1) + K \ln(\theta_2/\theta_1)]^{-1} \tag{I.2}$$

into (2.3), we obtain:

$$H(t) = \frac{S_0(\theta_1 e^{-t/\theta_1} - \theta_2 e^{-t/\theta_2}) + K(E_1(\frac{t}{\theta_2}) - E_1(\frac{t}{\theta_1})}{S_0(\theta_2-\theta_1) + K \ln(\theta_2/\theta_1)} \qquad (I.3)$$

$$\text{with } E_1(y) = \int_{x=y}^{\infty} \frac{e^{-x}}{x} dx$$

For: $\theta_1 << t << \theta_2$ this yields: $E_1(\frac{t}{\theta_2}) = -\gamma - \ln(\frac{t}{\theta_2})$

$$E_1(\frac{t}{\theta_1}) \approx 0$$

$$\theta_1 e^{-t/\theta_1} \approx 0$$

So (I.3) can be reduced to:

$$H(t) = \frac{-S_0 \theta_2 e^{-t/\theta_2} - K\gamma - K\ln t + K \ln \theta_2}{S_0(\theta_2-\theta_1) + K \ln(\theta_2/\theta_2)} \qquad (I.4)$$

Using $\frac{d}{d(\ln(t))} = t \frac{d}{dt}$, (I.4) we get:

$$\frac{dH}{d(\ln(t))} = t \frac{dH}{dt} = \frac{-S_0 \theta_2 - \frac{1}{\theta_2} e^{-t/\theta_2} t - K \frac{1}{t} t}{S_0(\theta_2-\theta_1) + K \ln(\theta_2/\theta_1)} \qquad (I.5)$$

Writing $t = e^{\ln(t)}$, (I.5) can be rewritten as:

$$\frac{dH}{d(\ln(t))} = \frac{S_0 e^{\ln(t) - \frac{1}{\theta_2} e^{\ln(t)}} - K}{S_0(\theta_2-\theta_1) + K \ln(\theta_2/\theta_1)} \qquad (I.6)$$

From (I.6) it is observed that $\frac{dH}{d(\ln(t))}$ is a function of ln(t), so H is a non-linear function of ln(t). When $S_0 = 0$, $\frac{dH}{d(\ln(t))}$ is constant and so H is a linear function of ln(t).

The loss modulus $E_1(\omega)$

A useful material function for the description of the constitutive behaviour in the frequency domain is the so-called complex modulus $\bar{E}(\omega)$ which can be written in terms of its real and imaginary parts:

$$\bar{E}(\omega) = E_s(\omega) + i.E_1(\omega) \tag{I.7}$$

$E_s(\omega)$ and $E_1(\omega)$ are called storage modulus and loss modulus, respectively. The loss modulus is related with the amount of hysteresis when excitating the viscoelastic material periodically. We will now derive expressions for the loss modulus $E_1(\omega)$ in terms of the material parameters S_0, K, θ_1 and θ_2 according to the continous relaxation spectrum $S(\tau)$:

$$S(\tau) = \begin{cases} S_0 + \frac{K}{\tau} & , \theta_1 \leq \tau \leq \theta_2 \\ 0 & , \tau < \theta_1, \tau > \theta_2 \end{cases} \tag{I.1}$$

The relaxation modulus G(t) may be written as:

$$G(t) = G_\infty (1 + \int_{\tau=0}^{\infty} S(\tau)\, e^{-t/\tau}\, d\tau) \tag{I.8}$$

G(t) is defined as the stress response to a unit step change of the strain ($\epsilon_0 = 1$):

$$\sigma(t) = G(t)\, \epsilon_0 \tag{I.9}$$

or, in the Laplace domain:

$$\hat{\sigma}(s) = \hat{G}(s)\, s\, \hat{\epsilon}(s) \tag{I.10}$$

with:

$\hat{\sigma}(s)$ = Laplace transform of $\sigma(t)$

$\hat{\epsilon}(s)$ = Laplace transform of $\epsilon(t)$

The Laplace transform of G(t) may then be written as:

$$\bar{G}(s) = \frac{G_\infty}{s} + \int_{\tau=0}^{\infty} G_\infty\, S(\tau)\, \frac{1}{s+1/\tau}\, d\tau \qquad (I.11)$$

The Fourier transform ($s = i\omega$) gives together with (I.10):

$$\bar{E}(\omega) = \frac{\bar{\sigma}(\omega)}{\bar{\varepsilon}(\omega)} = i\omega \frac{G_\infty}{i\omega} + \int_{\tau=0}^{\infty} G_\infty\, S(\tau)\, \frac{d\tau}{i\omega+1/\tau}$$

$$= G_\infty + i\omega\, G_\infty \int_{\tau=0}^{\infty} S(\tau)\, \frac{\tau(1-i\omega\tau)}{1+(\omega\tau)^2}\, d\tau$$

$$\bar{E}(\omega) = G_\infty \{1 + i\omega \int_{\tau=0}^{\infty} \frac{\tau\, S(\tau)}{1+(\omega\tau)^2}\, d\tau + \omega^2 \int_{\tau=0}^{\infty} \frac{\tau^2\, S(\tau)}{1+(\omega\tau)^2}\, d\tau\} \qquad (I.12)$$

Combining (I.7) and (I.12) gives:

$$E_1(\omega) = G_\infty\, \omega \int_{\tau=0}^{\infty} \frac{\tau\, S(\tau)}{1+(\omega\tau)^2}\, d\tau \qquad (I.13)$$

Now, we can substitute (I.1) into (I.13) to obtain:

$$E_1(\omega) = G_\infty\, \omega \int_{\tau=\theta_1}^{\infty} \frac{\tau(S_0+\frac{K}{\tau})}{1+(\omega\tau)^2}\, d\tau$$

$$E_1(\omega) = \frac{G_\infty\, S_0}{2\omega} \ln[\frac{1+\omega^2\theta_2^2}{1+\omega^2\theta_1^2}] + G_\infty\, K\, \{\arctan(\omega\theta_2) - \arctan(\omega\theta_1)\} \qquad (I.14)$$

Relation (I.14) gives the loss modulus for polypropene ($S_0 \neq 0$). For the glutaraldehyde-treated tissue S_0 has the value zero, so for this tissue the loss modulus may be written as:

$$E_1(\omega) = G_\infty\, K\, \{\arctan(\omega\delta_2) - \arctan(\omega\theta_1)\} \qquad (I.15)$$

Figure 2.8 shows the graphical representation of the relations (I.14) and (I.15). When $S_0 = 0$, the loss modulus is nearly frequency-independent for a wide range of frequencies. When $S_0 \neq 0$, an extra term is added to the loss modulus which is responsible for the presence of a maximum in the vicinity of the time constant θ_2.

Appendix II

Transformation of the continuous relaxation spectrum to a discrete spectrum, according to a generalized Maxwell model

In this appendix the transformation of the material parameters of the continuous relaxation spectrum to the parameters of the generalized Maxwell model is described.
In paragraph 2.3 the reduced relaxation function was expressed as a function of the Fung parameters K, θ_1 and θ_2, (equation (2.2)). Generally, the reduced relaxation function may be expressed in terms of the continuous relaxation spectrum $S(\tau)$:

$$G(t) = \frac{1 + \int_{\tau=0}^{\infty} S(\tau)\, e^{-t/}d\tau}{1 + \int_{\tau=0}^{\infty} S(\tau)d\tau} \qquad \text{(II.1)}$$

with

$$S(\tau) = \begin{cases} S_0 + \frac{K}{\tau} & \text{for } \theta_1 \leq \tau \leq \theta_2 \\ 0 & \text{for } \tau < \theta_1,\ \tau > \theta_2 \end{cases} \qquad \text{(II.2)}$$

When S_0 is taken zero, the model of Fung (Fung, 1972) is obtained. Substitution of (II.2) into (II.1) gives the expression for the reduced relaxation function based on a continuous relaxation spectrum:

$$G(t) = \frac{1 + S_0 \int_{\theta_1}^{\theta_2} e^{-t/\tau}d\tau + K \int_{\theta_1}^{\theta_2} \frac{1}{\tau} e^{-t/\tau}d\tau}{1 + S_0(\theta_2-\theta_1) + K \ln(\theta_2/\theta_1)} \qquad (2.4)$$

The reduced relaxation function based on a generalized (discrete) Maxwell model may be expressed as:

$$\hat{G}(t) = \frac{1 + \sum_{i=1}^{N} \hat{R}_i \, e^{-t/\hat{\tau}_i}}{1 + \sum_{i=1}^{N} \hat{R}_i} \qquad \text{(II.3)}$$

with $\hat{R}_i = \hat{C}_i / \hat{C}_0$

Here the symbol $\hat{}$ is used to denote that these values belong to the generalized Maxwell model.
To transform (2.4) to (II.1) some conditions must be fulfilled like:

$$G(t=0) = \hat{G}(t=0) = 1 \qquad \text{(II.2.a)}$$

$$G(t\to\infty) = \hat{G}(t\to\infty) \qquad \text{(II.2.b)}$$

Substituting t = 0 in relations (2.4) and (II.1) it can be seen that condition (II.2.a) is fulfilled. Substituting (2.4) and (II.1) in (II.2.b) gives:

$$\sum_{i=1}^{N} \hat{R}_i = S_0(\theta_2 - \theta_1) + K \ln(\theta_2/\theta_1) \qquad \text{(II.3)}$$

We divide the interval $[\ln(\theta_1), \ln(\theta_2)]$ into N subintervals (see fig. II.1) having equal size Δ according to:

$$\Delta = \frac{1}{N} \ln(\theta_2/\theta_1) \; l = \ln(\tau_{i+1}/\tau_i) \qquad \text{(II.4)}$$

with $i = 1,\ldots,N$; $\tau_1 = \theta_1$; $\tau_{N+1} = \theta_2$;

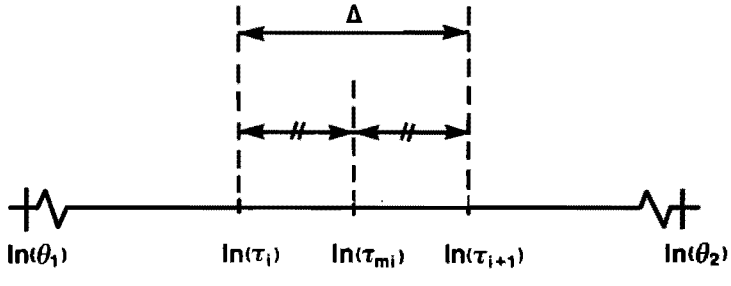

Fig. II.1. Dividing the interval $[\ln(\theta_1), \ln(\theta_2)]$ into N subintervals.

Furthermore we define a mean time constant τ_{mi} for the subinterval $[\ln(\tau_i),\ \ln(\tau_{i+1})]$:

$$\ln(\tau_{mi}) = \ln(\tau_i) + \frac{\Delta}{2} \quad \text{or} \quad \tau_{mi} = \tau_{mi} = \tau_i\, e^{\frac{\Delta}{2}} \tag{II.5}$$

From (II.4) follows

$$\tau_{i+1} = \tau_i\, e^{\Delta} \quad \text{or} \quad \tau_{i+1} - \tau_i = \tau_i(e^{\Delta}-1)$$

This yields with (II.5):

$$\tau_{i+1} - \tau_i = \tau_{mi}\, e^{-\frac{\Delta}{2}}\,(e^{\Delta}-1)$$

After series expansion of the exponential terms this can be written as $\tau_{i+1} - \tau_i \approx \tau_{mi}\,\Delta$ if $\Delta \ll 1$.

In the same way, G(t) (relation (2.4) may be divided:

$$G(t) = \frac{1 + \sum_{i=1}^{N} \left[S_0 \int_{\tau_i}^{\tau_{i+1}} e^{-t/\tau} d\tau + K \int_{\tau_i}^{\tau_{i+1}} \frac{1}{t}\, e^{-t/\tau} d\tau\right]}{1 + S_0(\theta_2-\theta_1) + K\, \ln(\theta_2/\theta_1)} \tag{II.6}$$

G(t) in relation (II.6) must be equal to $\hat{G}(t)$ in relation (II.1). This gives with the use of (II.3)

$$\hat{R}_i\, e^{-t/\tau_i} = S_0 \int_{\tau_i}^{\tau_{i+1}} e^{-t/\tau} d\tau + K \int_{\tau_i}^{\tau_{i+1}} \frac{1}{\tau}\, e^{-t/\tau}\, d\tau \tag{II.7}$$

For t = 0:

$$\hat{R}_i = S_0(\tau_{i+1} - \tau_i) + K\, \ln(\tau_{i+1}/\tau_i) \tag{II.8}$$

$$\hat{R}_i = S_0\, \Delta\, \tau_{mi} + K\, \Delta \tag{II.9}$$

Substitution of (II.9) into (II.7) gives:

$$(S_0 \Delta \tau_{mi} + K \Delta) e^{-t/\hat{\tau}_i} = S_0 \int_{\tau_i}^{\tau_{i+1}} \frac{1}{\tau} e^{-t/\tau} d\tau$$

$$\approx S_0 \int_{\tau_i}^{\tau_{i+1}} e^{-t/\tau_{mi}} d\tau + K \int_{\tau_i}^{\tau_{i+1}} \frac{1}{\tau} d\tau \, e^{-t/\tau_{mi}}$$

$$= S_0 e^{-t/\tau_{mi}} (\tau_{i+1} - \tau_i) + e^{-t/\tau_{mi}} K \ln(\tau_{i+1}/\tau_i)$$

$$= e^{-t/\tau_{mi}} (S_0 \tau_{mi} \Delta + K \Delta) \qquad \text{(II.10)}$$

Then, it can be seen that:

$$\hat{\tau}_i = \tau_{mi} \,, \quad \text{for } i = 1,N \qquad \text{(II.11)}$$

To compose the relaxation modulus of the continuous and discrete model, the elastic response of both models have to be considered. For these elastic responses applies:

$$\hat{F}_e(0) = \hat{c}_0 + \sum_{i=1}^{N} c_i \qquad \text{(II.12)}$$

and

$$F_e(0) = M \qquad \text{(II.13)}$$

in which M is the measured elastic response.

Combination of (II.9) and $\hat{R}_i = \frac{\hat{c}_i}{\hat{c}_0}$ gives:

$$\hat{c}_i = (S_0 \tau_{mi} + K) \Delta \hat{c}_0 \qquad \text{(II.14)}$$

Combining (II.12), (II.13) and (II.14) gives as a result:

$$M = \hat{c}_0(1 + \Delta \sum_{i=1}^{N} (S_0 \tau_{mi} + K)) \qquad \text{(II.15)}$$

and thus:

$$\hat{c}_0 = \frac{M}{1 + \Delta \sum_{i=1}^{N} (S_0 \tau_{mi} + K)} \qquad \text{(II.16)}$$

The transformation from the continuous relaxation spectrum to the discrete spectrum according to the generalized Maxwell model may be summarized as:

$$\hat{\tau}_i = \tau_{mi} = \theta_1 e^{(i-\frac{1}{2})\Delta}$$

$$\hat{c}_0 = \frac{M}{1 + \Delta \sum_{i=1}^{N} (S_0 \tau_{mi} + K)}$$

$$\hat{c}_i = [S_0 \tau_{mi} + K] \Delta \hat{c}_0$$

$$\Delta = \frac{1}{N} \ln(\theta_2/\theta_1)$$

Figure II.2 shows the reduced relaxation function of the glutaraldehyde-treated tissue and of polypropene, calculated for the generalized Maxwell model with N branches for N varying from 2 to 6. It can be seen that in both cases the relaxation function converges quickly to the function described with the continuous relaxation spectrum. Table II.1 shows the results of this transformation.

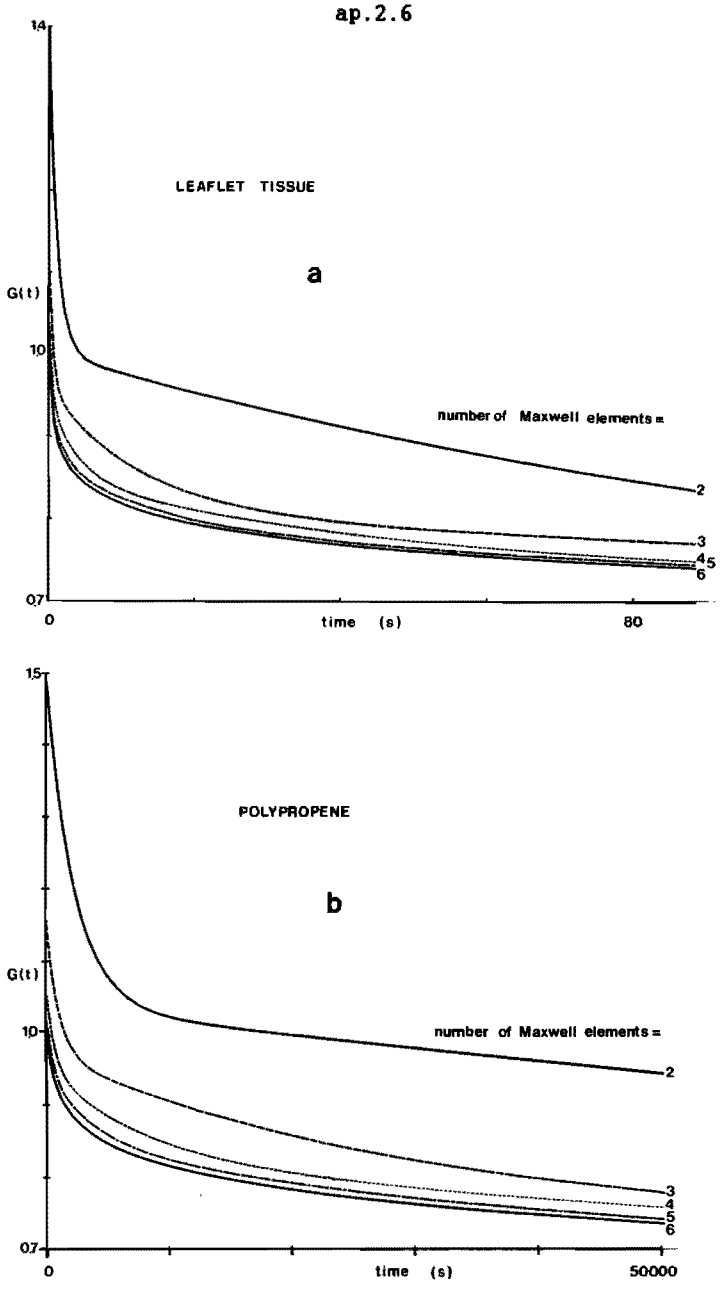

Fig II.2. The reduced relaxation function of the glutaraldehyde-treated tissue (a) and of polypropene, calculated for the generalized Maxwell model with 2N + 1 parameters. N is varied in both cases from 2 to 6.

		membrane	fibre	polypropene
parameters describing the continuous relaxation spectrum	M (N/mm^2)	1.8	23.0	1582
	v (-)	0.5	0.5	0.4
	S_0 (s^{-1})	-	-	$0.9265.10^{-5}$
	K (-)	0.05	0.05	0.1051
	θ_1 (s)	0.0019	0.0019	3.4
	θ_2 (s)	23	23	63270
parameters describing the generalized Maxwell model with 6 branches	C_0/M (-)	0.680	0.680	0.3909
	C_1/M (-)	0.053	0.053	0.0675
	C_2/M (-)	0.053	0.053	0.0675
	C_3/M (-)	0.053	0.053	0.0685
	C_4/M (-)	0.053	0.053	0.0736
	C_5/M (-)	0.053	0.053	0.0994
	C_6/M (-)	0.053	0.053	0.2327
	τ_1 (s)	0.0042	0.0042	4.61
	τ_2 (s)	0.0199	0.0199	39.71
	τ_3 (s)	0.0955	0.0955	204.42
	τ_4 (s)	0.4576	0.4576	1052.32
	τ_5 (s)	2.1927	2.1927	5417.12
	τ_6 (s)	10.5070	10.5070	27886.11

Table II.1. The material properties of the used materials, given with parameters of the continuous relaxation spectrum and with parameters describing the generalized Maxwell model.

Samenvatting

Het in dit proefschrift beschreven onderzoek heeft tot doel technische ontwerpspecificaties op te stellen waaraan een verbeterde vliesklepprothese dient te voldoen. Dit geschiedt aan de hand van een analyse van het mechanisch gedrag van een vliesklepprothese belast met een fysiologische drukbelasting tijdens een hartcyclus. In die hartcyclus kunnen twee fasen onderscheiden worden waarin ongunstige spannings- en rekverdelingen kunnen ontstaan. Dit zijn de fase waarin de klep gesloten is en de fase waarin de klep zich opent en sluit. De analyse van het mechanisch gedrag van een vliesklepprothese in gesloten toestand en het opstellen van ontwerpspecificaties voor die toestand is het hoofdonderwerp van dit proefschrift.

De bezwijkfenomenen van bestaande vliesklepprothesen zijn bestudeerd uit de literatuur. Globaal kunnen de bezwijkfenomenen worden verdeeld in 3 typen: scheuren in het vliesmidden, scheuren in het vlies langs de vliesophanging en verkalking van de vliezen. Met name de eerste 2 worden gedacht samen te hangen met de belasting in gesloten toestand.

Voor de analyse van het mechanisch gedrag van de gesloten klep is een numeriek model gemaakt van een bestaande vliesklepprothese. Deze klep is opgebouwd uit 3 dunne flexibele vezelversterkte vliesjes afkomstig van een glutaraldehyde behandelde aortaklep van een varken. Die vliesjes zijn gemonteerd in een flexibel polypropeen frame met 3 opstaande poten. De invoergegevens voor deze numerieke analyse zijn verkregen door bestudering van de geometrie en materiaalparameters van de klep. Hieruit volgde o.a. dat glutaraldehyde behandeld aortaklep weefsel stijver en minder visceus is dan vers weefsel. In alle gevallen is het materiaal na 120 s uitgerelaxeerd. Voor polypropeen daarentegen zijn zeer lange relaxatijden gevonden (> 50.000 s).

Het numerieke model is gebaseerd op de eindige elementenmethode, en is opgebouwd uit balkelementen (frame), membraanelementen (vliezen en vliesophanging) en kabelelementen (vezelversterking in de vliezen en de Dacron klepbekleding). De klep wordt belast met een fysiologisch drukverschil over het klepvlies en is star bevestigd langs de klepbasis. Dit numerieke model voorspelt grote von Mises spanningen in het vlies nabij de vliesophanging. In die gebieden worden ook de

maximale vezelspanningen aangetroffen. In gebieden die niet direct belast zijn met een gelijkmatig verdeelde drukbelasting (zoals in het coaptatiegebied) worden negatieve waarden van de minimum hoofdspanning gevonden in membranen tussen vezels. Dit zou kunnen duiden op plooivorming waardoor weer grote buigrekken zouden kunnen ontstaan. Tenslotte is voor 2 willekeurige punten de schuifspanning tussen vezel en membraan berekend. De resultaten van de numerieke analyse zijn experimenteel getoetst door de verplaatsingen van de 3 frametoppen en het vliesmidden gedurende een hartcyclus in-vitro te meten. De frametop verplaatsingen zijn nagenoeg lineair met de druk over de klep. De vlies-midden verplaatsing is niet-lineair en vertoont enige hysterese. Numerieke en experimentele resultaten komen redelijk goed met elkaar overeen.

Het ontwikkelde en geverifieerde numerieke model is vervolgens gebruikt voor een parameter variatie studie aan een nieuwe vliesklepprothese. Deze klep bestaat in principe uit 3 flexibele kunststof vliezen versterkt met vezels die vrijwel parallel lopen. De vliezen zijn direct verbonden aan een kunststof frame. Uit de parameterstudie, gebaseerd op de statistische theorie van proefopzetten, is naar voren gekomen dat met name 5 geometrie en materiaalparameters op niet triviale wijze van belang zijn voor de spanningsverdeling in de gesloten klep. Dit zijn: de vliesophanging (gekarakteriseerd door een hoek α), framestijfheid, vezeldikte, elasticiteitsmodulus van de vezels en de gemiddelde vezelafstand. Een acceptabel compromis wordt gevonden bij een hoek van 10^{o}, stijf frame, vezeldikte van 0.25 mm, elasticiteitsmodulus van vezel van 50 N/mm^2 en een gemiddelde vezelafstand van 1.5 mm.

Door middel van een relatief eenvoudige duurproef, waarbij polyurethaan proefstrookjes met een frequentie van 8 Hz wisselende buigrekvariaties ondergaan, is bestudeerd of de aanwezigheid van wisselende buigrekvariaties samenhangt met het ontstaan van scheurtjes en het optreden van verkalking. Uit dit onderzoek is naar voren gekomen dat wisselende buigrekvariaties inderdaad het verkalkingsproces versnellen. Verder onderzoek hiernaar is dan ook gewenst, samen met een mechanische analyse van de klep in geopende toestand.

Nawoord

De uitvoering van het hier beschreven onderzoek en de tot stand koming van dit proefschrift is alleen mogelijk geweest door de bijdrage van vele mensen. Langs deze weg wil ik hen hartelijk bedanken.
Met name ben ik zeer veel dank verschuldigd aan Anton van Steenhoven. Hij was gedurende het gehele onderzoek mijn grote steun en toeverlaat; vanaf de inspirerende discussies aan het begin tot en met de afronding van dit proefschrift. Zonder zijn bijdrage zou dit werk veel aan waarde verloren hebben. Dit geldt ook voor beide promotoren, Prof. Janssen en Prof. Huysmans, die steeds klaar stonden voor intensieve begeleiding.
Leo Wouters heeft in het gehele onderzoek zeer veelzijdig meegewerkt. Het zoeken naar geschikte materialen voor een prototype van een klepprothese en het verkalkingsonderzoek rustten vooral op zijn schouders. Ook zorgde hij voor de fabricage van de spoeltjes voor het inductief lengtemeetsysteem en heeft hij alle figuren in dit proefschrift op foto gezet. Tini van Hout was een grote steun bij de uitvoering en de verwerking van de materiaal beproevingsexperimenten. Zijn filosofische discussies hebben tot vele goede ideeën geleid. Frans van den Broek, Theo van Duppen en Nick van Dijk tekenen voor het buigbelastingapparaat. Op snelle wijze werd een zeer origineel apparaat bedacht en gemaakt. Jacques Cauwenberg zorgde ervoor dat de kernen van de precisie spoeltjes steeds op voorraad waren. Tevens had hij vele goede ideëen bij het ontwerpen van een toestel om hartklepprothesen versneld te belasten. Veel dank ben ik ook verschuldigd aan collega Jos van Heck, die zijn steun verleende bij het opstellen van een goed statistisch model voor het bepalen van de ontwerpspecificaties. Fons Sauren was voor mij een goede afstudeercoach en daarna een stimulerende collega. Hem wil ik speciaal bedanken voor de steun in het begin van het onderzoek, voor de stimulerende discussies tijdens het onderzoek en het corrigeren van het proefschrift op het Engels bij de afronding. Rob van Renterghem was een fijne collega die zorgde voor de verwezenlijking van het inductief spoeltjesmeetsysteem. De anatomische tekeningen van de natuurlijke aortaklep en de Hancock klep werden gemaakt door Hans Rensema en Guus van Rooy.

Els Scheepens heeft de tekst van het hele proefschrift op snelle en accurate wijze getypt. Hiervoor ben ik haar veel dank verschuldigd. In het kader van een afstudeer- of stagewerk zijn bijdragen geleverd door vele studenten. Met name wil ik hier bedanken Ton Flaman, voor de samenwerking tijdens het meten van de commissuurverplaatsingen; Ad van de Ven bedacht het reeds hiervóór genoemde ontwerp van een toestel om hartklepprothesen versneld te belasten en Roland van Venrooy leverde zijn bijdrage in het meten van de verplaatsing van het vliesmidden. Enkele medewerkers van DSM zorgden met name voor het bepalen van enkele materiaaleigenschappen en de analyse van enkele verkalkte preparaten.
Aan 2 mensen ben ik echter de meeste dank verschuldigd: pap en mam, jullie zijn het uiteindelijk geweest die dit alles hebben mogelijk gemaakt; bedankt. En Claire, ja, ondanks dat je hier niet genoemd had willen worden, wil ik je toch bedanken voor de grote steun die je me de afgelopen 2 jaren hebt gegeven.

Levensbericht

17- 4-1956	Geboren te Maastricht.
1968 - 1974	Atheneum-B gevolgd aan het Henric van Veldeke College te Maastricht.
1974 - 1980	Studie aan de Technische Hogeschool Eindhoven, Afdeling Werktuigbouwkunde.
1980 - 1985	Wetenschappelijk assistent aan de Technische Hogeschool Eindhoven, Afdeling der Werktuigbouwkunde, in het kader van het interafdelingsproject Hartklepprothesen.
1-3-1985	In dienst getreden als medewerker van de afdeling Ontwikkeling Kunststoffen bij de Concerndienst Research en Octrooien van DSM te Geleen.

STELLINGEN

behorende bij het proefschrift

MECHANICAL SPECIFICATIONS FOR A CLOSED LEAFLET VALVE PROSTHESIS

1. Polyetherurethaan rubbers zijn geschikt voor de fabricage van de vliezen van kunstmatige vliesklepprothesen vanwege de goede biocompatibiliteit en de mogelijkheid de gewenste stijfheid en vezelversterking te verkrijgen. Het calcificatie probleem is hierbij echter nog onvoldoende onderzocht.

2. De stelling dat een vliesklepprothese een flexibel frame moet bevatten omdat bij de natuurlijke aortaklep van een flexibele vliesophanging sprake is, is onjuist.

3. De analyse van de deformatie van een vliesklepprothese tijdens openen en sluiten van de klep om ontwerpspecificaties voor die toestand op te stellen verdient, met het oog op een optimaal ontwerp, een grote prioriteit. Met name de optredende buigrekken zijn van belang in verband met de mogelijkheid van calcificatie.

4. De meetresultaten van spanningen in de vliezen van een vliesklepprothese gedurende een belastingcyclus zoals door Reis et al. gerapporteerd moeten argwanend bekeken worden. (Reis et al., J. Thorac. Cardiovasc. Surg., 62, 683-689, 1971).

5. Bij het gebruik van glutaraldehyde behandeld pericardium weefsel voor de fabricage van de vliezen van bioprothesen dient terdege met de richting van de vezelstructuur in dat pericardiumweefsel rekening te worden gehouden. Dit is in de praktijk welhaast onmogelijk.

6. Het mechanisch gedrag van een zogenaamde geknoopte hechting en van een continue hechting bij de implantatie van hartklepprothesen is wezenlijk anders.

7. Het menselijk waarnemingsvermogen is de zwakste schakel in de medische beeldvormende diagnostiek.

8. In het curriculum voor werktuigbouwkundig ingenieur moet meer aandacht gegeven worden aan het constitutief gedrag van (vezelversterkte) kunststoffen en aan een experimentele bepaling daarvan.

9. De vrije studierichting der Biomedische en Gezondheidstechniek (variant Werktuigbouwkunde), die aan de Technische Hogeschool Eindhoven werd gerealiseerd, is een van de saillante uitingen van de belangrijke activiteiten die deze T.H. ontplooit in het gebied "technische wetenschappen-geneeskunde".

10. Naar mate het hebben van een klus veelvuldiger gebruikt wordt als verontschuldiging om ergens niet te hoeven verschijnen, moet deze smoes in deze tijd van werkloosheid aangemerkt worden als een steeds grotere zonde tegen de ethiek.

11. Closetpapier heeft meer dan de Franse revolutie de gelijkheid van de mensen in de hand gewerkt.

12. Humor is een vorm van plagerij tegen de ernst van het leven.

Eindhoven, 2 april 1985 E.P.M. Rousseau